Cholinergic signaling modulates astrocytic D-serine release

A thesis submitted by

Michaela Tolman

in partial fulfillment of the requirements for the degree of

Ph.D.

in

Neuroscience

Tufts University

Sackler School of Graduate Biomedical Sciences

August 2018

Advisor: Philip Haydon, Ph.D.

Abstract

Cholinergic signaling controls brain states, modulates circuit function, and is a primary therapeutic strategy for a number of diseases including schizophrenia and Alzheimer's disease. Recent work from our lab has demonstrated in mouse hippocampal slices that wakefulness-dependent acetylcholine (ACh) release acts on alpha 7 nicotinic acetylcholine receptors (α7nAChRs) expressed by astrocytes to control the availability of the obligatory NMDA receptor (NMDAR) co-agonist, D-serine. However, cholinergic dependent changes in hippocampal D-serine levels have not been measured in vivo. To do this, I established both high pressure liquid chromatography (HPLC) and microdialysis techniques. Using these two techniques, I found that the level of D-serine detected correlates with the wakefulness state of the mouse, that the α7nAChRs on astrocytes are necessary for maintaining normal hippocampal D-serine levels, social interaction, learning, and memory behaviors in male mice. These experiments expand our mechanistic understanding of cholinergic signaling by comparing the astrocyte α7nAChR conditional knock-out (cKO) mice to neuronal α7nAChR cKO mice.

Table of Contents

List of Tables

List of Figures

Copyrighted Materials

Reprinted with permission from Neuron: Papouin T, Dunphy JM, Tolman M, Dineley KT, Haydon PG. Septal Cholinergic Neuromodulation Tunes the Astrocyte-Dependent Gating of Hippocampal NMDA Receptors to Wakefulness. *Neuron* May 17 2017;94(4):840-854 e847.

Reprinted Figure 2 with permission from Springer Nature: Jones CK, Byun N, Bubser M. Muscarinic and nicotinic acetylcholine receptor agonists and allosteric modulators for the treatment of schizophrenia. *Neuropsychopharmacology* September 28 2011;37(1):16-42.

Reprinted Figure 1 with permission from Elsevier: Halassa MM, Fellin T, Haydon PG. The tripartite synapse: roles for gliotransmission in health and disease. *Trends in Molecular Medicine* January 4 2007;13(2):54-63.

Reprinted Figure 2 with permission from Cureus: Sattar Y, Wilson J, Khan AM, et al. A review of the mechanism of antagonism of N-methyl-D-aspartate receptor by ketamine in treatment-resistant depression. *Cureus* May 18 2018;10(5):e2652.

Abbreviations

A1R – adenosine 1 receptor
ACh – acetylcholine
AChE – acetylcholine esterase
AD – Alzheimer's disease
ADHD – attention-deficit/hyperactivity disorder
ALS – amyetrophic lateral sclerosis
Asc-1 – alanine-serine-cysteine-1
ASCT – alanine-serine-cysteine transporter
ATP – adenosine triphosphate
Aβ – amyloid beta
BChE – butyrylcholinesterase
BF – basal forebrain
CAMKII – calmodulin-dependent protein kinase II
ChAT – choline acetyl transferase
cKO – conditional knock-out
CNS – central nervous system
CSF – cerebrospinal fluid
CTL4 – choline transporter-like protein 4
DAAO – D-amino acid oxidase
DBB – diagonal band of broca
DISC1 – disrupted in schizophrenia 1
dnSNARE – dominant negative SNARE
GFAP – glial fibrillary acidic protein
GWAS – genome wide association studies
HPLC – high pressure liquid chromatography
KO – knock-out
LDTg – laterodorsal tegmental
LTD – long-term depression
LTP – long-term potentiation
MHb – medial habenula
MS – medial septum
NGF – nerve growth factor
NMDAR – N-methyl-D-aspartate receptor
PHGDH – phosphoglycerate dehydrogenase
PLC – phospholipase C
PNS – peripheral nervous system
PPtg – pedunculopontine
REM – rapid eye movement
SC – schaffer collateral
SNARE – soluble N-ethylmaleimide-sensitive factor activating protein receptor
SNP – single nucleotide polymorphism
SR – serine racemase
SSS – SLEEPLESS
TRPA1 – transient receptor potential ankyrin 1

VAMP2 – vesicle-associated membrane protein 2
α7nAChR – alpha 7 nicotinic acetylcholine receptor

Chapter 1: Introduction

1.1 Background

Cholinergic signaling controls brain states and modulates circuit function. Using pharmacology and mouse hippocampal slices, we demonstrated that wakefulness-dependent acetylcholine (ACh) release acts on alpha 7 nicotinic acetylcholine receptors (α7nAChRs) expressed by astrocytes to control the availability of the obligatory NMDA receptor (NMDAR) co-agonist, D-serine[1]. However, cholinergic dependent changes in hippocampal D-serine levels have not been measured in vivo. To do this, I established both high pressure liquid chromatography (HPLC) and microdialysis techniques. Using these two techniques, I found that the level of D-serine detected correlates with the wakefulness state of the mouse, that the α7nAChRs on astrocytes are necessary for maintaining normal hippocampal D-serine levels, social interaction, learning, and memory behaviors in male mice. These experiments expand our mechanistic understanding of cholinergic signaling and the astrocyte's role in translating cholinergic tone into the modulation of neuronal networks. Disruptions in cholinergic signaling and D-serine levels have been targeted for the treatment of schizophrenia and Alzheimer's disease. Our mechanistic insights will help to understand the underlying causes of these severe diseases and help to better direct drug discovery efforts.

1.2 Cholinergic Signaling

Acetylcholine (ACh) was the first neurotransmitter discovered in the early 1900s [2]. Henry Dale first isolated ACh as a contaminant in his bacterial cultures and later described its potent effects on nerve activity in the periphery[3]. Today, the mechanisms of the cholinergic system are still being investigated. We know that ACh plays crucial and

well conserved roles in both the peripheral and central nervous systems (PNS and CNS) of the body. While cholinergic transmission is synaptic and fast acting in the periphery, ACh release in the CNS is more diffuse, positioning it well for a slower acting role as a neuromodulator in the brain. Rather than forming direct synaptic structures, cholinergic neurons in the CNS release ACh through volume transmission [4]. Once released, ACh can be hydrolyzed by either ACh esterase (AChE) or butyrylcholinesterase (BChE). These reactions produce acetate and choline, which are transported back into the cell and used in lipid metabolism[5]. Cholinergic neuronal cell bodies cluster in specific nuclei then send their projections diffusely throughout the brain. These cholinergic nuclei include the pedunculopontine and laterodorsal tegmental areas (PPtg and LDTg), medial habenula (MHb)[6] and the basal forebrain (BF)[7] including the medial septum (MS). These projections and ACh release by volume transmission allow this well-known neurotransmitter to adjust the gain of neuronal circuitry based on cues from the periphery.

The cholinergic system senses signals from the PNS and the external environment and in turn modulates cognitive inputs and other neurotransmitter systems. The output of this modulation is the coordination of neuronal networks and the tuning of synaptic plasticity. To do this, ACh can act on dopaminergic[8], GABAergic, and glutamatergic[9] neurons and astrocytes[10, 11]. Evolutionarily, this has allowed animals to potentiate their responses to environmentally adaptive behaviors, such as the proximity of a predator, and decrease responses to ubiquitous, less urgent stimuli.

Since volume transmission does not have a direct post-synaptic structure designed to receive the signal, the effect ACh elicits largely depends on the location and subtype of receptor that receives the signal. There are two types of cholinergic receptors: ionotropic

nicotinic and metabotropic muscarinic. The nicotinic receptors are fast acting non-selective cation channels[12, 13]. They are made up of five subunits. α4β2 heteropentameres and α7 homopentameres are common subtypes[14], but many combinations can be formed with the α2-7 and β2-4 subunits. All flavors of these ionotropic receptors are permeable to Na^+, K^+, and Ca^{2+} ions, but the α7nAChR has the highest permeability to Ca^{2+} ions. nAChRs are found on presynaptic terminals, intracellular compartments, postsynaptic terminals, cell bodies, and axons. Each subtype in different locations can affect the release of multiple transmitter systems[15-17]. Metabotropic muscarinic ACh receptors (mAChRs) act more slowly than the ionotropic, nAChR subtypes. The M1, 3, and 5 subunits are coupled to G_q proteins and activate phospholipase C (PLC). The M2 and 4 subunits are coupled to $G_{i/o}$ proteins and negatively regulate adenylate cyclase[18]. mAChRs can be found on both pre and postsynaptic compartments with differing effects. For example, presynaptic M2/4 mAChRs can act as inhibitory autoreceptors on cholinergic terminals[19, 20]. Whereas M1/5 mAChRs can stimulate dopamine release from striatal synaptosomes[21] or increase the excitability of cortical pyramidal neurons when on postsynaptic compartments[19, 22]. Thus, the receptor subtype and location largely dictate how ACh affects the local environment once released.

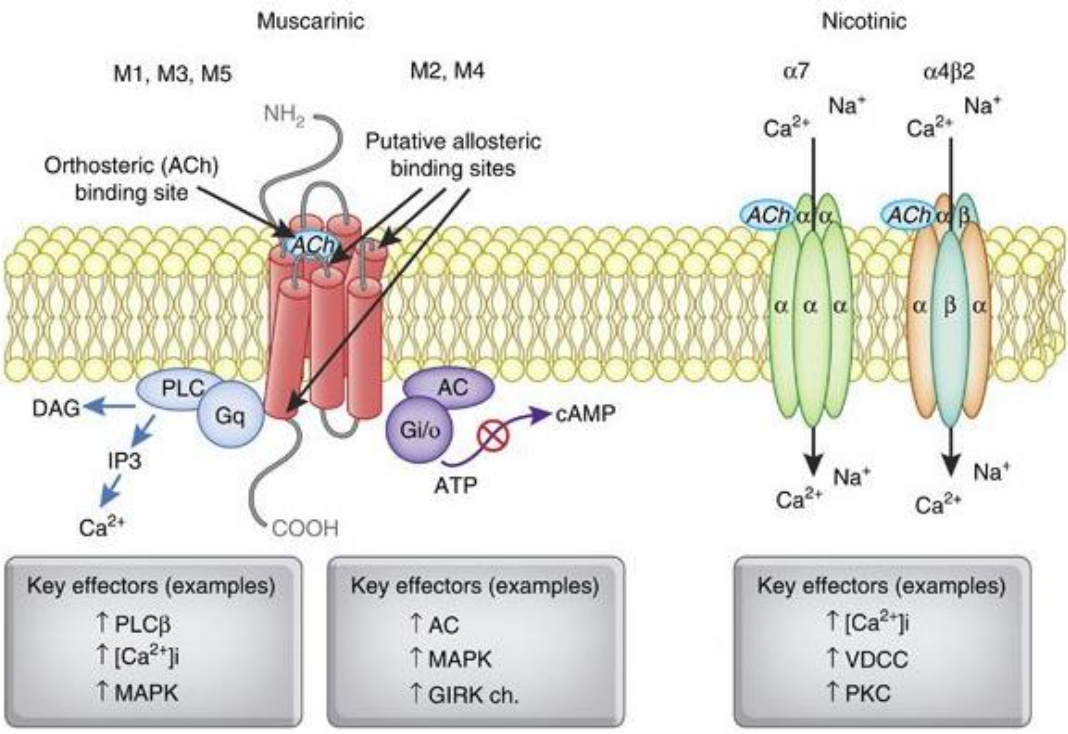

Figure 1.1: Cholinergic receptor signaling pathways. The structure and signaling pathways of mAChRs and nAChRs. Each mAChR subtype is a seven-transmembrane protein, which belongs to two major functional classes based on G-protein coupling. The M_1, M_3, and M_5 mAChRs selectively couple to the Gq/G11-type G-proteins resulting in the generation of inositol-1,4,5-trisphosphate (IP3) and 1,2-diacylglycerol (DAG) through activation of the phosphoinositide-specific phospholipase-Cβleading to increased intracellular calcium levels. The M_2 and M_4 mAChRs preferentially activate Gi/Go-type G-proteins, thereby inhibiting adenylate cyclase, reducing intracellular concentration of cAMP, and prolonging potassium channel opening. All mAChR subtypes show a high sequence homology across species, particularly in the orthosteric ACh-binding sites. Neuronal nAChRs are pentameric ligand-gated ion channels. The most abundant neuronal subunits are α_4, β_2, and α_7, with the heteromeric $\alpha_4\beta_2$ receptor subtype in highest abundance. The heteromeric $\alpha_4\beta_2$ receptor subtype can exist in two different forms: $(\alpha 4)_2(\beta 2)_3$ receptors show low Ca^{2+} permeability and high affinity to ACh and nicotine, whereas $(\alpha 4)_3(\beta 2)_2$ receptors have high Ca^{2+} permeability. By contrast, the α_7 nAChR also shows high permeability to Ca^{2+} relative to the heteromeric $\alpha_4\beta_2$ nAChRs. The action of $\alpha_4\beta_2$nAChRs can enhance intracellular levels of Ca^{2+} by secondary activation of VOCCs, whereas α_7 nAChRs preferentially increase Ca^{2+} release from ryanodine-sensitive intercellular stores through CICR. The capacity of these different nAChR subtypes to couple to VOCC or CICR mechanisms results in distinct patterns of Ca^{2+} signaling that can provide a broader control of synaptic plasticity and neurotransmitter release, as well as gene transcription. Reprinted from (Jones, et al., 2012)[23]

The coordination of ACh release and receptors mediate essential functions in the CNS. In the early 1990s, it was discovered that electrically stimulating the cholinergic nucleus in the MS could improve long term memory retention[24]. A decade later, it was determined that ACh mediates θ rhythms in the hippocampus, which are key to learning and memory[25]. These θ rhythms depend on activation of the MS and are exhibited during exploration and rapid eye movement (REM) sleep. Inducing θ oscillations decreases the threshold for long-term potentiation (LTP), the cellular mechanism for learning and memory[26]. Activation of both n and mAChRs is necessary to produce the balanced timing-dependent changes in hippocampal synaptic plasticity.

Through both experimental models and human studies, ACh has been implicated in the coordination of a number of other complex behaviors. In fruit flies, it was discovered that a protein called SLEEPLESS (SSS) is tethered to postsynaptic membranes and negatively regulates nAChRs. SSS promotes sleep by decreasing nAChRs' affinity for ACh[27]. In mammals, the Lynx1 protein was shown to play a similar role and when knocked out, the investigators found greatly increased nAChR currents and neuronal cell death[28]. Early on in human studies of depression, it was found that increasing levels of ACh correlated with symptoms of the disease[29]. A decade later, it was shown that amplification of the cholinergic system enhanced anxiety and depression-like behaviors[30]. Similarly, stress increases ACh in the hippocampus and cortex[31] and results in altered splicing of the AChE mRNA in the hippocampus[32]. On the other hand, there are also issues when there is not strong enough cholinergic signaling. Genome wide association studies (GWAS) were performed and found that mutations in cholinergic receptors are linked to patient's severity of and susceptibility to nicotine and alcohol

addiction[33, 34]. Mutated cholinergic receptors have also been associated with attention-deficit/hyperactivity disorder (ADHD)[35].

Many have sought to better understand the mechanisms of cholinergic signaling through the optogenetic and pharmacological manipulation of ACh release. General cholinergic agonists enhance LTP in the CA1 region[36]. Stimulation of the MS or its projections through the diagonal band of broca (DBB) causes both depolarization and hyperpolarization through muscarinic receptors on interneurons in the CA1 region of the hippocampus[37]. While the mAChRs are clearly important, learning and memory deficits due to lesioning of the cholinergic projections can be rescued by nAChR agonists, such as nicotine[38]. Using optogenetics, it was found that the α4β2 mAChR in particular was responsible for modulating the activity of GABAergic interneurons in this region[39]. It was determined that both direct activation of GABAergic interneurons in the stratum oriens and the indirect modulation of pyramidal neurons in the CA1 region is necessary to induce timing-dependent synaptic plasticity[40-42]. These bursts of ACh induced inhibitory activity that works to synchronize the hippocampal network[37, 43, 44]. To add to the complexity of orchestrating this response, astrocytes in the hippocampus also express cholinergic genes and respond to altered ACh levels[45].

Understanding how to activate the cholinergic system is crucial for drug development. Tsanov, 2015 reviews results from a number of groups using optogenetics to activate cholinergic neurons in the MS. The results consistently show that activation of the MS increases Θ power when the animal is anesthetized or in a state of quiet wakefulness[46]. When the animal is in an active state, either there is no effect of stimulating the MS since ACh levels are saturated or a weaker level of stimulation is

required to increase Θ power. Gu et al. also found that they could alternately induce LTP or long-term depression (LTD) in the CA1 depending on when they added activation of the cholinergic projections relative to stimulation of the Schaffer collateral projections. LTP was disrupted by amyloid β (Aβ) and α7nAChR or NDMAR antagonists[41]. These studies show the complex nature of cholinergic signaling in the hippocampus and challenges involved with developing cholinergic agonists for the treatment of cognitive disorders. Future work is needed to better understand these cellular mechanisms in vivo and in the context of multiple disease states before we can develop next generation cholinergic modulators for patients.

1.3 Dysregulation of Cholinergic Signaling

Dysregulation of the cholinergic system has severe consequences and contributes to a number of disease etiologies[47-50]. Deficits in cholinergic signaling have been intensely studied in Alzheimer's disease (AD). It was first thought that cholinergic neurons in the BF deteriorate with normal aging[51], but more recent work has shown that normal aging is only associated with synaptic changes, but little cell death[52]. Loss of cholinergic neurons is one of the first pathological signs of AD. This may be in part due to their high energy demands[53]. While cholinergic cell death is a large contributor, other disruptions to cholinergic signaling have also been linked to disease pathology. Clinical dementia correlates with decreased levels of cholinergic markers, such as choline acetyl transferase (ChAT), mAChRs, nAChRs, and ACh levels[54]. Aβ also binds with high affinity to the α7nAChR[55]. At low concentrations, it activates the receptor, but at high concentrations it causes receptor desensitization[56]. The consequences of decreased cholinergic signaling in the hippocampus include deficits in attention, learning, and

memory[57]. As a result, the majority of treatments options for AD have focused on boosting cholinergic tone to produce temporary improvements in cognition, but are not able to alter the disease progression.

Others have reviewed the cholinergic modulators used to treat AD[58]. Most of the current treatments focus on boosting ACh levels and the subsequent cognitive enhancing effects are thought to be mediated through the hippocampus[59]. Newer generation cholinergic drugs have tried to target specific m or nAChR subtypes. Since scopolamine, an mAChR antagonist, induces memory deficits in healthy patients, reminiscent of AD, there has been interest in developing mAChR agonists for the treatment of AD[60]. Xanomeline, for example, was developed as an M1/4 agonist, but failed to reach clinical significance in its phase III trial[61, 62]. Many other subtype-specific cholinergic agonist have advanced to clinical trials, but have seen complications with activation of cholinergic receptors in the periphery[63]. At this point, it is clear that the development of cholinergic treatments for AD would benefit greatly from new targets derived from a better understanding of the mechanisms underlying the cholinergic signaling.

Recent cholinergic drug discovery efforts have turned to schizophrenia. Schizophrenia is a psychiatric disorder characterized by positive symptoms (i.e. delusions and hallucinations), negative symptoms (i.e. anhedonia and social withdrawal), and cognitive impairments (i.e. disturbances in attention and working memory)[64]. Initially, it was thought that the dopaminergic system was the key target, but many of the dopaminergic therapies were only partially affective and came with prohibitive side effects. With a better understanding of the disease etiology, it is now recognized that NMDARs, $GABA_A$Rs, and AChRs all play a role[65-68]. The underlying cause of

schizophrenia likely involves hundreds of genes and environmental factors[69], but post mortem studies have shown that there is a significant decrease in m and nAChR expression in the prefrontal cortex, striatum, and hippocampus[70-72]. Interestingly, smoking rates are much higher in schizophrenic patients, reaching over 80%[73]. It is thought that this may be a form of self-medication, but that the beneficial effects of nicotine subside quickly[74]. As a therapeutic target, nicotine has been avoided due to its liability for abuse and its cardiac affects. Supporting the hypothesis that m and nAChRs play an important role in schizophrenia etiology, researchers have shown that cholinergic inhibition can cause psychosis in healthy individuals, whereas AChE inhibitors can improve cognition[75, 76]. The α7nAChR gene specifically has been linked to a vulnerability to develop schizophrenia[77]. Similarly, the α7nAChR subtype specifically shows decreased levels in schizophrenic patients[78]. With these histological and pharmacological data, it is clearly shown that the cholinergic system is altered in and contributes to schizophrenia etiology.

In early clinical trials, cholinergic modulators have shown promise for affecting both positive and negative symptoms of schizophrenia as well as the cognitive deficits. If successful, these would be a huge improvement over the current standard of care. As mentioned previously, activation of peripheral receptors has limited the clinical potential of these drug candidates, however. The M1/4 agonist xanomeline improved both positive and negative symptoms in schizophrenic patients[79], but development was halted after gastrointestinal side effects arose in the long-term clinical studies. The α7nAChR agonist DXMB-A showed efficacy in phase I and II trials[80], but there was no longer a significant difference between groups after four weeks of dosing[81]. The chief concern with these

studies is desensitization of the receptor and nicotine use in the patients. Many allosteric modulators have been developed in hopes of circumventing this issue[23]. Additional challenges to cholinergic drug discovery in schizophrenia include the lack of predictive mouse models and the lack of conservation between species in the regulation of ACh metabolism[82]. Ideally, the field of cholinergic modulation in schizophrenia would benefit greatly from a better understanding of the cellular mechanisms tuning neuronal networks and the identification of new therapeutic targets in these pathways.

1.4 Astrocytic Contribution to Neuronal Networks

Astrocytes were first described 100 years ago as a subtype of glia or support cell. Since early neuroscientists used electrical signals to record from brain and spinal cord tissue, they missed the complex chemical and structural interactions supplied by the 'glue' cells. With new tools, there has been tremendous progress in glial research in the last 50 years. Just 20 years ago the term 'tripartite synapse' emerged with the confirmed hypothesis that astrocytes are far from glue or passive support cells; they are active participants at the synapse[83]. We now know that 60-90% of synapses are contacted by astrocytic processes in the hippocampus and each astrocyte contacts thousands of synapses[84, 85]. This gives astrocytes a unique vantage point from which they can integrate signals and modulate neuronal outputs. For example, it has been shown that astrocytes sense neuromodulators such as norepinephrine and ACh in vivo[10, 86] and subsequently tune neuronal networks to sensory stimuli or brain states[45, 87-89]. The types of stimulation, age of the animal, and experimental parameters used to activate and record the response of astrocytes varies widely in the literature, causing some varied results. It has been shown that astrocytes exert their effects on neuronal networks in part by releasing

gliotransmitters, however. These gliotransmitters can have differing effects on the network. For example, adenosine triphosphate (ATP) is release from astrocytes and rapidly hydrolyzed into adenosine. Adenosine can then act presynaptically on adenosine 1 receptors (A1Rs) to inhibit release of neurotransmitters[90] or potentiate post synaptic responses[91]. D-serine, an obligatory co-agonist of the NMDAR, is also released by astrocytes and modulates synaptic plasticity[92, 93]. Astrocytes can release gliotransmitters via soluble N-ethylmaleimide-sensitive factor activating protein receptor (SNARE)-dependent vesicle-associated membrane protein 2 (VAMP2) vesicular release or through channels[94-96]. Better understanding the specific signals and intracellular mechanisms that lead to release of different gliotransmitters will be key to developing new classes of cognitive therapies targeting astrocytic modulation of neuronal networks.

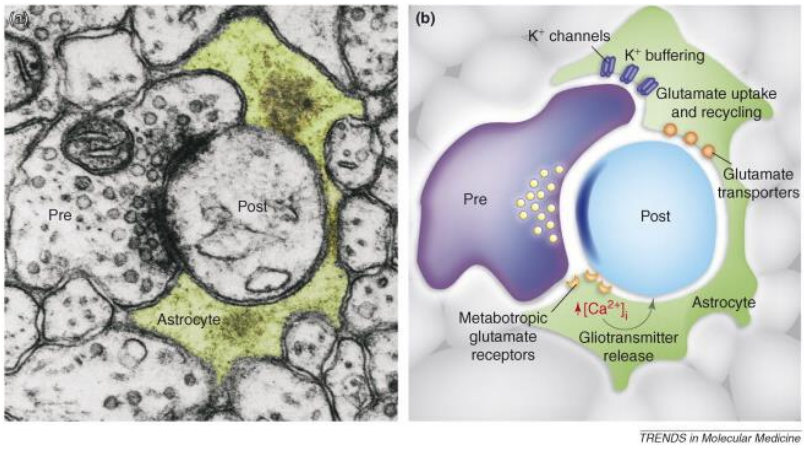

Figure 1.2: The astrocytic process is the third active element forming the tripartite synapse. **(a)** Electron micrograph showing a presynaptic (Pre) and postsynaptic (Post) terminal enwrapped by the astrocytic process (green) forming the tripartite synapse. **(b)** The close association of the astrocytic process with the presynaptic and postsynaptic terminals exerts crucial roles in clearing K^+ ions that accumulate following neuronal activity, and in the uptake of the synaptic transmitter glutamate by the activity of plasma-membrane glutamate transporters. Additionally, neurotransmitter release from presynaptic terminals can activate astrocytic metabotropic receptors, which induce the inositol (1,4,5)-trisphosphate (Ins(1,4,5)P_3)-dependent release of Ca^{2+} from internal stores, which in turn triggers the release of several neuroactive compounds (gliotransmitters) from these cells. Locations of astrocytic transporters and receptors in

this figure do not necessarily represent their exact spatial distribution. (Panel (a) was modified, with permission, from Peters O.A. 1991 The fine structure of the nervous system). (Reprinted from Halassa, et al., 2007)[97]

1.5 D-serine

Traditionally, it was not thought that there were abundant D-enantiomer amino acids in the brain, but in the early 1990s D-serine was found in the CNS[98]. Not only was D-serine present in the brain, it was found to act on one of the most important receptors, the NMDAR. D-serine binds to the GluN1 subunit while glutamate binds to the GluN2-3 subunit to activate the receptor. Glycine was first found to bind to this site, hence the name 'the glycine binding site', but D-serine was later found to be the main co-agonist at synaptic NMDA receptors throughout the adult brain[98]. Acting as an obligatory co-agonist, the concentration, localization, and timing of D-serine release emerged as an important modulator of NMDAR gated functions such as learning, memory, and social interactions[99-101]. Thus, the mechanisms of D-serine synthesis, release, and reuptake has been widely studied.

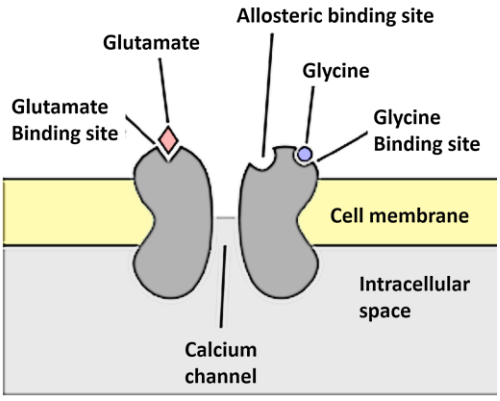

Figure 1.3 NMDA receptor signaling.
(Reprinted from Sattar, et al., 2018)[102]

In the brain, D-serine is synthesized from L-serine via the enzyme serine racemase (SR). When SR is genetically knocked-out, D-serine levels are decreased by

90% which causes changes in activity levels and memory deficits in male mice[103]. The location of SR and therefore the cell-type that regulates its extracellular availability has been hotly debated. Some found that SR was mainly localized to astrocytes using immunostaining[104-106]. Later on, a different antibody was used in rat forebrain tissue sections and it was found that SR was primarily localized to neurons[107]. Once the SR knock-out (KO) mouse was developed, it was used as a negative control in further immunohistochemistry studies. These groups found that SR was localized to excitatory and inhibitory neurons, but not to astrocytes[108]. Overall, three groups find significant levels of SR in astrocytes[105, 109, 110] and two groups find higher levels of SR in forebrain neurons[107, 111] using immunohistochemistry. As genetic tools progressed, Benneyworth et al. used cell-type specific promoters to KO SR in either astrocytes or neurons[112]. They reported that knocking-out SR in calmodulin-dependent protein kinase II (CamKII) expressing neurons decreased overall SR levels by 65%. When they knocked-out SR from glial fibrillary acidic protein (GFAP) expressing astrocytes, they only saw a 10% reduction in SR levels. At this point, the field is far from a universal conclusion. It is likely that both neurons and astrocytes contribute to D-serine synthesis. Further functional studies should be done to see which cell types and which cellular mechanisms are important for both its production and release.

Since the source of D-serine in the brain is still debated, it is not surprising that the release, transport, and reuptake mechanisms are not completely understood. Using in vivo microdialysis, some suggest that D-serine is released through alanine-serine-cysteine-1 (Asc-1) transporters[113]. Blocking these transporters lowered D-serine levels and impaired LTP[114]. Shigetomi et al. used genetic tools to KO the transient receptor

potential Ankyrin 1 (TRPA1) channels in astrocytes and also found impaired LTP in the CA1 region of the hippocampus and lower D-serine levels as measured by biosensors[115]. D-serine has also been localized to vesicular structures in rat cortical astrocytes[110]. Using the dn-SNARE mouse model, researchers found that blocking vesicular release from astrocytes inhibited D-serine release and dendritic spine plasticity in adult born neurons of the dentate gyrus[116]. These mechanisms likely all contribute to D-serine release rather than acting mutually exclusively. In this line of research, a 'shuttle' hypothesis has emerged. Since astrocytes have the machinery to make L-serine from glucose[117, 118], one group has proposed that astrocytes synthesize L-serine and then shuttle it over to neurons for the synthesis of D-serine. This hypothesis notes that a key enzyme in the L-serine synthesis reaction, phosphoglycerate dehydrogenase (PHGDH) is exclusively found in astrocytes. When PHGDH is knocked-out, there was a subsequent decrease in neuronal D-serine levels[119]. Mutations in this enzyme have also been found in human patients, resulting in microcephaly, psychomotor retardation, seizures and decreased D-serine in the cerebrospinal fluid (CSF)[120]. Once released, D-serine can be taken up through either a Na^+-dependent alanine-serine-cysteine transporter (ASCT)[121] or through the Na^+-independent transporter Asc-1[122]. The balance between these two forms of transport has important implications for neuronal excitability. When neurons are active, intracellular Na^+ levels increase, potentially prohibiting the reuptake of D-serine through the ASCT and keeping extracellular D-serine levels high. Regardless of the mechanism of release or reuptake, the extracellular regulation of D-serine is incredibly important for modulating complex behaviors.

Changes in D-serine levels have been implicated in a number of disease states. Many studies have looked at D-serine levels in schizophrenic patients and found decreased levels in the serum, plasma, and CSF[123-128]. Mutations in D-serine related genes also confer an increased risk of developing schizophrenia including SR[129], D-amino acid oxidase (DAAO) the enzyme that degrades D-serine[130, 131], and disrupted in schizophrenia 1 (DISC1) a protein that binds to SR[132]. It was also found that DAAO protein levels are increased in schizophrenia, leading to an overactive degradation of D-serine in the extracellular space[133]. In rodent studies, traditional antipsychotic treatments targeting the monoamine pathways do not affect D-serine levels[134, 135], but adding D-serine to the treatment regimens of schizophrenic patients improved both positive and negative symptoms[123, 136-138]. Improvements during the treatment of schizophrenic patients also correlates to D-serine levels in their plasma[139]. D-serine levels also decrease over time during normal aging[140] and NMDAR related deficits in aging can be rescued by D-serine[141]. Unfortunately, to introduce therapeutic levels of D-serine to the brain, high concentrations have to be ingested, which leads to toxicity over time. The deficit of D-serine in schizophrenic patients and its demonstrated efficacy in the clinic highlight the importance of better understanding the mechanisms of its regulation to identify new therapeutic targets. My current work creates a novel link in the mechanistic understanding of both cholinergic signaling and D-serine modulation.

Chapter 2: Septal cholinergic neuromodulation tunes the astrocyte-dependent gating of hippocampal NMDA receptors to wakefulness[1]

[1] Papouin, T., Dunphy, JM., Tolman, M., Dineley, KT., Haydon, PG. 2017. *Neuron*. 94(4):840-854.e7. Reprinted here with permission from publisher.

2.1 Summary

The activation of the N-methyl D-aspartate receptor (NMDAR) is controlled by a glutamate-binding site and a distinct, independently regulated, co-agonist-binding site. In most brain regions, the NMDAR co-agonist is the astrocyte-derived gliotransmitter D-serine. We found that D-serine levels oscillate in mouse hippocampus as a function of wakefulness, in vitro and in vivo. This causes a full saturation of the NMDAR co-agonist site in the dark (active)-phase that dissipates to sub-saturating levels during the light (sleep)-phase, and influences learning performance throughout the day. We demonstrate that hippocampal astrocytes sense the wakefulness-dependent activity of septal cholinergic fibers through the α7-nicotinic acetylcholine receptor (α7nAChR), whose activation drives D-serine release. We conclude that astrocytes tune the gating of synaptic NMDARs to the vigilance state and demonstrate that this is directly relevant to schizophrenia, a disorder characterized by NMDAR and cholinergic hypofunctions. Indeed, bypassing cholinergic activity with a clinically-tested α7nAChR agonist successfully enhances NMDARs activation.

2.2 Introduction

N-methyl D-aspartate receptors (NMDARs) play a direct role in many aspects of brain physiology, such as learning and memory. They are also involved in a variety of disorders, and a hypofunction of synaptic NMDAR signaling is the main hypothesis for the etiology of schizophrenia, a chronic and severe mental disorder that affects 2.6 million adults in the United States[142, 143]. Activation of NMDARs requires the presence of a co-agonist, in addition to their agonist glutamate[144, 145], and D-serine plays this role in many brain regions, in particular the hippocampus[93, 146]. Because D-serine is thought to

be a gliotransmitter released by astrocytes[109, 110, 146, 147] an interesting corollary is that astrocytes could regulate the availability of D-serine at synapses to control NMDAR independently of neuronal activity. However, because the conditions and stimuli that govern D-serine release are unidentified, it is still unknown whether astrocytes can modulate the concentrations of D-serine they supply to NMDARs under certain conditions of brain activity.

Brain disorders often shed light on the physiological pathways at play in the healthy brain, and our current understanding of the etiology of schizophrenia points to a possible link between brain cholinergic activity and NMDAR co-agonist gating. D-serine levels are lowered in the plasma of schizophrenic patients[126, 127] and many human mutations associated with schizophrenia result in a hypofunction of NMDAR co-agonist binding site by decreasing its affinity or by directly impairing D-serine availability[132, 148]. In parallel, a dysregulation of the cholinergic system is a hallmark of schizophrenia[142, 149], and recent clinical trials aimed at improving cognitive symptoms of schizophrenic patients with cholinergic modulators[142].

Cholinergic neurons in the medial septum send scattered projections to cortical regions where their activity results in ambient levels of acetylcholine (ACh), or extracellular ACh "tone", involved in long-range and long-lasting effects[150]. In these regions, the ACh tone fluctuates with changes in vigilance state: the highest levels are found during active wakefulness and the lowest during slow wave sleep[151-153]. Interestingly, ACh is known to influence NMDAR activity and NMDAR-dependent functions[154-158], and activates intracellular signaling in astrocytes through various ACh receptors (AChRs)[10, 159-161]. Combined with evidence that ACh can promote D-serine

synthesis and/or release[10, 155, 162], these data point to a link between vigilance state-dependent cholinergic activity and NMDAR co-agonist gating via astrocytic D-serine.

This hypothesis greatly aligns with the most recent view of astrocytes function. Indeed, the time course of astrocytic activity is several orders of magnitude slower than neurons[163]. This makes astrocytes good candidates to receive, integrate and relay information about the neuromodulatory state of the brain, such that their impact on neuronal and brain function has become increasingly relevant in the scope of behavioral states[86-88, 90, 109]. This is supported by evidence that astrocytes are exquisite sensors of neuromodulators, such as norepinephrine and acetylcholine, that are involved in sensory modalities and vigilance states[10, 45, 86, 88, 152, 159-161, 164]. Here we used a variety of in vivo and *in vitro* approaches to examine fluctuations of endogenous D-serine availability throughout the day and their link with cholinergic activity. We found that the wakefulness-dependent cholinergic activity from the medial septum governs astrocytic release of D-serine via the activation of astrocytic α7nAChRs, thus tuning the gating of hippocampal NMDARs to wakefulness. We also show that bypassing the endogenous cholinergic activity with an α7nAChR partial agonist, used in a Phase III clinical trial for the treatment of schizophrenia, successfully enhances D-serine levels, highlighting the relevance of our findings to the therapeutic approach of schizophrenia.

2.3 Materials and Methods

2.3.1 Contact for reagent and resource sharing

Further information and requests for resources and reagents should be directed to and will be fulfilled by the Lead Contact, Philip Haydon (Philip.haydon@tufts.edu).

2.3.2 Experimental model and subject details

All animal experiments were conducted in accordance with the guideline of the Animal Care and Use Committee of Tufts University.

2.3.3 Animals, housing and genotyping

Adult male mice (3-6 months old) were used throughout this study with the exception of Figure 2.13 where experiments were occasionally performed on α7nAChR$^{flox/flox}$ or α7nAChR$^{+/+}$ females. All animals were kept on a 12-12 light-dark cycle and housed in groups of 2-5 siblings with water and food *ad libitum*. No mouse was single-housed for more than 24h under any circumstances, including after surgery where littermates were housed back together as soon as sternal recumbency was reached. Behavior and electrophysiology experiments were conducted by a male experimenter. Littermates of the same sex were randomly assigned to experimental groups.

ChAT-ChR2-eYFP BAC transgenic mice were purchased from Jackson Laboratory (*B6.Cg-Tg(Chat-COP4*H134R/EYFP)6Gfng/J*, Stock #014546) and bred in our facility (2 females and 2 males founders). Genotyping was performed on tails samples taken from 7 day old pups using the same set of primers and PCR cycling conditions described in Zhao et al., 2011. Mice referred to as ChAT-ChR2-eYFP$^{-/-}$ (of ChR2$^{-/-}$) were littermate non-carriers of the transgene.

Heterozygous α7nAChR$^{floxed/+}$ mice in which exon 4 of the *Chrna7* gene is flanked by loxP sites (*B6-Chrna7*^{LBDEx4007Ehs}) originated from Dr. K. Dineley's lab (Department of Neurology, University of Texas, Medical Branch, Galveston, TX 77555) where they were generated as described in Hernandez et al., 2014. They were cleared fron quarantine after

2 weeks, backcrossed with C57Bl/6 mice and bred in our facility. Primers used for genotyping were: (forward) GTG CCA GAC CAC ATG TGC ATT GG and (reverse) GGT CAC TGA GCA GTG GTG GAC AG, giving a 474 base pair (bp) band for the endogenous *Chrna7* allele and a ~650bp band for the floxed allele (See Figure 2.14).

The dnSNARE mice were bred and genotyped as previously described[94, 116]. In these mice, the expression of the tetracycline transactivator (tTA) is driven by the GFAP promoter, which ensures the selective expression of the construct in astrocytes of adult mice. In the absence of Doxycycline (Dox), tTA binds to the tetracycline response element which permits the expression of the dnSNARE and eGFP transgenes. The dnSNARE transgene codes for the cytosolic portion (96 amino acids) of the vesicle associated membrane protein VAMP2 which acts as a dominant-negative that inhibits vesicular exocytosis[116]. Importantly, breeders were maintained on a Dox-containing diet (40mg/kg) at all times and pups (all genotypes) were kept on Dox until they were weaned (4 weeks), in order to prevent *in utero* and developmental expression of the transgene. This is of paramount importance since GFAP promotor activity, although selectively restricted to astrocytes in adults (see Zhang et al., 2014 and http://web.stanford.edu/group/barres_lab/cgi-bin/igv_cgi_2.py?lname=gfap), is found in a population of neuronal precursor cells during early post-natal development[165]. GFAP-tTA negative mice were used as single gene controls (Figure 2.13). Animals were used 8 weeks after Dox removal from diet. Additionally, 12 dnSNARE mice were put back on a Dox-containing diet at ~P80 for 4 weeks before being used for electrophysiology (Figure 2.13) in order to shut off transgene expression and control for possible off-target long-lasting cellular effects of dnSNARE expression ("dnSNARE on Dox"). Importantly,

some doubts have been raised by Fujita et al., 2014 about the cell-selectivity of the expression of the dnSNARE construct in these mice. In their publication, they reported broad and marked expression of the transgene GFP reporter in hippocampal and cortical neurons. This is not the case for the dnSNARE line originating from and bred in our lab and we encourage readers to refer to Figure 2.5 were we performed immunohistochemistry and extensive cell counting that demonstrate the absence of neuronal expression of the transgene in our line. In particular we show that not a single eGFP-positive neuron was found among 5,884 and 5,887 neurons counted (by two separate investigators) in confocal z-stacks of images taken from dnSNARE off Dox mice from our lab (See section on Immunohistochemistry, fluorescence imaging and cell counting, below). This is in agreement with all but one publication that have used dnSNARE mice since they were generated in 2005, and in strikingly contrasts with results from Fujita et al., suggesting possible genetic drift of the line used by Fujita et al. or technical/procedural issues in their study (such as the absence of Dox during development).

2.3.4 Zeitgeber time scale

The Zeitgeber time (ZT) scale arbitrarily sets the origin of the 24h period (ZT0) to the onset of the light-phase, allowing comparison among studies independently of the actual clock-time settings of animal facilities. Onset of light (ZT0) was at 7am during daylight saving time and 6am otherwise in our facility. It should be noted that for electrophysiology experiments at ZT0, mice that were still awake in their home cage at that time were favored over mice already nested. This criterion was applied to avoid mitigating effects due to periods of rest of unknown duration prior to light onset. We

measured that an average of 3 min elapsed between taking the mouse cage off the rack in the animal facility to the decapitation of the animal.

2.3.5 Slice preparation

Experiments were carried out on acute hippocampal slices from adult male mice (3-6 months). After decapitation under isoflurane anesthesia, the brain was quickly removed from the skull and placed in ice-cold artificial cerebrospinal fluid (aCSF) saturated with 95% O_2 and 5% CO_2 and containing 2mM Mg^{2+} and 1mM Ca^{2+} to limit excitotoxicity. Hippocampal coronal slices (350 µm) were incubated 35 min at 33°C in 1.5 mM Mg^{2+} and 2 mM Ca^{2+}-containing aCSF and then allowed to recover for 45 min at room temperature. Slices were then transferred into a recording chamber, where they were perfused with aCSF (~1 mL/min) saturated with 95% O_2/5% CO_2. The aCSF composition was (in mM): 125 NaCl, 2.5 KCl, 1.25 NaH_2PO_4, 26 $NaHCO_3$ and 10 glucose (pH 7.3, 290-300 $mOsm.L^{-1}$).

2.3.6 Field recordings

Schaffer collaterals were electrically stimulated at 0.05 Hz with a concentric tungsten electrode placed in the *stratum radiatum*. Evoked field excitatory post-synaptic potentials (fEPSPs) were recorded using a glass electrode (2-4 MΩ) filled with aCSF and placed in the *stratum radiatum*. Intensity of stimulation (< 120 µA, 100 µs, except for Figure 2.10 Panel A where a different stimulator was used) was set appropriately to avoid population spikes, and the slope of field responses was monitored throughout. Experiments were performed at 33°C in the presence of 2 mM Ca^{2+} and 50 µM picrotoxin. NMDAR-mediated responses were isolated in low Mg^{2+} concentration (0.2 mM) with 10 µM NBQX to block AMPA/Kainate receptors. When AMPAR-mediated

responses were recorded (Figure 2.10), NBQX was omitted and the concentration of Mg^{2+} was 1.3 mM. Data were recorded with an Axopatch C (Axon Instruments, Inc.), and collected and analyzed using Clampex9.2 and Clampfit9.2 software (Axon Instruments, Inc.). Average traces were obtained from 20-30 min of stable recordings. Unless major run-up, rundown or electrical noise appeared on the recordings that prevented accurate analysis, no experiments were excluded.

2.3.7 Optogenetics

For ChR_2 excitation in slices from ChAT-ChR2-eYFP BAC transgenic mice, square pulses of blue light (460/50 nm, 20 ms duration) were delivered through the 40X water immersion objective of a Prairie Technologies Uncager microscope equipped with a 75 W mercury lamp (Olympus, U-LH75XEAPO). Illumination was applied to the entire visual field centered on the tip of the recording pipette and the output light power measured at the microscope objective was 600-800 µW. Trains of light-pulses were delivered using a high-speed shutter (Uniblitz VMM-D4, Vincent Associates). The frequency and duration of trains (5 Hz, 10sec) were controlled by an A310 Accupulser (World Precision Instruments) triggered by Clampex9.2. When brain slices were obtained from ChAT-ChR2-eYFP BAC transgenic mice, care was taken to reduce exposure to light during the slicing procedure and when slices were manipulated under the microscope.

2.3.8 Drugs

With the exception of EVP-6124 hydrochloride (MedChem Express) that was injected i.p. at 0.4 mg/kg, drugs were purchased from Tocris or Sigma, prepared as 1000X aliquots (stored at -20°C) in distilled water, DMSO (CPT) or 90% alcohol

(picrotoxin) and bath applied at concentrations indicated in the main text with a 1:1000 dilution. D-serine was also injected i.p. at 200mg/kg for behavioral experiments. $ZnCl_2$ 250 nM (Sigma) was used in 10 mM Tricine (Sigma) with the relation $[Zinc]_{free} = [Zinc]_{applied}/200$[93, 166]. It should be noted that Zinc and Ro25-6981 are partial antagonists that inhibit ~70-80% and ~90% of the current flowing through GluN2A-NMDARs (GluN1/GluN1/GluN2A/GluN2A) and GluN2B-NMDARs (GluN1/GluN1/GluN2B/GluN2B), respectively[166]. The subunit composition of NMDARs impacts many of their properties and in particular their affinity for glycine and D-serine[167], and remains unchanged throughout the 24h period in our study guarantees that their affinity for exogenous D-serine is unchanged.

EVP-6124 (or vehicle: 0.04% DMSO in saline) was injected i.p. at ZT0 in awake mice (9 mice total for this experiment), in the animal facility. Mice were then immediately returned to their home cage with their siblings and left undisturbed for 4 hours (ZT4). During this time, they were closely monitored to check for possible behavioral effects of EVP-6124 injection. All of the 9 injected mice nested and were immobile in the hour following the injection. None of the mice injected with EVP-6124 showed any sign of prolonged wakefulness or enhanced locomotor activity (see below).

2.3.9 D-serine biosensor measurements in conditioned medium

For D-serine measurements with amperometric biosensors, slices were obtained exactly as described above for electrophysiology experiments. Typically, 6-8 hemi-slices were obtained for those experiments, approximately spanning from Bregma -1.5 to -2.6. After 30min at 33°C and 45min recovery at RT, slices were taken individually to carefully separate the hippocampus from the rest of the slice. To minimize manipulation

and damage to slices, a small portion of cortex immediately above the hippocampus (motor and somatosensory cortex typically) was left attached and therefore participated in the following incubation. Hippocampal-cortical slices were then allowed an additional 15min of recovery before being placed in 3mL of aCSF gently oxygenated with 95% O_2/5% CO_2, where they were incubated for 90min at RT. Ca^{2+} and Mg^{2+} concentration were 2mM and 1.5mM respectively. To favor oxygenation and access to glucose, this incubation was performed in two separate 1.5 mL tubes that received 3-4 hippocampal slices each. The conditioned medium (CM) was then carefully drained and immediately frozen (-80°C) until used for D-serine measurement (see below). Incubated tissue was frozen too (-80°C) until protein extraction was performed using a Pierce™ BCA protein assay kit. On average, the concentration of protein for all incubated 6-8 slices was, in WT: 13.8 ± 0.7 mg/ml of protein at ZT0 and 13.1 ± 0.4 mg/mL at ZT6; and in dnSNARE: 10.1 ± 0.8 mg/ml of protein at ZT0 and 12.7 ± 0.8 mg/ml of protein at ZT6. Two CM measurements fell under the detection limit of our sensors, raising uncertainties about their accuracy, and were excluded from the analysis (Figure 2.13F). D-serine and null biosensor electrodes, 0.5 mm in length and 50-60 µm in diameter, were purchased from Sarissa Biomedical and used according to manufacturer's instructions (Dale et al., 2005 and http://www.sarissa-biomedical.com/products/sarissaprobes.aspx). These biosensors consist of platinum electrodes coated with D-serine degrading enzyme (DAAO) embedded in a perm-selective layer (the null-sensor consisting of the perm-selective layer alone is used to subtract non-selective signals). The degradation of D-serine by DAAO involves the stoichiometric use of 2 electrons, which provides a linear electronic readout of D-serine concentration. Calibration experiments showed that the

biosensor electrodes reliably and linearly detect D-serine for concentrations of 0.1 to 50 µM (Figure 2.1), in line with manufacturer specifications. The electrodes were mounted on Scientifica micromanipulators to allow submersion and positioning in the recording chamber of the electrophysiology setup at 33°C in a vehicle solution (aCSF made the day of slice incubation). Control of biosensors' potential and measurement of current through biosensors were operated using a bipotentiostat (Digi-IVY, Model DY2023). Biosensors and null sensors were rehydrated at 33°C for 30 min to 1h under continuous perfusion of the vehicle solution. Cycling from -500 to +500 mV and back was carried out several times as suggested by manufacturer, and biosensors were then allowed to polarize to +500 mV for 60 min until capacitive decay was imperceptible. The CM was then perfused in the recording chamber where the biosensors were submerged. The aCSF made on the day of CM collection was used as the baseline and wash-out vehicle solution. The volume of CM incubated with slices (3 mL) was set by preliminary experiments aimed at determining the minimal volume of CM allowing plateau detection by the biosensors with this method. As seen on traces of Figure 2.1F, artifacts usually appeared on recordings as the perfusion system was switched to the CM or from the CM back to the vehicle solution (after the 3 mL had passed through). A similar artifact was purposefully generated during perfusion of the calibrating (1 µM) D-serine solution when 3 mL had passed through, by gently tapping the recording chamber. As can be seen on the calibration trace (Figure 2.1F bottom) the plateau detection is fully reached by the time 3 mL have been perfused (artifact on the trace). Though no current was generally observed on the null-sensor, currents measured on this sensor electrode were subtracted from currents measured on the D-serine sensor electrode to obtain a pure "D-serine-

induced" amperometric signal. Sensors were calibrated at the end of every experiment with 0.1, 0.5, 1 and 10 µM D-serine to measure their sensitivity (in our hands, some biosensor electrodes successfully detected D-serine amounts as low as 50 nM). This allowed a determination of the absolute concentration of D-serine in CM.

Classical use of these biosensors consists of penetrating brain slices with the biosensor electrode itself, which typically results in an immediate peak detection of tens of µM of D-serine, likely due to tissue destruction and irreversible damage to neurons and glia, causing intracellular D-serine (which accounts for most of brain D-serine) to be released into the extracellular space. After tens of minutes of decay this is expected to stabilize to a steady-state level thought to reflect the endogenous extracellular concentration of D-serine in slices[115]. Instead, this is more likely to reflect residual amounts of D-serine escaping the scarring/dying tissue surrounding the biosensor. Additionally this approach is highly dependent on how deep sensors are forced into the slice, which dictates how much of the sensor is in contact with damaged tissue and therefore how much D-serine is detected. Last but not least, we found that such a method could cause deterioration of the sensor itself upon penetration in the slice. Together these concerns encouraged us to employ a different approach (conditioned medium approach), described above.

2.3.10 Enforced-wakefulness and enriched-environment housing

Enforced-wakefulness (EW) is usually achieved by "gentle handling" which consists of exposing animals to unknown and potentially stressful stimulations for about 6 hours (new bedding, new cage, handling, novel objects, noise and poking, rattling on the cage grid)[168]. In an effort to achieve EW with minimal stress to the animals, EW was

carried out over a shorter duration and without handling at all. Since D-serine availability decreases within the first hour of the light-phase (Figure 2.1) we were able to assess the effect of only 2 hours of EW. This is still sufficient to distinguish between a circadian and a wakefulness-dependent mechanism (see main text) while avoiding any confounding effects from long periods of EW that increase locomotor activity and cause stress as shown by dramatic elevation of corticosterone levels. This also allowed EW to occur in home cages without handling the mice, removing the bedding, grid, water or food and without presentation of any novel object. The cage was simply placed in a new room. Typically, no further action was required to maintain animals awake for the first hour since this was enough to elicit classic exploratory behavior and social interaction. For the following hour, the cage was occasionally gently displaced to maintain the animals alert and by 1.5h into the EW, the filter-lid was partially removed from the top of the cage. Subsequent olfactory stimulation provided enough arousal to keep mice awake until ZT2. Enriched environment housing (EEH) consisted of novel objects such as plastic hamster tunnels, igloos, cubes, slides and platforms of different colors and textures dispersed around that cage (objects were wiped with alcohol beforehand). Items were not fixed to the bottom of the cage and mice were free to displace them. Three to five males from the same litter were housed in the same, large cage (26 x 47 x 20 cm). The grid was removed and the cage top was covered with high-ceiling lid so that mice could also explore their environment vertically. Food was provided *ad libitum* and water was provided via two 40 mL water dispensers (BioServInc #9019), also contributing to novelty. Finally, at the onset of the dark-phase (ZT12), mice were provided a running metallic wheel that was

removed at the onset of the light-phase (ZT0). EEH was provided for at least 2 consecutive days and limited to a maximum of 5 days in order to prevent habituation.

2.3.11 In vivo microdialysis and HPLC

Cannula implantation: 6-8 week old male C57/B6 mice (Jackson Laboratory, 000664) received a unilateral cannula implantation surgery. Briefly, mice were anesthetized using isofluorane. Buprenorphine (0.05mg/kg, sub cutaneous) was given pre-operative and post-operative as needed. Hippocampal coordinates were measured (-2mm, left 1.5mm) from Bregma and the midline. The guide cannula (CMA P000138) was inserted just above the cortex and secured with dental cement and two contra lateral anchor screws. Mice recovered 7 days before sampling. Cannula implantation was verified at the end of the experiments following transcardiac 4% PFA perfusion and brain sectioning. Placement of the cannula was assessed by a separate investigator and animals showing mistargetting were excluded from the HPLC analysis. All procedures were approved by Tufts IACUC. *Microdialysis*: Mice were habituated to single housing for at least 7 days prior to sampling. On the day of sampling, probes (CMA P000082) were inserted through the guide cannula at ZT0. ACSF (Harvard Appparatus, 597316) was perfused through the probe at a rate of 0.5ul/minute for 6 hours. Dialysis samples were collected every hour and frozen at -80C. During sampling, mice were video recorded using Pinnacle video capture software. *Video scoring*: Animals were scored as active (mobile or immobile but awake) or inactive (nested and absence of movement) each minute of the 6 hour recording. The average activity over the 6 hour sampling was then compared to the average concentration of D-serine collected in the dialysis sample. *High precision liquid chromatography*: D-serine detection was performed using HPLC and an Accucore C18

column (Thermo Fisher, 17126-152130). An organic phase (methanol) and aqueous phase (50mM phosphate buffer, pH 4.34) were perfused at a rate of 200ul/minute in a step protocol: 0-6 min 3% organic, 6.5-10 min 20% organic, 11-14 min 80% organic, and equilibrated at 3% organic for 7 minutes. Samples were diluted in half with aqueous mobile phase and derivatized using o-Phthaldialdehyde (Pickering, O120) and N-Acetyl-L-Cysteine (Sigma, A8199). After derivatization, 1M acetic acid was added. 1ul of sample was injected and run on the column, followed by a second replicate run from the same sample. Standards were prepared from D- and L-serine (Sigma) in aqueous mobile phase at a ratio of 1:10. The area under the D-serine peak was used to calculate the sample concentration relative to standards. For each animal, the average activity was plotted versus the average D-serine concentration. Statistical significance was assessed using a correlation analysis.

2.3.12 Wakefulness assessment, EEG-EMG recordings and analysis

The implantation of electroencephalogram (EEG) electrodes (Pinnacle Technology) was conducted stereotaxically under isoflurane anesthesia on 6-8 week old male C57/B6 mice (Jackson Laboratory, 000664). The skull surface was exposed and four insulated wire electrodes were placed and screwed as follows: two extradural cortical electrodes were inserted bilaterally in the frontal areas and the other two were inserted bilaterally in the parietal areas. Two insulated wire electrodes were inserted bilaterally into the nuchal muscle for electromyogram (EMG) recordings. Electrodes connected to a micro-connector (Pinnacle technology) were secured at the surface of the skull with dental acrylic. Mice received buprenorphine (0.08 mg/kg) and saline i.p. and allowed 5 days of recovery. Lightweight recording cables (Pinnacle Technology) were

connected to the head implants and mice were placed in Pinnacle Plexiglas cages containing water and food ad libitum for acclimation for 2-3 days. EEG and EMG signals were amplified and bandpass filtered at 0.5–100 Hz and 10–100 Hz, respectively, using a 15 LT Bipolar Physiodata amplifier system (Grass Technologies) and sampled at 400 Hz with a MP150 data acquisition system (BIOPAC Systems). The system was equipped with infra-red cameras to monitor mice behavior and activity throughout the recording. EEG and EMG waveforms were then analyzed as in Kohtoh *et al.* 2008 using SleepSign for Animal software (Kissei Comtec) with minor changes. Briefly, waveforms were analyzed by 10s epochs (1024 FFT points). Each Epoch was divided in 5 regions that were FFT calculated with a Hanning Window and averaged. Three frequency bands were calculated: δ (0.75-4Hz), θ (4-8Hz) and α (8-12Hz) and the values were used to determine vigilance states using the following algorithm with the indicated order of priority: 1-Clear locomotion or EEG integral > 3-5 μV/sec = active wakefulness; 2- EEG integral < 3-5 μV/sec and EEG δ power > 250-500 μV^2 = Non-REM sleep; 3- EEG integral < 3-5 μV/sec and EEG θ/(δ+ θ) ratio and/or EEG α /(δ+ α) > 45% = Non-REM sleep; 4- otherwise = quiet wakefulness. For experiments in which mice were administered saline or EVP-6124 i.p. (Figure 2.9), their activity was assessed in home cage for the following 4hrs through video monitoring and scored by minute bins as in Figure 2.13 (score 1: wakefulness, locomotor activity or otherwise active behavior; score 0: immobility).

2.3.13 Fear conditioning

All mice used for behavior were exclusively handled by a male investigator (TP) who also performed cage change over the few weeks prior to experiments. Here again,

mice were fully adult (3 to 6 months old) and housed in groups of 2-5. We measured that an average of 2 min elapsed between the time the mouse cage was taken off the rack in the facility to moment animals were all placed in the 4 fear conditioning chambers (i.e., 5min or less until first shock). Mice were naïve, had undergone no previous procedure (except for i.p. injections where applicable, see below) and were sacrificed within 24h after the training session. Mice that were used for fear conditioning were not re-used for electrophysiology or any other type or procedures or experiments. Out of 155 animals used for fear conditioning experiments, only 3 were excluded from the analysis for the following reasons: blindness, escaping the fear enclosure, impaired baseline locomotor and exploratory behavior.

Four conditioning chambers (Coulbourn Instruments, H10-11R-TC) were situated inside a sound-attenuating isolation cabinet (Coulbourn Instruments, H10-24T). They consisted of metal rod floors, two metallic walls, one of which was mounted with a dim ceiling-facing white light bulb, a metallic ceiling, a rear plexiglass panel and a front plexiglass opening. Grid floor was connected to a precision shocker (Coulbourn Instruments H13-15) administering 0.5mA, 2s shocks. The tray, grid floor, ceiling and all four wall panels of the chamber, as well as the inside of the sound-attenuating cabinet were thoroughly wiped with 70% alcohol solution and dried before and after each session. A Panasonic WV-BP334 B/W camera was mounted in the celling of each chamber connected to a PCI-1410 (ACT-610) interface, allowing subsequent automated detection and measurement of freezing responses using FreezeFrame and FreezeView software (Coulbourn Instruments). Freezing was defined as a complete and continuous absence of movement, except for respiratory motion, for at least 1 second.

Training consisted of a single 5min session during which two shocks were delivered (at t = 180 and 240 s). No auditory stimuli were provided. Mice were then immediately placed back in their home cage and returned to the animal facility. Testing was carried out 24h later for all groups, except for acquisition/short-term memory assessment that was performed 1h after training (Figure 2.11E). Testing consisted of a single session of 3 min during which no shocks were delivered. Context B consisted of visual, olfactory, textual, dimensional and lighting differences to context A. It was obtained by using a small plastic enclosure (17 cm wide X 27 cm long X 17 com high) with a distinctive plastic smell, positioned in the center of the original conditioning chamber. Its walls were high enough to mask the rest of the conditioning chamber and covered with a black and white checkered motif. The floor of the enclosure was padded with lab diapers to mask the underlying grid floor. Diapers texture was new to mice and very distinctive from the metallic rods through which the shocks were delivered during training. Brighter lighting was provided. No auditory stimulus was presented in either context. For the ZT23 group, handling of mice was carried out under red light, except for the dim lighting of the contextual chamber. Mice were returned to the animal facility at least 30min prior to light onset.

For D-serine administration experiments, littermates were randomly separated into receiving a different treatment and run simultaneously. Brain extracellular D-serine concentration peaks ~ 1 hour after i.p. D-serine injection and lasted at least 1h[169]. D-serine (200 mg/kg) and vehicle (0.9% saline) were therefore injected i.p. into wild-type littermates 1h prior to conducting behavior training. This dose of D-serine was efficient at increasing extracellular brain D-serine, as shown by micro-dialysis measurements (Figure

2.5B). The 1h delay between injection and training also prevented cueing the training with the unpleasant injection procedure.

2.3.14 Adeno-associated viruses and stereotaxic surgeries

Two to three month old mice from the α7nAChR^{floxed} line were anesthetized by isoflurane inhalation. Buprenorphine HCl (0.1 mg/kg) was administered subcutaneously as a pre-emptive analgesic. Once under deep anesthesia, mice were immobilized in a Kopf stereotaxic apparatus using intra-aural positioning studs to stabilize the skull and a hole was drilled on the surface of the skull at the appropriate coordinates. Using a 30G needle and Neuros syringe (Hamilton Co.), 2 µL of AAV5-GFAP(0.7)-eGFP-T2A-iCre (2.6×10^{10} genome copies, Vector Biolabs Inc #VB1131) were injected into area CA1 with the following coordinates (anterior, lateral, depth [mm] relative to Bregma): (-2.0, +1.5, -1.5) or 1µL of AAV9-eSYN-eGFP-T2A-iCre (7.8×10^9 genome copies, Vector Biosystems Inc #VB1089) into the CA1 and CA3 areas: (-2.0, +1.5, -1.5) and (-2.0, +2.6, -2.2) respectively. Injection rates of 100 nL/min were controlled by a micro syringe pump controller (World Precision Instrument Micro4). After injection, the incision site was sutured with 6-0 nylon sutures (Unify, #XS-N618R11). Animals were postoperatively monitored until recovered.

Recordings were obtained from slices of AAV5-GFAP(0.7)-eGFP-T2A-iCre or AAV9-eSYN-eGFP-T2A-iCre injected a7nAChR$^{flox/flox}$ animals or α7nAChR$^{+/+}$ littermates at three different ZT times (see main text). eGFP fluorescence in slices was visualized under 460 nm light, and recording and stimulating electrodes were placed accordingly in regions of interest (ROI) of the CA1 *s. radiatum* with the best levels of fluorescence. Immediately after recordings, slices were briefly mounted on a slide and the

location, spread and penetrance (% fluorescent cells) of the infection was inspected by appreciating the eGFP fluorescence under an epifluorescence microscope. For the AAV9-injected animals, the infection was considered successful when eGFP fluorescence was observed both in CA3 and CA1 pyramidal neurons, including cell bodies, dendrites and Schaffer collaterals. Transduction failures in either of these regions typically resulted in the cell bodies not being fluorescent (despite strong fluorescence in surrounding layers due to projections from transduced regions). Results from slices showing no or low infection in either CA3 or CA1 were discarded from the final analysis. For either virus serotype, results from slices showing no transduction at all were pooled and considered as "sham" (ie, surgery/injection controls) in Figure 2.13L.

2.3.15 Immunohistochemistry, fluorescence imaging and cell counting

Mice were anesthetized with isoflurane then transcardially perfused with PBS followed by 4% paraformaldehyde (PFA). Brains were extracted, post-fixed and cryoprotected by immersion in 30% (w/v) sucrose in PBS at 4°C. Brains were sectioned (50 μm thick) using a sliding microtome (Leica SM2000R). Sections were washed with PBS containing 0.3% Triton X-100 (PBS-Tx), and non-specific labeling was blocked using 5% bovine serum albumin (BSA). Sections were incubated with primary antibodies diluted in 1% BSA/0.3% Tx in PBS overnight at 4°C on an orbital shaker. The following primary antibodies were used: anti-GFP (1:1000, Invitrogen, A11122), anti-ChAT (1:200, Millipore, AB144P), anti-NeuN (1:1000, Millipore, ABN78), and anti-GFAP (1:1000, AbCam, ab4674). The following day, sections were washed three times in PBS-Tx then incubated with the appropriate AlexaFluor 488, 594, 633 secondary antibody (1:1000, Life Technologies) for 2 hours at room temperature on an orbital shaker. After

the incubation, sections were rinsed with PBS-Tx three times then mounted on Superfrost Plus slides (VWR) and coverslipped with Vectashield HardSet Mounting Medium with DAPI (Vector Laboratories). Whole section imaging was performed using the 10x lens of a Keyence BZ-X710 fluorescence microscope. Confocal stacks were taken using a Nikon A1R confocal microscope equipped with a 20x (N.A. 0.75) and 40x oil-immersion lens (NA 1.0). Images were acquired with a resolution of 1024 x 1024 pixels. Images were adjusted for brightness and contrast in Fiji (Schindelin et al, 2012). Anti-GFP and anti-ChAT immunostaining in Figure 2.11 was performed as in Zhao et al, 2011. Sections from dnSNARE mice were immunostained with anti-GFAP and anti-NeuN.

Cell counting in Figure 2.13 and Figure 2.8 was performed independently by two investigators (TP and JD) on at least 12 high-resolution z-stacks (3 animals, 2 sections per animal, 2 stacks per section) spanning the 50 µm range of tissue at 1-2 µm increments. The Cell Counter plug-in in Fiji (Schindelin et al, 2012) was used to colocalize each cell's nucleus (DAPI staining) with a cell-specific marker (GFAP or NeuN) and the reporter (GFP) by scanning through the z-planes manually. In results shown in Figure 2.13B-D and 7I-K, both the AAV5 virus and the AAV9 virus were remarkably selective for astrocytes and neurons respectively. For the AAV5 virus, we found that 100% (investigator 1, JD) and 99.8% (investigator 2, TJP) of eGFP expressing cells (1271 and 1174 eGFP+ cells counted respectively; 90-100 cells per stack) were GFAP+ (i.e. astrocytes). On average 80.0 ± 2.0% (JD) and 80.4 ± 3.0% (TJP) of all astrocytes (GFAP+) in the ROI (total astrocytes JD: 1592, TJP: 1467) were eGFP+ (expressing iCre). In sections from AAV9 injected mice, we found that virtually all eGFP+ cells in area CA1 and 98 to 99% of eGFP+ cells in CA3 were NeuN+ (i.e.

neurons) and that ~75% of all neurons (JD: 73.4 ± 5%; TJP: 78.8 ±%6%) in the ROI expressed iCre recombinase (eGFP+).

2.3.16 Quantification and statistical analysis

When applicable (field recordings, D-serine biosensor measurements in conditioned medium, in vivo micro-dialysis and HPLC, fear conditioning, adeno-associated viruses and stereotaxic surgeries), exclusion criteria are explained in the corresponding method section above. Briefly, no electrophysiology experiments were excluded unless major rundown, run-up or noise prevented accurate analysis. Two C.M. measurements were excluded from the analysis because they fell under the biosensors detection limit. Only 3 out of 155 animals were excluded in the fear conditioning experiments due to blindness, lack of locomotor activity or escaping the enclosure. Finally, viral infections and micro-dialysis probes were excluded in case of lack of infection and/or mistargetting. In all electrophysiology experiments, n indicates the number of independent slices analyzed. In behavior experiments, n indicates the number of independent animals. For in vivo micro-dialysis/HPLC experiments, n indicates the number of animals from which one dialysate was obtained. For fluorescence imagine, n is the number of individual cells counted. This information is explicitly reported in all figures either as a number in the bar graph or as individual data points. An analysis of variance was preformed with a Shapiro-Wilk normality test to verify normality of data distribution whenever applicable and determine the appropriate subsequent statistical analysis. Statistical tests used in this study are paired or unpaired Student's *t* tests, Pearson tests, an agreement test, a Wilcoxon Matched-pairs signed rank test, and one-way or repeated measures ANOVAs followed, whenever appropriate, by Bonferroni post

hoc tests. Statistical tests used are reported in figure legends and/or in the text along with the n-value, the test-value (F(df1, df2), *t*(df) etc…) and the exact p-value. P-value of 0.05 was used as the significance threshold throughout this study. When statistical results are reported for a group of comparisons using the same test, the test-value is omitted and the closest p-value is reported. In figures, p-values are illustrated as follow, for all tests used: $p > 0.05$: n.s.; $p < 0.05$: *; $p < 0.01$, **; $p < 0.001$: ***.

2.4 Results

2.4.1 D-serine availability oscillates over the 24h period

To determine whether there are daily fluctuations in D-serine levels, we first performed extracellular recordings of synaptic NMDAR-mediated field excitatory post-synaptic potentials (NMDA-fEPSPs) in the *stratum radiatum* of acute hippocampal slices (Figure 2.2A-C and Star Methods). Slices were obtained at different Zeitgeber times (ZT; ZT0 being the onset of light) across the 24h period, and the endogenous occupancy of the NMDAR co-agonist-binding site was determined by adding a saturating concentration of exogenous D-serine (50 µM; Figure 2.2A-D). We found that the effect of D-serine application was highly dependent on the time-of-day at which slices were obtained (Figure 2.1A, $F(6,50) = 9.889$, $P < 10^{-6}$, one-way ANOVA and Figure 2.2E-G). Exogenous D-serine failed to potentiate NMDA-fEPSPs at ZT0 (Figure 2.1A&B, $t(9) = 0.87$, $P = 0.407$, paired Student's *t* test), indicating that the NMDAR co-agonist site was already fully saturated, but produced significant ($P < 0.01$, paired Student's *t* tests) and increasing effects in slices obtained from ZT1 through ZT13 (Figure 2.1A and Figure 2.2G, ZT1: 17 ± 2.4%; ZT2: 20.9 ± 3.3%; ZT6: 25.7 ± 3.6%; ZT13: 28.7 ± 5.8%). In the dark (active)-phase, the occupancy of NMDARs progressively increased as revealed by

weakening effects of D-serine application from ZT13 to ZT23 (Figure 2.1A&B, P = 0.001, Bonferroni post-*hoc* test and Figure 2.2A-G). Importantly, these fluctuations were not due to changes in the co-agonist site's affinity for D-serine since the subunit composition of NMDARs, assessed with the GluN2A- and GluN2B-NMDAR specific antagonists Zinc (250 nM) and Ro25-6981 (2 µM) respectively, did not change over the 24h period (Figure 2.1C, $F(2,18) = 0.298$ and $F(2,22) = 0.649$, $P > 0.05$, one-way ANOVAs). Together, these data suggest that the amount of endogenous co-agonist available to NMDARs fluctuates across the 24h period.

Since D-serine is the endogenous co-agonist of NMDARs at CA3-CA1 synapses[93], we directly assessed extracellular D-serine levels (Figure 2.1D-E and Star Methods). Hippocampal slices obtained at ZT0 and ZT6 were incubated in aCSF for 90 min and D-serine concentration in this conditioned medium (CM) was then measured using amperometric biosensors[170]. D-serine amounts, both absolute (-32%) and normalized to the protein content of incubated tissue (-27%), were significantly lower in the CM obtained from ZT6 slices (Figure 2.1F&G, $P < 0.05$ Student's *t* tests) supporting the existence of daily fluctuations of free extracellular D-serine levels in hippocampal slices. We concluded that the oscillations in the occupancy of NMDARs co-agonist site are caused by oscillations in the endogenous concentration of D-serine. Therefore, the "saturation index" is used thereafter as a proxy for the amount of D-serine available to synaptic NMDARs (ZT6: 0.800 ± 0.020; ZT0: 0.985 ± 0.018, $t(18) = 6.84$, $P < 0.0001$, Student's *t* test, Figure 2.1H). It is directly calculated from the increase in NMDA-fEPSP slope caused by exogenous D-serine (Figure 2.2B&C and Star Methods) and represents

the baseline occupancy of NMDAR co-agonist site: the higher the concentrations of endogenous D-serine, the higher the saturation index.

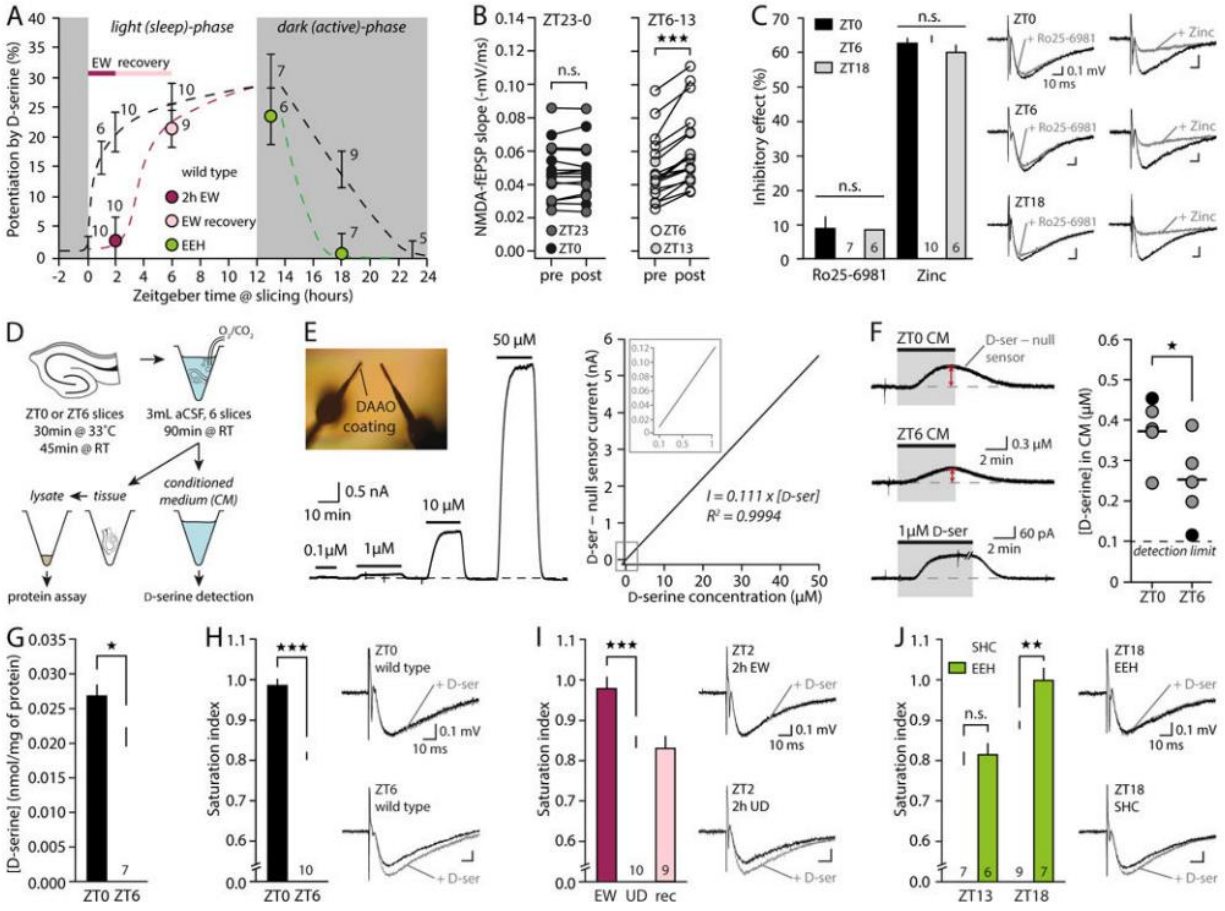

Figure 2.1: Daily oscillations of D-serine availability are driven by wakefulness. **A**, Effect of D-serine application on NMDA-fEPSPs in slices obtained at different Zeitgeber times (ZT) from wild-type mice, mice subjected to enforced-wakefulness (EW), EW mice after 4h of recovery, and mice in enriched environment housing (EEH). Dotted lines are provided as visual guides. **B**, Individual slopes of NMDA-fEPSPs before (pre) and after (post) D-serine application, at indicated ZTs. **C**, Inhibitory effect of the GluN2B-NMDAR antagonist Ro25-6981 (2 µM) and GluN2A-NMDAR antagonist Zinc (250 nM) at ZT0, ZT6 and ZT18 and illustrative traces. **D**, Schematic showing the collection of conditioned medium (CM). **E**, Calibration of the D-serine biosensors showing their linearity, including for sub-micromolar D-serine (right inset). **F**, D-serine measurements in ZT0 and ZT6 CM. Each circle indicates the value obtained from one animal. Color-code shows "pairs" of ZT0 and ZT6 CMs run on the same set of biosensors. Horizontal bars represent average. **G**, Average D-serine concentration in CM normalized to the weight of tissue incubated (mg of protein). **H-J**, Saturation index of NMDARs at ZT0 and ZT6 (**H**); at ZT2 in slices from EW mice, undisturbed (UD) mice, or EW mice after 4h of recovery (rec) (**I**); and at ZT13 and ZT18 in slices from mice housed in EEH or in

standard home cages (SHC) (**J**). Pooled data are shown as mean ± SEM. See also Figure 2.2 and 2.3.

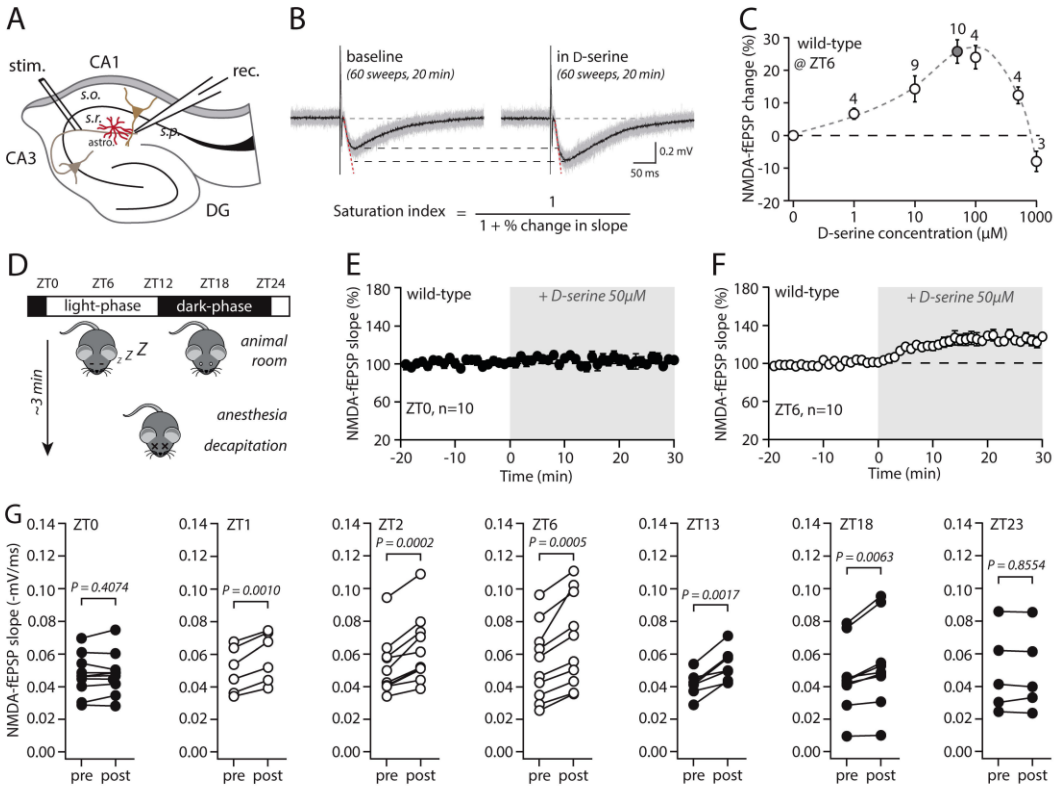

Figure 2.2: D-serine availability fluctuates across the 24h period
A, Schematic illustrating the electrophysiological recording setup used in Figure 2.1. Collateral axons from CA3 neurons (Schaffer collaterals) were stimulated at 0.05 Hz with a tungsten electrode (stim.) placed in the *s. radiatum* (s.r.) at the junction between area CA3 and CA1. Field responses from CA3-CA1 synapses were recorded in the CA1 area with a glass electrode (rec.) placed in the *s. radiatum* about 150 µm from the stimulation site. Astrocytes (astro.) have been shown to play an active part in synaptic transmission at CA3-CA1 synapses through the release of various types of gliotransmitters (see main text). In particular, abundant literature has shown that the NMDAR co-agonist, D-serine, is released by astrocytes at CA3-CA1 synapses. **B**, The slope of NMDA-fEPSPs (dotted red line), in baseline condition or after addition of exogenous D-serine, was measured from average trace (black) representing 20 min of stable recording (60 consecutive sweeps, gray background traces). The percentage of increase caused by exogenous D-serine application was then used to calculate the saturation index of NMDARs under baseline condition via a simple equation. The only assumptions tied to this equation are that 1) the increase of NMDA-fEPSPs by exogenous D-serine reflects a submaximal baseline occupancy of the co-agonist binding site of synaptic NMDARs that participate to the field response, 2) the amount of exogenous D-serine applied is sufficient to cause a maximal occupancy of the co-agonist binding site of NMDARs at CA3-CA1 synapses (GluN2A-NMDARs *K*d < 1µM for D-serine and see panel C), and 3) the affinity of NMDARs for D-serine is unchanged (see main text and Figure 1C). **C**, Dose-response

curve showing the percentage of potentiation of NMDA-fEPSP slope for increasing concentrations of exogenous D-serine. Note that the maximal potentiation is obtained for D-serine concentrations of 50 μM and 100 μM. However, for concentrations higher than 100 μM, D-serine application induced a well-documented internalization of NMDARs that prevented potentiation or caused a decrease of NMDA-fEPSP. This prompted us to use applications of 50 μM of D-serine to assess NMDAR saturation, rather than 100 μM. **D**, Mice were taken at different times of 24h period and were transported from the animal facility to the electrophysiology area in their home-cage. Typically no more than 3min elapsed between the moment mice were fetched in the animal facility and their decapitation. **E-F**, Average time course effect of the effect if exogenous D-serine application on NMDA-fEPSP in slices obtained from wild type mice at ZT0 (**E**) and ZT6 (**F**). D-serine application caused an average 25% increase of the slope of NMDA-fEPSPs at ZT6, plateauing 10-15min after the onset of application (**F**). In contrast, D-serine failed to increase NMDA-fEPSP in slices taken at ZT0 (**E**). **G**, Individual raw data showing the slope of NMDA-fEPSPs for each experiment before (pre) and after (post) D-serine application at indicated ZTs. Paired Student's *t* tests were used. Pooled data is shown as mean ± SEM.

2.4.2 D-serine fluctuations are driven by wakefulness, not circadian rhythms

D-serine is present at saturating levels at the end of the dark (active)-phase, rapidly declines to non-saturating levels in the light (sleep)-phase and progressively builds-up again through the dark-phase (Figure 2.1), seemingly following daily levels of wakefulness (Figure 2.3). To understand whether D-serine oscillations are governed by wakefulness and activity or by an intrinsic 24-hour circadian rhythm, mice were subjected to enforced-wakefulness (EW) between ZT0 and ZT2 before hippocampal slices were obtained (Star Methods and Figure 2.3A&B). This should be without effect on D-serine supply if it is determined by the time-of-day through a circadian mechanism. However, EW should prevent the rapid decline of D-serine at the onset of the light-phase if D-serine supply is driven by wakefulness. We found that after 2h of EW, the saturation index was significantly greater than that measured at ZT2 from undisturbed mice (Figure 2.1A&I, $t(18) = 3.97$, $P = 0.0009$, Student's *t* test). This effect was only transient and the saturation index returned to control levels after 4 hours of rest following EW (Figure

2.1A&I). Since prolonging wakefulness through the light-phase can maintain saturating levels of D-serine, we asked whether favoring active exploratory behavior with enriched environment housing (EEH) could accelerate D-serine accumulation during the dark-phase (Star Methods, Figure 2.3A&C). We found that EEH increased wakefulness in the dark-phase, especially during the first 6 hours (Figure 2.3A&C) and that the saturation index measured in ZT18 slices was enhanced in mice kept in EEH (Figure 2.1A&J, $t(14) = -3.2$, $P = 0.0064$, Student's *t* test), indicating that increased activity accelerated the buildup of D-serine. Together these results demonstrate that oscillations in D-serine availability at CA3-CA1 synapses are not driven by circadian rhythms but instead follow a mechanism wherein wakefulness and activity promote the accumulation of D-serine while rest/sleep favors its clearance.

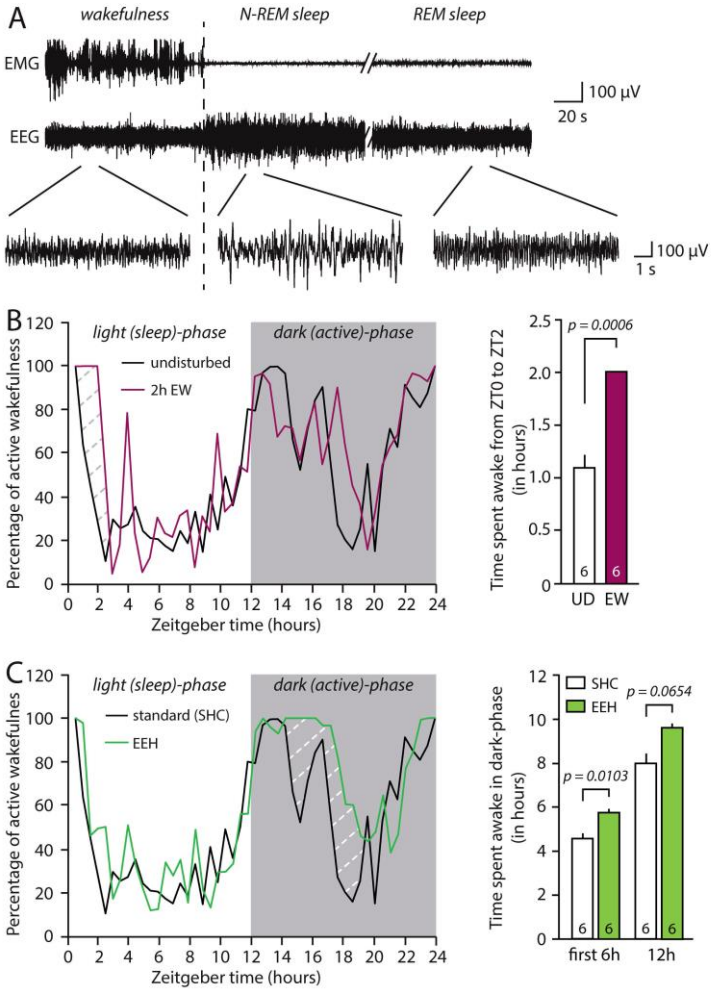

Figure 2.3: EEG/EMG monitoring of wakefulness throughout the 24h-period
A, Waveforms illustrating the three main vigilance states used for scoring: wakefulness, Non-REM and REM sleep. **B,** *Left:* Stage graph showing the average percentage of active wakefulness (measured with EEG/EMG) by 30min epochs through the 24h period, in undisturbed mice (UD) and mice subjected to 2 hours of enforced-wakefulness (EW) from ZT0 to ZT2. *Right:* Bar graph depicting the amount of time spend awake (in hours) from ZT0 to ZT2 by UD mice and mice kept awake from ZT0 to ZT2 (EW). **C,** *Left:* Same as H for mice kept in a standard environment (SHC) or in enriched environment housing (EEH). *Right:* Bar graph depicting the amount of time spend awake (in hours) for the first 6 hours of the dark phase (ZT12 to ZT18) and for the total duration of the dark phase (from ZT12 to ZT24) by mice kept in a SHC and in EEH. EEH increased wakefulness in the dark-phase, especially during the first 6 hours (SHC: 4.6 ± 0.2 h spent awake, EEH: 5.8 ± 0.2 h spent awake, $t(9) = -4.61$, $P = 0.0103$, Student's *t* test).

2.4.3 D-serine levels fluctuate with wakefulness in vivo

To validate these findings in a more physiological setting, we collected samples via in vivo micro-dialysis from area CA1 of the hippocampus of freely behaving mice from ZT0 to ZT6, while video-monitoring their activity during the entire 6 hours of micro-dialysis (Figure 2.4A&B and Star Methods). The absolute D-serine and L-serine concentration in the dialysate was then determined through high performance liquid chromatography (HPLC) on a C18-column using concentration standards (Figure 2.4C and Star Methods). The average concentration of D-serine (1.8 ± 0.3 μM) and L-serine (13.3 ± 1.2 μM) measured across mice was very similar to that found in the literature (Figure 2.4D,[169]). However, we also observed that the concentration of D-serine measured in the dialysates was significantly correlated to the percentage of time mice spent active during the 6 hours of micro-dialysis (P=0.0018, one-tailed Pearson correlation test, Figure 2.4E). The lowest D-serine concentrations were found in the dialysate of mice that spent 70-80% of the time nested and immobile, while the highest amounts were measured in mice with levels of activity greater than 60%. This correlation was specific for D-serine since L-serine levels were not correlated to activity (P = 0.3823, Figure 2.4F), and a correspondence test independently validated that actograms obtained from video-monitoring are a faithful proxy of wakefulness measured by EEG/EMG recordings (Figure 2.4G; 95.2% agreement, kappa-value = 0.876 and see Figure 2.5A). Together, these experiments indicate that D-serine levels measured in vivo with micro-dialysis reflect the overall wake/sleep history of the mouse during the dialysate collection. This conclusively demonstrates that D-serine concentration fluctuates with wakefulness in the mouse hippocampus, varying more than 5-fold between rest (~0.5

µM) and wakefulness (3 µM), thus nearly spanning the entire range of NMDAR co-agonist site sensitivity[167].

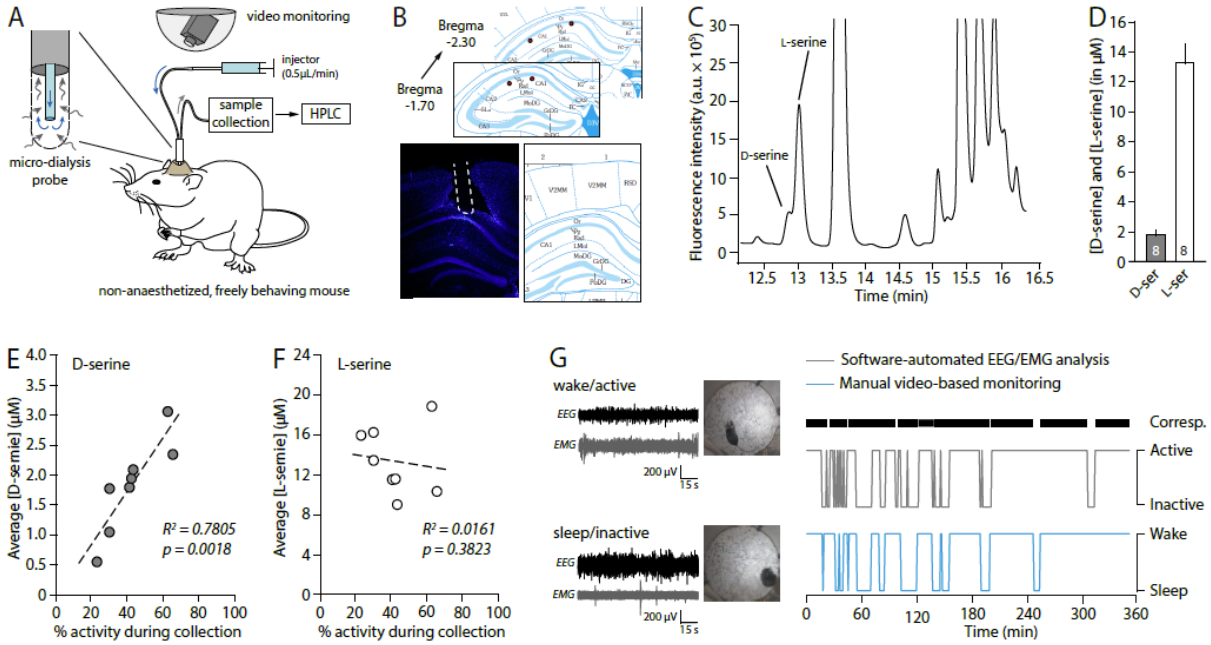

Figure 2.4: Wakefulness-dependent fluctuations of D-serine concentration in vivo. **A**, Experimental set-up for in vivo micro-dialysis and video-monitoring from ZT0 to ZT6. **B**, Histological targeting of micro-dialysis probes on the Allen Brain Atlas (top) determined on DAPI-stained hippocampal section (bottom). **C**, HPLC chromatogram showing L-serine and D-serine peaks. **D**, Average D-serine and L-serine concentrations in 8 different mice. **E**, Individual D-serine concentrations in dialysates as a function of the average percentage of time the mouse spent active during micro-dialysis. **F**, Same as E for L-serine. **G,** *Left*: Video snapshots and EEG/EMG traces representing the active/resting state and the wake/sleep state. *Right*: Actograms (6 hours) of the same mouse obtained using video-based or EEG/EMG scoring of activity/wakefulness. The black horizontal bar indicates the sections of correspondence (corresp.) between the two scoring systems. See also Figure 2.5.

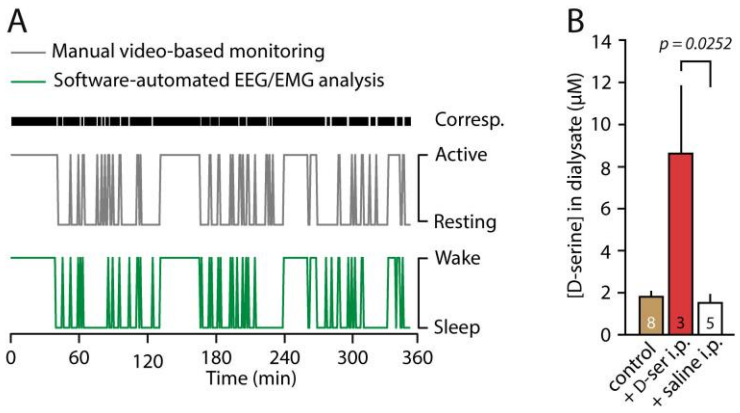

Figure 2.5: EEG/EMG versus video monitoring and D-serine dosing
A, Additional 6 hours long actograms obtained using manual video-based or EEG/EMG based scoring of activity/wakefulness (see methods). The black horizontal bar indicates the sections of correspondence (corresp.) between the two scoring systems (90.8% agreement, kappa-value = 0.812). **B**, D-serine concentration measured in dialysate collected during 4 hours of *in vivo* micro-dialysis following i.p. administration of D-serine (200mg/kg) or saline (as in Figure 3 experiments). The levels of D-serine detected in the dialysate are 400% higher following i.p. Dserine administration (8.6 ± 3.2 μM) when compared to saline injections (1.5 ± 0.4 μM). Also note that saline injections do not improve D-serine levels compared to control.

2.4.4 Daily D-serine fluctuations impact learning and memory

In order to evaluate the significance of such endogenous D-serine oscillations to behavior, we probed an NMDAR-dependent learning and memory assay. We examined contextual fear memory, a task that relies on hippocampal NMDARs[171, 172] and in which mice learn to associate foot shocks with the context where they are delivered. Mice were trained at different ZTs, re-exposed to the context 24h later and the amount of time they spent freezing was measured (Figure 2.6A). Mice trained at ZT0 and tested 24 later had greater levels of freezing (+62%) compared to mice trained at ZT6 and tested 24h later (P = 0.0017, Bonferroni post-*hoc* test, Figure 2.6B&C), revealing a more efficient formation of hippocampal memory at ZT0 consistent with higher levels of D-serine (Figure 2.1G&H). The immediate response to shocks (Figure 2.6B) was similar in all groups, indicating that there were no differences in sensitivity/aversion to the electrical stimuli

during training. As expected for this task, the difference between the ZT0 and ZT6 groups was also context-dependent: mice tested in a different context (Context B, Star Methods) had low and identical levels of freezing (Figure 2.6D, $t(22) = 1.07$, P = 0.2962, Student's *t* test).

Mice are less active during the light-phase, which could diminish their capability to explore and encode the environment and its aversive nature at ZT6. To test if the reduced memory at ZT6 was attributable to weaker acquisition, mice were trained at ZT0 or ZT6 and tested 1h later in the original context. Both groups showed strong freezing levels and performed identically (Figure 2.6E, $t(25) = 0.14$, P = 0.8897), indicating that mice can acquire and retrieve short-term contextual memory equally, regardless of the ZT at training.

ZT6-trained mice had 6 hours of light-phase remaining after training whereas ZT0-trained mice had almost 12 hours (Figure 2.6A). Because memory consolidation occurs during episodes of sleep after training[173], we considered this confounding factor by assessing the performance of mice trained at ZT1 (when D-serine is low in slices, similar to ZT6, Figure 2.1) and tested 24h later (~11 hours of light-phase remaining after training, like at ZT0). This group showed reduced levels of freezing that were identical to the ZT6 group (Figure 2.6B&C, P = 0.846, Bonferroni post-*hoc* test), indicating that enhanced memory in the ZT0 group was not the result of a greater time spent in light-phase after training. Finally, to explore the possibility that mice performed better at ZT0 because they cued the task with light onset, a group of mice was trained and tested in the dark-phase (ZT23, a time when D-serine levels are high in slices similar to ZT0, Figure 2.1). Handling of mice was carried out under red light, except for the dim lighting of the

contextual chamber. Levels of freezing in this group were similar to the ZT0 group and greater than the ZT6 group (Figure 2.6B&C, P = 0.0410, Bonferroni post-*hoc* test), ruling out the possibility that ZT0-trained mice used light onset as a learning strategy.

Overall, the magnitude of contextual fear memory oscillates from ZT0 to ZT23 (Figure 2.6C, F(3,47) = 4.26, P = 0.0088, one-way ANOVA) and recapitulates both the saturation level of NMDARs in slices and the finding that in vivo D-serine levels depend on overall wakefulness. This suggested that daily oscillations of hippocampal D-serine contribute to this behavioral effect. If true, increasing brain D-serine with i.p. administration (200 mg/kg i.p, Figure 2.5B,[169]) should improve fear memory at ZT6 but not at ZT0, since D-serine is naturally saturating at ZT0 but not at ZT6. In agreement with this assumption, D-serine treatment (200mg/kg i.p. 1h prior to training, Figure 2.6A) significantly increased the percentage of freezing in the ZT6-group compared to saline ($t(26) = -2.16$, P = 0.0402), whereas it failed to improve freezing levels at ZT0 (Figure 2.6F&G, $t(24) = 0.41$, P = 0.685). That D-serine-treated mice performed identically to saline-treated littermates at ZT0 also indicates that D-serine did not enhance overall motor or cognitive skills. Together, these results indicate that the oscillations in D-serine levels occur over a range of concentrations that is relevant to behavior, such as learning and memory**.**

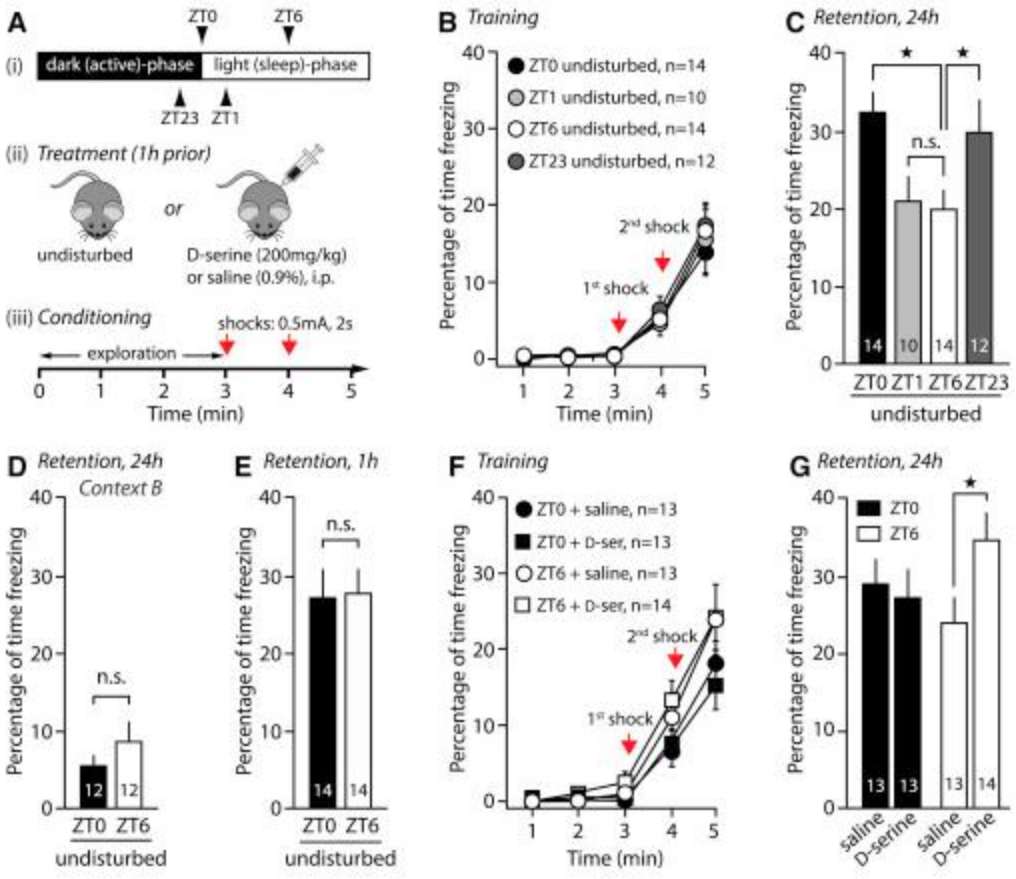

Figure 2.6: Oscillations in NMDAR occupancy impact learning and memory. **A**, Schematic of the timing, injection and training paradigm for contextual fear conditioning. **B**, Immediate freezing responses of undisturbed mice during training at different ZTs. **C**, Freezing response 24h later for mice trained in (B). **D**, Freezing response in a different context, 24h after training at ZT0 and ZT6. **E**, Freezing response of mice 1h after training at ZT0 and ZT6. **F**, Immediate freezing responses of mice during training at ZT0 and ZT6, 1h after i.p. injections of saline or D-serine. **G**, Freezing responses, 24h later, for mice trained in (F). All panels show mean ± SEM. See also Figure 2.5.

2.4.5 Astrocytes are the source of activity-dependent D-serine supply

D-serine is considered a gliotransmitter but it can also be found in neurons[174]. Therefore, we examined the contribution of astrocytes to daily oscillations of D-serine availability by assessing NMDAR saturation index in slices obtained from astrocyte-specific dnSNARE mice (Figure 2.7A). In these mice, the tetO-dnSNARE:GFAP-tTA

transgenic construct drives the expression of the cytoplasmic domain of the vesicular protein VAMP2 selectively in astrocytes (astrocyte-specific GFAP promoter), following removal of doxycycline (Dox) from the diet (Star Methods). This impairs the formation of the SNARE complex in astrocytes by a dominant-negative effect, reducing by 91% the exocytotic release of gliotransmitters, including D-serine[94, 116]. It should be noted that, in agreement with the vast majority of the astroglial literature that used dnSNARE mice, a systematic examination performed by two independent investigators in both area CA1 and CA3 failed to identify a single eGFP-expressing neuron among 5,884 and 5,887 neurons counted in 24 stacks from 5 different animals (Figure 2.8A-D). This careful assessment is in striking contrast to and refutes the claims from Fujita et al., 2014, and confirms the cell-specificity of transgenes expression in dnSNARE mice (Figure 2.7A&B). In slices from dnSNARE mice off Dox, we found that the effect of exogenous D-serine on NMDA-fEPSPs was independent of the time of day (Figure 2.7C, $F(2,28) = 0.085$, $P = 0.918$, one-way ANOVA), in contrast with slices from single gene controls (GFAP-tTA negative) in which the same oscillations found in WT mice were observed ($F(2,15) = 8.666$, $P = 0.0032$). In slices obtained at ZT0 from dnSNARE mice off Dox, D-serine significantly augmented NMDA-fEPSPs (Figure 2.7D, $t(9) = 4.39$, $P = 0.0017$, paired Student's *t* test and see Figure 2.8E&F) and the resulting saturation index was identical to that found at ZT6 (Figure 2.7E, $t(18) = 0.44$, $P = 0.665$, Student's *t* test). Consistently, NMDAR subunit composition was the same in ZT0 and ZT6 slices (Figure 2.7H, $P > 0.05$, one-way ANOVAs) and amperometric measurements revealed similar levels of D-serine in ZT0 and ZT6 slices from dnSNARE mice off Dox (Figure 2.7F&G, $P > 0.05$, Student's *t* tests). Importantly, reintroducing Dox into the diet for a month to

suppress transgene expression ("dnSNARE on Dox", Star Methods) was sufficient to restore daily oscillations of D-serine (Figure 2.7C, $F(2,24) = 8.042$, $P = 0.0024$, one-way ANOVA) and the differential saturation at ZT0 and ZT6 (Figure 2.7E, $t(14) = 3.52$, $P = 0.0034$, Student's *t* test). Together, these data demonstrate that D-serine oscillations rely on astrocytic SNARE-dependent supply of D-serine during the dark-phase.

D-serine and its synthesizing enzyme serine racemase are also present in neurons[174, 175], suggesting a potential contribution of neurons to D-serine supply. This has prompted the proposal of an "L-serine/D-serine shuttle" wherein 1) astrocytes provide L-serine to neurons, 2) D-serine is synthesized in neurons from L-serine and 3) neurons release D-serine[175]. According to this view, an alternative interpretation of our results would be that neuronal D-serine release is impaired in dnSNARE mice due to the lack of L-serine supply from astrocytes. However, providing exogenous L-serine (20 µM, 45min) did not restore the saturation index in dnSNARE slices at ZT0 (Figure 2.8G&H), indicating that the expression of the dnSNARE transgene directly prevented the release of D-serine, not L-serine, by astrocytes.

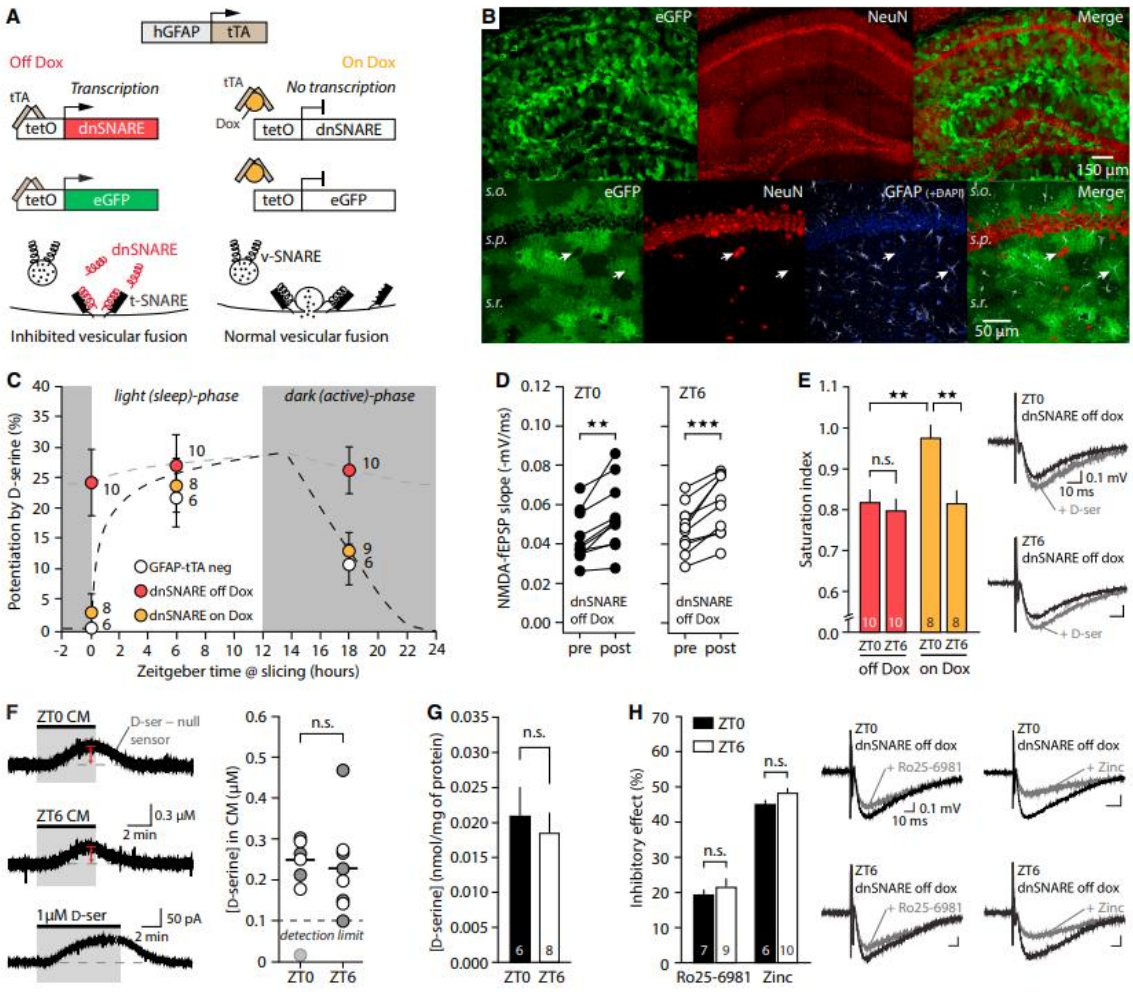

Figure 2.7: Inhibition of SNARE-mediated vesicular release in astrocytes abolishes D-serine oscillations. **A**, Schematic of conditional astrocyte-specific expression of dnSNARE and eGFP transgenes in dnSNARE mice. Animals are raised on Dox until weaning. **B**, *Upper panels*: Composite confocal images showing the mosaic expression of the eGFP reporter in hippocampal astrocytes of a dnSNARE mouse kept off Dox for 8 weeks after weaning (stitch of 20 images 20x, NA: 0.75). *Lower panels*: confocal (40x) images of DAPI nuclear staining, eGFP fluorescence, and NeuN (neuronal) and GFAP (astrocytic) immunoreactivity (*so*, *stratum oriens*; *sp*, *stratum pyramidale*; *sr*, *stratum radiatum).* Arrows show an eGFP-negative neuron and an eGFP-positive astrocyte. **C**, Effect of D-serine application on NMDA-fEPSPs in slices obtained from GFAP-tTA-negative animals (single gene control) and dnSNARE mice off or on Dox, at different ZTs. Dotted lines serve as visual guides. **D**, Individual slopes of NMDA-fEPSPs before (pre) and after (post) D-serine application at ZT0 and ZT6 in slices from dnSNARE mice off Dox. **E**, Saturation index at ZT0 and ZT6 in slices from dnSNARE mice off or on Dox. **F**, D-serine measurements in ZT0 and ZT6 CM from dnSNARE mice off Dox. **G**, Average D-serine concentration in CM normalized to the weight of tissue incubated (mg of protein). **H**, Effect of the GluN2B-NMDAR antagonist Ro25-6981 and the GluN2A-

NMDAR antagonist zinc on NMDA-fEPSPs in ZT0 and ZT6 slices from dnSNARE mice off Dox. Pooled data are shown as mean ± SEM. See also Figure 2.8.

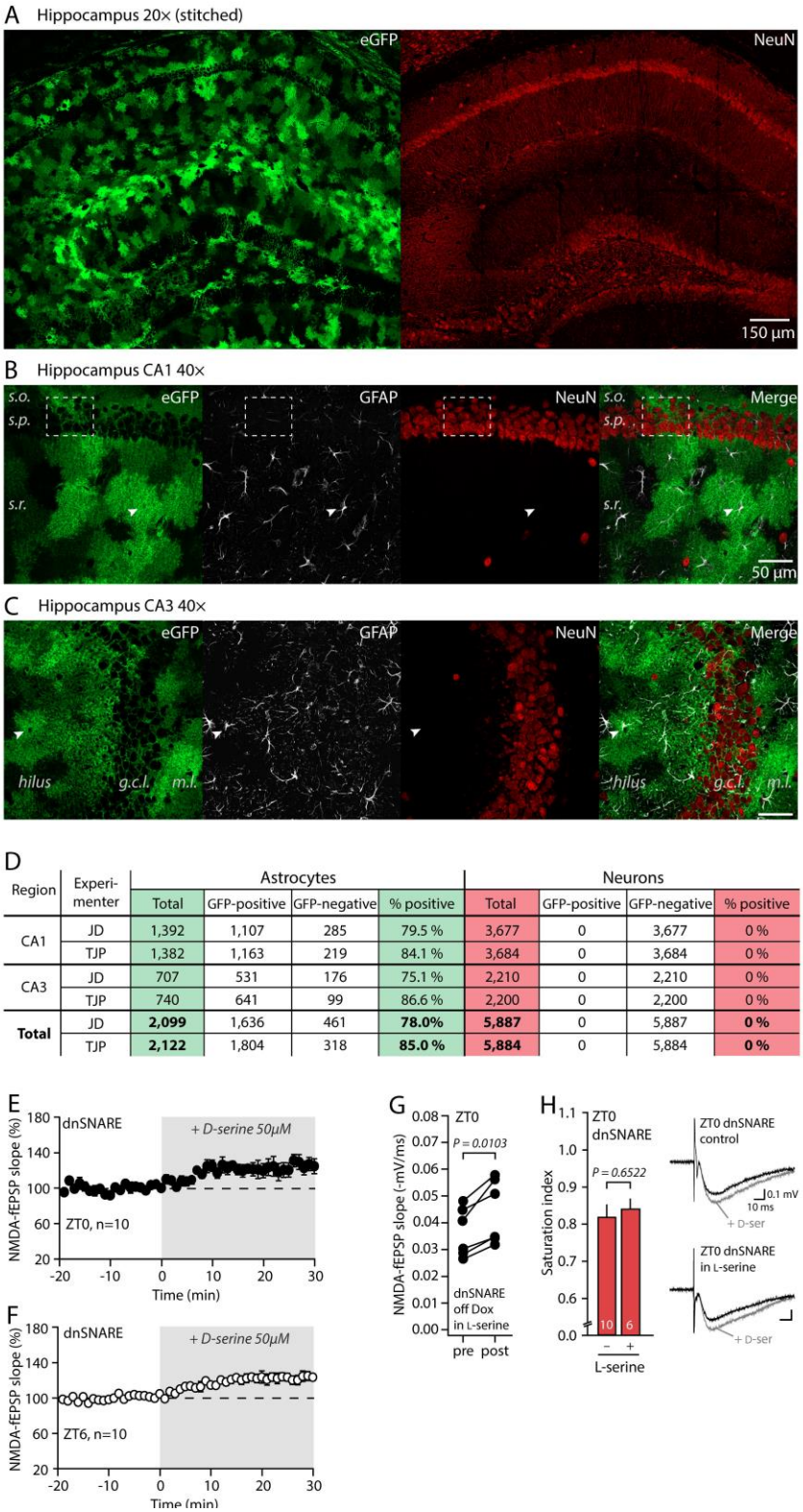

D

Region	Experimenter	Astrocytes				Neurons			
		Total	GFP-positive	GFP-negative	% positive	Total	GFP-positive	GFP-negative	% positive
CA1	JD	1,392	1,107	285	79.5 %	3,677	0	3,677	0 %
	TJP	1,382	1,163	219	84.1 %	3,684	0	3,684	0 %
CA3	JD	707	531	176	75.1 %	2,210	0	2,210	0 %
	TJP	740	641	99	86.6 %	2,200	0	2,200	0 %
Total	JD	**2,099**	1,636	461	**78.0%**	**5,887**	0	5,887	**0 %**
	TJP	**2,122**	1,804	318	**85.0 %**	**5,884**	0	5,884	**0 %**

Figure 2.8: Astrocyte-specificity of dnSNARE transgenes expression
A, Mosaic expression of the eGFP reporter (left) in hippocampal astrocytes typically seen in astrocyte-specific dnSNARE mice (generated by Pascual et al., 2005 and most recently used and further characterized by Sultan et al., 2015), and NeuN immunostaining of neurons (right) for comparison. The 20x confocal images (NA: 0.75, no gamma function used) were obtained from a dnSNARE male kept off Dox for 8 weeks after weaning, and stitched (20 in total). Note the very distinctive absence of transgene expression in the pyramidal layer on the left image, typical of the dnSNARE line generated and bred in our lab (Pascual et al., 2005). **B**, Individual 40x confocal image showing the eGFP fluorescence and the GFAP (astrocyte) and NeuN (neuron) immunoreactivity in area CA1 of a hippocampal section obtained from a 10 week-old adult dnSNARE mouse taken off Dox after weaning. Here again, note the mosaic expression of the transgene eGFP reporter in astrocytes: no clear eGFP fluorescence could be detected in about 15-20% of astrocytes. Importantly, no eGFP fluorescence at all could be found in any neurons surveyed. This was further quantified in D. Doted square shows area where the high density of astrocytic processes penetrating the pyramidal layer could be mistaken for eGFPpositive neurons upon imprecise examination. Arrowhead points to a typical eGFP-positive astrocyte. **C**, Same as B in area CA3. g.c.l.: granule cell layer. m.l.: molecular layer. Scale bar is the same as in B. **D**, Table summarizing the results of the cell counting performed by two independent investigators (JD and TJP) in both area CA1 and CA3. Note that among 5,884 and 5,887 neurons counted, not a single eGFP-positive neuron was found (0%). **E-F**, Average time course of exogenous D-serine application on NMDA-fEPSPs in slices obtained from dnSNARE mice off Dox at ZT0 (E) and ZT6 (F). Note that D-serine application caused an average 25% increase in the slope of NMDA-fEPSPs in both cases, in contrast with results obtained in wild types (Figure 2.2 E&F). **G**, Individual slopes of NMDA-fEPSPs before (pre) and after (post) Dserine application in the presence of physiological extracellular concentrations of L-serine in the aCSF (20 μM, 45min to 1h) in slices obtained from dnSNARE off Dox at ZT0. A paired Student's *t* test was used. **H**, Average saturation index of NMDARs in slices from dnSNARE mice off Dox, in the presence L-serine (calculated from G). An unpaired Student's *t* test was used. This experiment was performed to test the possibility that dnSNARE expression in astrocytes impaired L-serine release, instead of D-serine release. NMDARs remained unsaturated in the presence of 20 μM L-serine, ruling out this possibility (see main text). Pooled data are shown as mean ± SEM

2.4.6 Cholinergic tone drives wakefulness-dependent D-serine release from astrocytes

In addition to being tightly correlated with vigilance states[151-153], cholinergic signaling potentiates NMDAR activity and modulates NMDAR-dependent functions[154-158]. ACh also elicits intracellular Ca^{2+} signaling in astrocytes through muscarinic receptors[10], α4β2- and α4β4-nAChRs receptors[176], or α7nAChRs[160, 161] and can promote

D-serine release or synthesis[10, 155, 162]. Therefore, we hypothesized that ACh is the signal that tunes D-serine levels to wakefulness and tested whether cholinergic agonists can enhance the saturation index of NMDARs in ZT6 slices (Figure 2.9A). Application of a broad AChR agonist, carbamylcholine (Carba, Table 1), caused a full saturation of NMDARs (Figure 2.9A, $P < 10^{-7}$ vs control, Bonferroni post-*hoc* tests) that persisted in the presence of atropine (P = 0.899 vs Carba), suggesting the involvement of nicotinic (nAChRs), rather than muscarinic, receptors. The most abundant nAChRs expressed by hippocampal astrocytes in C57Bl/6 mice are α4β2- and α4β4-nAChRs[176] but Carba still caused a full saturation of NMDARs in the presence the α4β4- and α4β2-nAChR antagonist DHβE (P = 0.889). In contrast, we found that the effect of Carba was prevented by the α7nAChR antagonist MLA (Figure 2.9A, $P < 10^{-9}$), in line with observations that α7nAChR activation promotes NMDAR activity[155, 157, 158] and favors D-serine release[162]. As expected from this finding, the α7nAChR selective agonist AR-R17779 (AR-R) alone elicited a full saturation of NMDARs ($P < 10^{-8}$ vs control), which was attenuated by the co-application of MLA ($P < 10^{-4}$ vs AR-R). Importantly, stimulation of α7nAChRs did not change the subunit composition of NMDARs (Figure 2.10A), indicating that it did not change NMDAR affinity for D-serine but rather increased extracellular D-serine levels. Finally, in line with studies reporting the presence of α7nAChRs on astrocytes[161, 176-178], we found that neither application of Carba nor AR-R altered the saturation index in slices from dnSNARE mice off Dox (Figure 2.9A, $F(2,24) = 0.0031$, P = 0.997, one-way ANOVA), suggesting that α7nAChR stimulation elicits D-serine release from astrocytes.

That the stimulation of α7nAChRs elevates D-serine levels in ZT6 slices suggested that the saturating levels of D-serine found at ZT0 could be due to a basal activation of α7nAChRs. We tested this hypothesis and found that incubations of ZT0 slices with MLA for 60 min or more reduced NMDAR saturation index to a level similar to that normally found at ZT6 (Figure 2.9B&C, $t(19) = 8.78$, $P < 10^{-6}$, Student's *t* test), while it had no effect in slices obtained at ZT6 ($t(16) = 0.8$, $P = 0.4354$), or in ZT0 slices from dnSNARE mice off Dox ($t(18) = 0.66$, $P = 0.5176$). Altogether these results indicate that the daily oscillations in NMDAR co-agonist site occupancy are driven by the wakefulness-dependent endogenous activation of α7nAChRs upstream of astrocytic exocytosis.

Similar to ACh, the activity of noradrenergic neurons is phased to vigilance-state[179] and norepinephrine (NE) directly impacts astrocyte Ca^{2+} activity through α1 adrenergic receptor α1AR[86, 88]. We thus asked whether adrenergic activity could also influence the release of D-serine and found that the saturation index in ZT6 slices was neither altered by the presence of NE nor by the specific α1AR agonist methoxamine (Figure 2.9A, $P > 0.05$ Bonferroni post-*hoc* tests). Similarly, we found that oscillations in D-serine availability do not originate from changes in purinergic tone across the 24h period (Figure 2.10C-G), demonstrating that wakefulness-dependent release of hippocampal D-serine is selectively influenced by cholinergic neuromodulation.

Our findings suggest a direct and specific mechanistic link between α7nAChR activity and NMDAR co-agonist site, which is highly relevant in the context of schizophrenia. Indeed, the α7nAChR is the target of several therapeutics that have been taken into clinical trials to improve cognitive deficits associated with schizophrenia[142, 149,

[180]. Yet, the mechanism underlying their beneficial effect is ill-defined. We asked whether the most recent of them, EVP-6124 (FORUM Pharmaceuticals, Phase III clinical trial NCT01716975), was capable of enhancing NMDAR saturation index. Pharmacokinetic studies have shown that EVP-6124 reaches peak brain concentration 2h after administration, and remains at effective concentrations for at least 4 hours[181]. We administered EVP-6124 to wild-type mice at ZT0 (0.4 mg/kg i.p single dose, as in Prickaerts et al., 2012; Figure 2.9D) and found that this significantly increased the saturation index of NMDARs in slices obtained 4 hours later ($t(19) = -3.37$, $P = 0.0032$, Student's *t* test) without causing prolonged wakefulness or enhanced locomotor activity (Figure 2.10B). This indicates that α7nAChR-targetting therapeutics can enhance NMDAR activity, likely via D-serine, raising the possibility that this is the mechanism of action that mediates their beneficial effects on cognition.

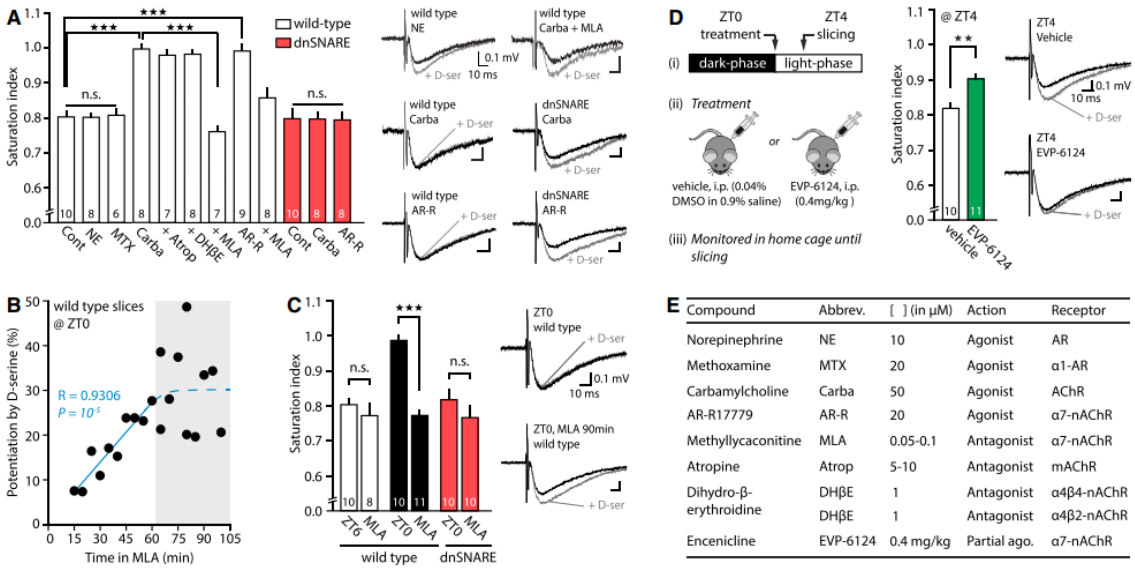

Figure 2.9: Endogenous cholinergic signaling controls D-serine availability across the 24h period. **A**, NMDAR saturation index in slices from WT and dnSNARE mice off Dox in the presence of adrenergic and cholinergic agonists/antagonists: norepinephrine (NE, 10 µM), α1AR agonist (MTX, 20 µM), AChR broad agonist (Carba, 50 µM), Carba and the muscarinic AChR antagonist atropine (+ Atrop, 5-10 µM), Carba and the α4β2- and α4β4-nAChR antagonist DHβE (+ DHβE, 1 µM), Carba and the α7nAChR antagonist MLA (+ MLA, 50-100 nM), the α7nAChR agonist AR-R17779 alone (AR-R, 20 µM) and the combination of AR-R and MLA. See Table 1. **B**, Effect of MLA incubation on NMDA-fEPSPs potentiation by D-serine. Individual experiments are shown. Plateau effect is reached after 60 min incubation (gray area). **C**, Effect of MLA incubation (>60 min) on NMDAR saturation index in ZT0 and ZT6 slices from WT mice, and ZT0 slices from dnSNARE off Dox. **D**, Experimental set-up for i.p. injections of EVP-6124 or vehicle in WT mice (*left*) and saturation index of NMDARs in slices obtained 4h later (*right*). ***E***, Table summarizing the various compounds, their abbreviation, concentration, action and target. Pooled data are shown as mean ± SEM. See also Figure 2.10.

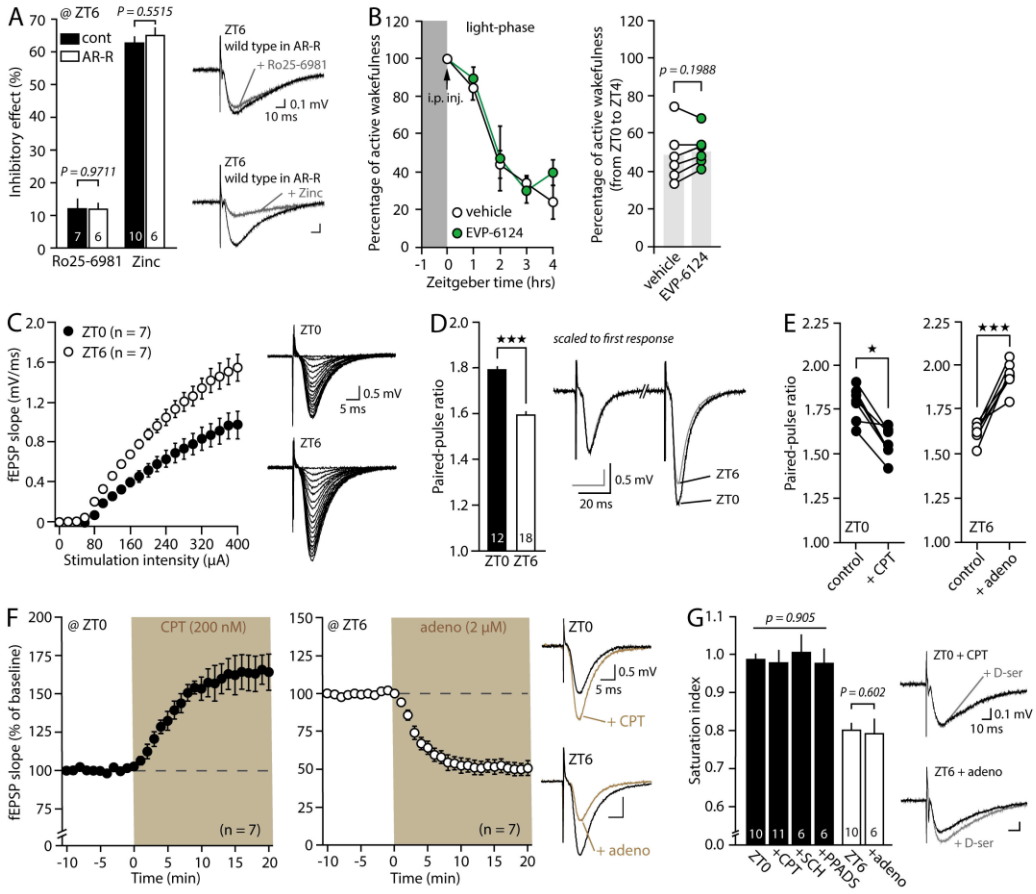

Figure 2.10: D-serine oscillations are driven by ACh and independent of purinergic signaling

A, NMDAR subunit composition is unchanged under α7nAChR stimulation, as shown by the effect of the GluN2A- and GluN2B-heterodimer antagonists Zinc (250 nM in Tricine) and Ro25-6981 (2 µM) on NMDA-fEPSPs recorded in the presence of the α7nAChR agonist AR-R17779 (P > 0.05, unpaired Student's *t* tests). **B**, Control experiment relative to main Figure 5D and performed on a separate cohort of animals. *Left:* Stage graph showing the percentage of time spent awake between ZT0 and ZT4 by mice injected with either EVP-6124 or vehicle solution at ZT0 (1 hour bins). Six animals received vehicle/EVP-6124 i.p. injection on day 1 and EVP- 6124/vehicle on day 2. $F(1,5) = 2.128$, $P > 0.05$, Repeated Measures ANOVA. *Right:* Individual (paired) percentage of time awake for the 4 hours following either EVP-6124 or vehicle i.p. administration: $t(5) = -1.46$, $P = 0.1988$, paired Student's *t* test. Mice activity was assessed through video-monitoring (as in experiments presented in Figure 2). **C**, Input-output curves obtained in ZT0 and ZT6 slices from WT animals and representative AMPA-fEPSP traces. **D**, Paired-pulse ratio (PPR) for 100 ms stimulation interval in ZT0 and ZT6 slices and representative traces. For comparison purposes, traces were scaled to the first responses. **E**, Effect of A1R antagonist CPT (at ZT0), and adenosine (at ZT6) on PPR. **F**, Effects of CPT and adenosine applications on AMPA-fEPSPs at ZT0 and ZT6 along with representative traces. **G**, Saturation index of NMDAR in ZT0 slices in the presence of CPT (200 nM), SCH (1 µM) and PPADS (10 µM), and in ZT6 slices in the presence of

adenosine (2 μM). Pooled data are shown as mean ± SEM. These experiments were performed to verify that D-serine oscillations are independent from daily fluctuations in adenosine tone. Indeed it was shown that wakefulness-dependent astrocyte-mediated oscillations in adenosine/ATP modulate presynaptic release probability through adenosine receptor 1 (A1R, Schmitt et al., 2012). In agreement, we found that synaptic strength was reduced in ZT0 slices compared to ZT6 (**C**). This was associated with a reduction in release probability at ZT0 (**D**, $P < 0.001$ Student's *t* test) that could be reversed by the A1R antagonist CPT (200 nM) and mimicked by adenosine (2 μM) in ZT6 slices (**E**, $P < 0.05$ paired Student's *t* tests). To test the possibility that D-serine oscillations could be secondary to daily adenosine variations, we blocked A1R (CPT), A2AR (SCH, 1 μM) or P2R (PPADS, 10 μM) ATP/adenosine receptors in ZT0 slices, and mimicked ZT0 adenosine tone in ZT6 slices (adenosine, 2 μM) for 30-60 min prior to assessing NMDAR saturation index. Despite striking effects on fEPSPs (**F**), these pharmacological manipulations were without effect on NMDAR saturation index (**G**, ZT0: $P = 0.905$, one-way ANOVA, ZT6: $P = 0.601$, Student's *t* test), indicating that D-serine oscillations do not originate from changes in purinergic tone across the 24h period.

2.4.7 Activity of MS-DBB cholinergic fiber drives the release of D-serine in the hippocampus

To confirm that *in situ* release of endogenous ACh elicits D-serine elevations, we employed the ChAT-ChR2-eYFP BAC transgenic mouse line that selectively expresses channelrhodopsin (ChR2) in cholinergic fibers[182]. These mice display strong expression of ChR2-eYFP in the medial septum (MS) and the ventral diagonal band of Broca (DBB), where the cholinergic fibers innervating the hippocampus originate (Figure 2.11A&B; Teles-Grilo Ruivo and Mellor, 2013). In slices obtained at ZT4, optical stimulation of these fibers (460 nm, 10 sec @ 5Hz / min for 15 min, Star Methods, Figure 2.11C and Figure 2.12B-F) caused a slow and long-lasting enhancement of NMDA-fEPSPs (Figure 2.11D, 24.0 ± 11.2% at 50-70 min (2) vs baseline (1), $t(9) = 2.82$, $P = 0.0198$, paired Student's *t* test) that was not observed in ChAT-ChR2$^{-/-}$ mice (Figure 2.12G). This effect was not observed on AMPA-fEPSPs either (Figure 2.12H), indicating that it was specific to NMDARs and not due to an overall increase in synaptic strength.

Importantly, application of exogenous D-serine 70 min after optical stimulation had no further effect on NMDA-fEPSPs (Figure 2.11D, 2.8 ± 1.9% (3) vs (2), $t(9) = 1.57$, P = 0.150), revealing a full saturation of NMDARs caused by the optical stimulation. Consistently, optical stimulation was unable to potentiate NMDA-fEPSPs when delivered in the presence of saturating levels of exogenous D-serine (Figure 2.11E, $t(9) = -1.32$, P = 0.217), confirming that the release of endogenous ACh by direct stimulation of cholinergic fibers causes an increased occupancy of the NMDAR co-agonist site. To ask whether α7nAChR mediates this effect, we repeated the experiment in the presence of the α7nAChR antagonist MLA and found that optical stimulation failed to cause an increase of NMDA-fEPSPs (Figure 2.11F, $t(9) = 0.06$, P = 0.953) while subsequent D-serine application produced a standard 20.2 ± 4.2% potentiation ($t(9) = -4.44$, P = 0.003). This indicates that NMDARs had remained unsaturated following the optical situation and that α7nAchR indeed mediates D-serine elevations driven by ACh transmission. As a last validation, we reasoned that optical stimulation of cholinergic fibers should have no effect in slices obtained at ZT0, in which we found that both ACh and D-serine are already present at elevated levels. Accordingly, NMDA-fEPSPs remained unchanged following optical stimulation and D-serine application in ZT0 slices (Figure 2.12I).

We conclude that the release of endogenous ACh from MS-DBB cholinergic fibers scattered in the hippocampus elicits a long-lasting surge in D-serine concentration that causes a long-term potentiation of NMDAR activity, via the stimulation of α7nAchRs.

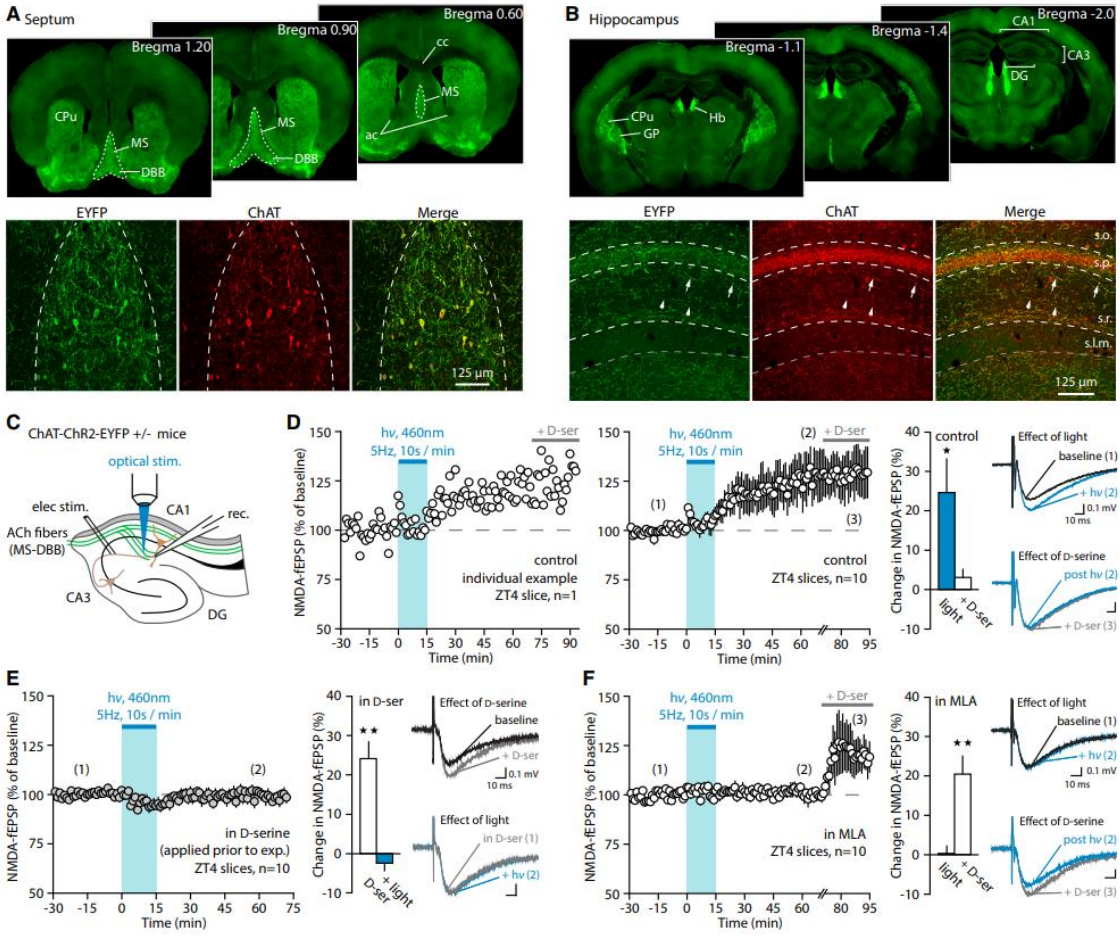

Figure 2.11: Cholinergic volume transmission elicits a long-lasting increase of NMDAR co-agonist site occupancy. **A&B**, Upper panels: eYFP fluorescence in the ventral diagonal band of Broca (DBB) and medial septum (MS) of ChAT-ChR2-eYFP mice, and their hippocampal projections. Anatomical structures are indicated for guidance and comparison with Zhao *et al.*, 2011: caudate putamen (CPu), corpus callosum (cc), anterior commissure (ac), globus palidus (GP), habenula (Hb) and dentage gyrus (DG). Lower panels: 20x confocal images (maximum projection of 3 z-planes) of eYFP fluorescence and ChAT immunoreactivity in the MS (showing numerous cholinergic neurons) and the hippocampus (showing cholinergic fibers (arrowheads) and varicosities (arrows)). **C**, Setup of optogenetic experiments. **D**, Individual example (left) and average effect over time (right) of the optical stimulation of hippocampal cholinergic fibers on NMDA-fEPSPs. D-serine was applied at the end of the experiment to assess NMDAR saturation. Bar graphs show the average effect of light (2), compared to the baseline (1), and that of D-serine application (3), compared to the post-light plateau (2). **E & F**, Same as (D) in the presence of D-serine from the start of the experiment (**E**) or in the presence of MLA (**F**). In (E) the effect of D-serine is not shown on the time course. Data are shown as mean ± SEM. See also Figure 2.12.

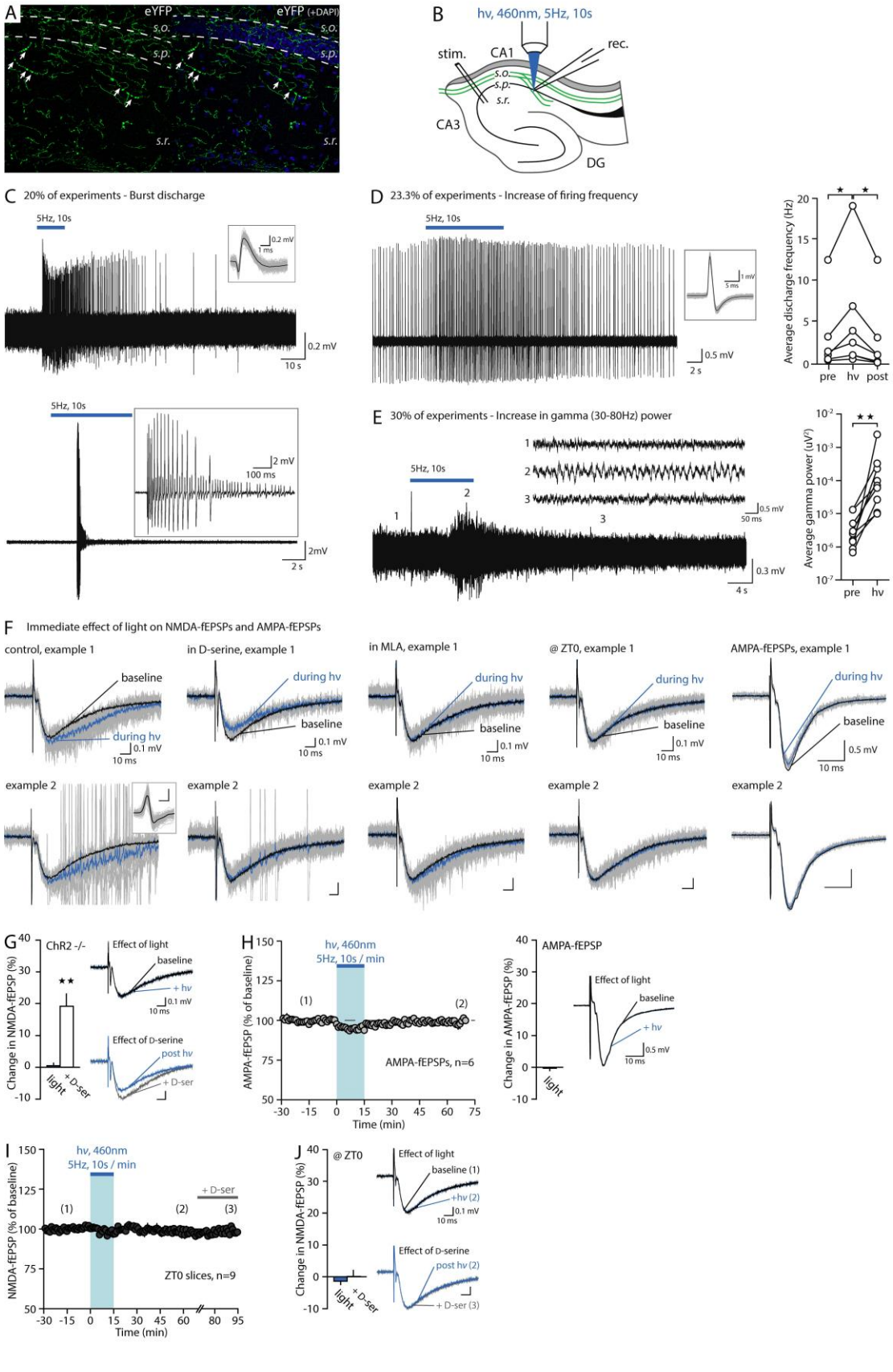
A
eYFP
eYFP (+DAPI)
s.o.
s.p.
s.r.
B
hv, 460nm, 5Hz, 10s
stim.
CA1
rec.
CA3
DG
C
20% of experiments - Burst discharge
5Hz, 10s
0.2 mV
1 ms
10 s
2 mV
100 ms
2mV
2 s
D
23.3% of experiments - Increase of firing frequency
0.5 mV
2 s
Average discharge frequency (Hz)
pre
hv
post
E
30% of experiments - Increase in gamma (30-80Hz) power
0.5 mV
50 ms
0.3 mV
4 s
Average gamma power (uV²)
F
Immediate effect of light on NMDA-fEPSPs and AMPA-fEPSPs
control, example 1
in D-serine, example 1
in MLA, example 1
@ ZT0, example 1
AMPA-fEPSPs, example 1
baseline
during hv
0.1 mV
10 ms
0.5 mV
example 2
G
ChR2 -/-
Effect of light
Effect of D-serine
post hv
+ D-ser
Change in NMDA-fEPSP (%)
light
+ D-ser
H
hv, 460nm
5Hz, 10s / min
AMPA-fEPSP (% of baseline)
AMPA-fEPSPs, n=6
Time (min)
AMPA-fEPSP
Change in AMPA-fEPSP (%)
I
NMDA-fEPSP (% of baseline)
ZT0 slices, n=9
J
@ ZT0
+hv (2)
post hv (2)
+ D-ser (3)

Figure 2.12: Optogenetic activation of cholinergic fibers
A, 40X confocal image of eYFP fluorescence (and DAPI staining) in a section from a ChAT-ChR2- eYFP+/- animal illustrating the high density of cholinergic fibers in the different layers of the area CA1, and the virtual absence of intrinsic ACh producing neurons. In particular, note the presence of 'varicosities' (arrows) that were reported to be release sites of ACh facing no defined post-synaptic structure (Duffy et al., 2011). **B**, Schematic of the experimental setup for recording neuronal activity in the pyramidal layer with extracellular recording. **C-E**, Extracellular juxta-cellular recordings of neuronal activity carried out in the pyramidal layer of slices from ChAT-ChR2-eYFP+/- mice. It has been documented that stimulation of cholinergic fibers causes a variety of effects on hippocampal neurons, including action potential (AP) firing, synaptic discharges and network gamma oscillations. In a set of preliminary experiments we used these markers to ensure that our optical stimulation protocol was efficient at stimulating cholinergic fibers in slices from ChAT-ChR2-eYFP+/- mice. An extracellular glass electrode was slowly moved through the pyramidal layer of area CA1 while stimulating Schaffer collaterals. This allowed the positioning of the recording pipette near neuron cell bodies detected by their AP firing in response to Schaffer collateral stimulation. Schaffer collateral stimulation was then stopped, and the optical stimulation was delivered after a brief baseline recording. We found that delivering 10 s trains of blue light (460 nm, 20 ms squares) at 5 Hz (the endogenous firing frequency of cholinergic fibers, see Lee et al., 2005) caused (**C**) in 20 % of the experiments (6 out of 30 experiments): clear bursts of synaptic discharges (upper panel, the inset shows the average synaptic event elicited by optical stimulation) or burst firing of APs in nearby neurons (lower panel, the inset shows the occurrence of large and small APs indicative that at least two distinct cells fired during this epoch), (**D**) in 23.3% of the experiments (7 out of 30 experiment): a transient increase in the frequency of AP firing in the nearby neuron ($P < 0.05$, paired Student's *t* test, inset shows average of 50 individual APs fired during the epoch), and (**E**) in 30 % of experiments (9 out of 30): an increase in gamma power (30-80 Hz band, $P = 0.0039$, Wilcoxon Matched-pairs signed rank test, upper traces are expanded epochs of the lower trace at indicated times; note the clear gamma oscillations on the middle trace (2)). No distinctive effect of light was noticed in 26.7 % of experiments (8 out of 30). **F**, Set of representative traces (2 examples each), illustrating the immediate effect of light (particularly obvious on AMPAfEPSPs, panel G) on NMDA-fEPSPs in control condition, in the presence of D-serine, in the presence of MLA, at ZT0 or on AMPA-fEPSPs. The black trace represents the baseline (average of 60 sweeps, 20 min). The gray background traces are the 15 raw traces immediately following each of the 10s, 5Hz optical stimulations. The deep blue trace is the average of these 15 raw traces. Note the presence of APs on top of the synaptic field response in some of the traces (control, example 2) reminiscent of the observations made in the preliminary experiments described above. **G**, Bar graphs and representative traces showing the absence of effect of the optical stimulation on NMDA-fEPSP in slices from ChAT-ChR2-eYFP -/- mice ($t(5) = 0.4$, $P = 0.705$). The effect of light was compared to the baseline, and that of D-serine application was compared to the post-light plateau. **H**, Average effect over time of the optical stimulation of hippocampal cholinergic fibers on AMPA-fEPSPs. Bar graph shows the average effect of light ($t(6) = -0.59$, $P = 0.584$). **I**, Average effect over time of the optical stimulation of hippocampal cholinergic fibers on NMDA-fEPSPs in slices obtained at

ZT0. Bar graph shows the average effect of light and subsequent D-serine application ($P > 0.05$). The effect of light (2) was compared to the baseline (1), and that of D-serine application (3) was compared to the post-light plateau (2). Pooled data are shown as mean ± SEM. **: $P < 0.01$, ***: $P < 0.001$.

2.4.8 Astrocytic a7nAChRs mediate ACh-driven D-serine oscillations

There have been increasing reports of the presence α7nAChR on astrocytes[176, 177] along with confirmations that such receptors are functional and play a signaling role[160, 161]. However, α7nAChRs are expressed by all cell types in the hippocampus and while the RNAseq database shows expression in astrocytes, it is less abundant than in neurons[176, 178]. We thus asked whether α7nAChRs required for the wakefulness-dependent regulation of D-serine availability are located on astrocytes or neurons. We used mice in which exon 4 of *Chrna7* is floxed (α7nAChR$^{flox/flox}$, Star Methods, Figure 2.14, Hernandez et al., 2014) and performed stereotaxic injections of adeno-associated viruses encoding Cre recombinase and GFP reporter. Mice were injected with an AAV5 encoding GFAP(0.7)-eGFP-T2A-iCre into area CA1 to selectively transduce astrocytes (Figure 2.13A), or with an AAV9 encoding eSYN-eGFP-T2A-iCre both in areas CA3 and CA1 to transduce neurons (Figure 2.13H). Mice were sacrificed at 35 ± 6 days post-injection and sections were immuno-stained for the astrocyte marker GFAP and the neuronal marker NeuN to confirm cell-type specificity of the transduction. As shown in Figure 2.13B-D and 13I-K, both the AAV5 and AAV9 viruses were highly selective for astrocytes and neurons, respectively.

NMDAR saturation index was assessed in slices from these animals, and these experiments were carried out blind to mouse genotype (Star Methods). We found that the effect of D-serine application was independent of the time-of-day in slices from AAV5-

α7nAChR$^{flox/flox}$ mice (Figure 2.13E, F(2,42) = 0.4439, P = 0.6446, one-way ANOVA) while it was ZT-dependent in slices from AAV5-α7nAChR$^{+/+}$ mice (F(2,20) = 5.5778, P = 0.0119). At ZT0, D-serine applications yielded a significant increase of NMDA-fEPSPs in slices from AAV5-α7nAChR$^{flox/flox}$ (Figure 2.13F, $t(15) = 8.2$, $P < 10^{-5}$, paired Student's *t* test) revealing that the saturation index was impaired and similar to that found at ZT6 (Figure 2.13G, $t(29) = 0.8$, P = 0.4278, Student's *t* test). Thus, the loss of α7nAChR on astrocytes abolishes the oscillations in NMDAR saturation index. In contrast, the effect of D-serine application remained time-of-day dependent in AAV9-α7nAChR$^{flox/flox}$ slices (Figure 2.13L, F(2,34) = 8.6824, P = 0.0009, one-way ANOVA) in which NMDARs were fully saturated at ZT0 (Figure 2.13M, $t(12) = 0.91$, P = 0.3825; Figure 2.13N, $t(22) = 4.36$, P = 0.0002), indicating that the genetic deletion of the α7nAChR in pre and postsynaptic neurons (as well as *s. radiatum* interneurons) is without effect on the daily fluctuations of NMDAR co-agonist site occupancy. We conclude that astrocytic α7nAChRs are required for converting ACh drive into oscillations of NMDAR co-agonist site occupancy.

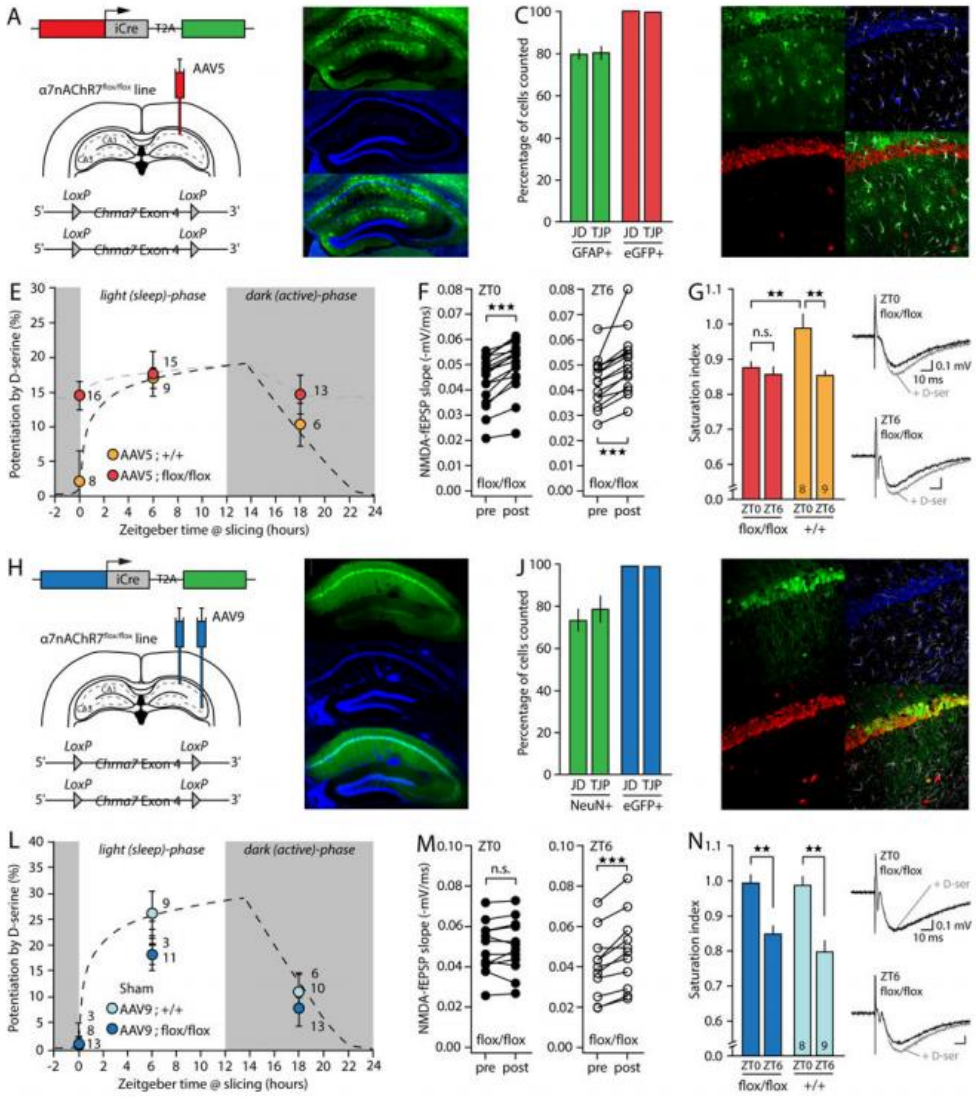

Figure 2.13: Astrocyte-specific α7nAChR knock-out abolishes D-serine oscillations. **A**, Schematic of stereotaxic injections of Cre-encoding AAV5 virus in area CA1 of α7nAChR$^{flox/flox}$ and α7nAChR$^{+/+}$ littermates. **B**, eGFP fluorescence and DAPI staining in the hippocampus, 35 days after AAV5 injection. **C**, Percentage of GFAP+ cells (astrocytes) that are eGFP+ (expressing iCre) and percentage of eGFP+ cells that are GFAP+, counted by two independent investigators (JD and TJP). **D**, Astrocyte-specificity of the viral transduction: Confocal (40x) images showing DAPI nuclear staining, eGFP fluorescence, NeuN (neuron) and GFAP (astrocyte) immunoreactivity. **E**, Effect of D-serine on NMDA-fEPSPs in slices obtained from AAV5-injected α7nAChR$^{flox/flox}$ and α7nAChR$^{+/+}$ littermates at different ZTs. **F**, Individual slopes of NMDA-fEPSPs before (pre) and after (post) D-serine application, at ZT0 and ZT6 in slices from AAV5-injected α7nAChR$^{flox/flox}$. **G**, Saturation index at ZT0 and ZT6 in slices from AAV5-injected α7nAChR$^{flox/flox}$ and α7nAChR$^{+/+}$ mice. **H-N**, Same as above for AAV9-injected animals. Note the neuronal-specificity of the transduction. Sham: injected animals that showed no signs of virus transduction. Pooled data show mean ± SEM. See also Figure 2.14.

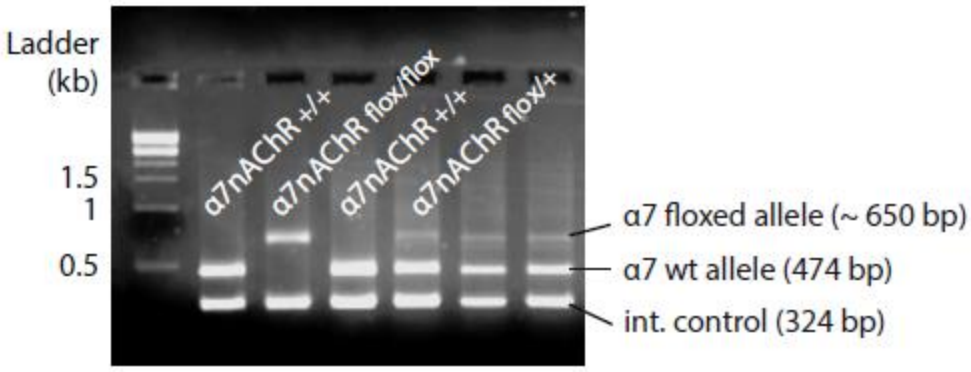

Figure 2.14: α7nAChR flox mouse genotyping
A, Representative gel of PCR reactions used to genotype mouse pups from the α7nAChRflox/+ line. A portion of the exon 4 of *Chrna7* gene was amplified using the primers and cycling parameters described in Experimental Procedures. The sequence amplified from the wild type allele is 474 bp. Mice with both *Chrna7* alleles floxed (α7nAChRflox/flox) have a ~ 650 bp but no band at 474 bp. β-actin was used as an internal control (324bp).

2.5 Discussion

We demonstrate that by sensing wakefulness-dependent release of acetylcholine through α7nAChRs, astrocytes modulate the amount of D-serine they provide to synaptic NMDARs throughout the day (Figure 2.15). There are three main consequences to this finding. First, this represents a new mechanism whereby NMDARs, and NMDAR-dependent functions, are controlled by vigilance state-dependent cholinergic activity through their co-agonist site. Second, we show that astrocytes are central to this mechanism: they locally shape synaptic properties to the ongoing brain activity by monitoring the neuromodulator environment, a new function we term *contextual guidance*. Third, by linking cholinergic activity, α7nAChRs, astrocyte-derived D-serine, and NMDARs, this new pathway is greatly relevant to schizophrenia, and we demonstrate that the stimulation of α7nAChRs with a clinically tested drug (EVP-6124) is sufficient to enhance NMDAR function.

The degree of occupancy of the co-agonist binding site directly dictates the ability of NMDARs to be activated by glutamate[145]. Since glutamate is fully saturating to NMDARs during synaptic transmission[183], D-serine availability is the limiting factor to NMDAR activation. We found that D-serine levels fluctuate in vivo as a function of wakefulness over a range of concentrations that spans NMDAR co-agonist site sensitivity. Therefore, the wakefulness-dependent control of D-serine we describe represents a new and major mechanism for the regulation of NMDAR activation throughout the day. It allows more robust NMDAR activity and higher learning capabilities during windows of higher behavioral alertness, in line with the well-documented memory enhancing effect of nicotine. Such "on-demand" control of NMDAR activation also allows maintaining lower levels of hippocampal NMDAR activity during periods of rest, which could be relevant to synaptic downscaling and to memory consolidation that occur during slow wave sleep[173]. Overall, we predict that D-serine levels are regulated on-demand in other brain regions as a function of their involvement in a specific behavioral task, vigilance state or response to the hormonal status of the animal.

Behavioral states are intrinsically bound to neuronal population dynamics and to the activity of neuromodulator systems. For instance, states of wakefulness and attention coincide with bursting patterns of septal and/or locus coeruleus neurons and with volume transmission of NE and ACh[152, 153, 164, 179]. A significant body of evidence has now brought astrocytes into this scheme and suggests that astrocytes can sense brain states through volume transmission[10, 45, 87, 88, 159]. Our study validates and extends this emerging view by showing that hippocampal astrocytes sense wakefulness-dependent ACh

neuromodulation, and use this information to tune synaptic NMDARs activation via D-serine release. Based on similar reports that NE shapes astrocytes interactions with neurons in a context-dependent manner[88], we postulate that the capability of hippocampal astrocytes to sense information about the brain state and use it to appropriately tune synaptic properties can be generalized to other neuromodulator systems and gliotransmission pathways. Therefore, we propose a new function for astrocytes wherein, by monitoring the neuromodulator environment and releasing appropriate gliotransmitters, astrocytes locally shape synaptic properties to the ongoing brain context thus providing *contextual guidance* to synapses.

Multiple human mutations associated with schizophrenia point to a compromised function of the NMDAR co-agonist binding site, and this has become a leading hypothesis for the etiology and treatment of this disorder[142, 143]. This includes mutations that impair the synthesis, availability, or binding of D-serine such as mutations associated with *srr*, *DAO* and *Grin1*, respectively coding for D-serine synthesizing enzyme serine racemase (SR), D-serine degrading enzyme D-amino acid oxidase (DAAO), and NMDAR GluN1 subunit that arbors the co-agonist binding site[132, 148]. Similarly, the mutation of *Disc*-1 (Disrupted-In-Schizophrenia-1), a direct regulator of SR, is among the most notorious mutations associated with schizophrenia and causes a depletion of D-serine[132]. In line with this genetic evidence, clinical studies reported decreased D-serine levels in the plasma of schizophrenic patients[126, 127] and administration of D-serine improves negative, positive and general symptoms of schizophrenia[138]. In parallel, the dysregulation of the cholinergic system has historically been a hallmark of schizophrenia[142] and clinical attention is particularly focused on the α7nAChR. Indeed,

α7nAChR modulators seem to significantly improve the cognitive deficits associated with schizophrenia in clinical trials[142, 149, 180] even though no mechanisms have been proposed to explain such beneficial effects. Our work demonstrates that these two major hypotheses for the etiology and treatment of schizophrenia are mechanistically linked, via astrocytes. We show that impairing cholinergic signaling results in reduced D-serine availability and that, conversely, endogenous cholinergic activity can be bypassed with a clinically tested α7nAChR partial agonist to successfully enhance NMDARs activation. This provides mechanistic insights into the effects of clinically used α7nAChR modulators and highlights their potential to restore D-serine levels in schizophrenic patients, which is relevant when considering the nephrotoxicity of direct D-serine administration[184]. More importantly, our work places astrocytes at the center of this pathway, offering a new functional framework for the treatment of schizophrenia and opening the search for innovative approaches and targets to the field of glial biology.

In this context, the details of the signal transduction pathway linking the activation of α7nAChR to corresponding synaptic levels of D-serine will need to be defined. The α7nAChR is a highly Ca^{2+}-permeable ionotropic receptor and its activation triggers localized Ca^{2+} surges in astrocytes[160, 161]. Since D-serine release is SNARE- and Ca^{2+}-dependent[110, 116, 146], we presume that α7nAChR activation generates the optimal intracellular Ca^{2+} conditions that stimulate the release of D-serine containing vesicles. Interestingly, evidence also exist that muscarinic AChRs induce an IP_3R2-mediated release of D-serine from astrocytes[10] or that TRPA1 channels regulate D-serine release[115]. Together, these results suggest that a complex and diversified set of local (membrane channels) and global (IP_3R2-dependent) Ca^{2+} sources control the release of D-serine. Our

results also identify a pool of wakefulness-independent D-serine that remains unaffected by the blockade of α7nAChRs and SNARE-mediated vesicular release. This suggests the existence of a tonic source of D-serine that could be either astrocytic, but non-vesicular[115], or neuronal[175]. That multiple sources and routes of D-serine co-exist could constitute another interesting therapeutic target to control D-serine levels with, or independently of, wakefulness.

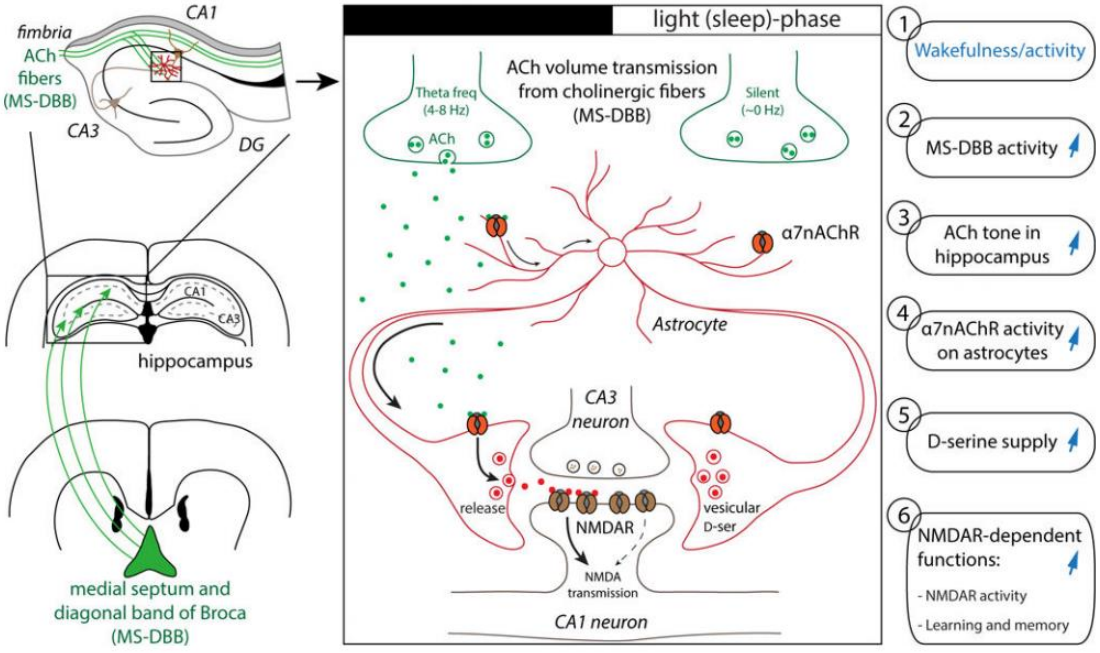

Figure 2.15: Cholinergic transmission tunes the gating of NMDARs through astrocyte-dependent D-serine release. The medial septum and diagonal band of Broca (MS-DBB) send scattered cholinergic projections to the hippocampus. During active wakefulness (1) MS-DBB neurons fire in the theta frequency (2) which elicits the release of acetylcholine in the extracellular space (3). This cholinergic tone is sensed by astrocytes through α7nAChRs (4). This drives the vesicular release of astrocytic D-serine at synapses (5) to enhance NMDAR activity and NMDAR-dependent functions (6). The cessation of MS-DBB activity (during sleep and rest) suppresses the cholinergic-induced activation of α7nAChRs on astrocytes and reduces D-serine release.

Chapter 3: Cholinergic signaling modulates behavior through astrocytes[2]

[2] Tolman, M., Papouin, TJ., and Haydon, PG. To be submitted to *Glia*.

3.1 Introduction

Neuromodulation allows the brain to 'tune' its functioning based on cues from the environment. For example, adjusting the gain of neuronal networks so that during active wakefulness long-term potentiation (LTP) and learning can occur, whereas during sleep the threshold for inducing LTP is higher and memory consolidation can occur[151, 185]. The cholinergic neurons are nicely positioned to modulate these whole brain states; their cell bodies reside in the basal forebrain and they project throughout the cortex and hippocampus[186]. Optogenetic activation of the cholinergic neurons induces state-dependent changes in hippocampal θ rhythms and LTP[185]. Disruptions in cholinergic signaling have been intensely studied in the context of Alzheimer's disease and schizophrenia[187, 188]. Pharmacological potentiation of the cholinergic system has proved a successful strategy for cognitive enhancement[189], but a lot of work is needed to understand the mechanisms underlying these disease states and even the basic mechanisms involved in translating cholinergic tone into the modulation of neuronal networks.

Recent work from our lab has shown a novel role for astrocytes in sensing cholinergic tone and modulating neuronal networks through the release of D-serine[1]. Astrocytes are known to respond to neuromodulators[88], express cholinergic genes[45], form networks across large regions through gap junctions[190], and contact thousands of synapses[191]. This positions them well for both sensing cholinergic tone and modulating neuronal networks. Astrocytes can both regulate the concentration of neurotransmitters[192] and release gliotransmitters at the synapse[193]. Understanding the precise cues that instruct these uptake and release functions is an area of active research, however. We found that

the activation of the α7nAChR on astrocytes specifically led to an increase in the release of D-serine in the hippocampus[1].

Since glutamate is released at saturating levels, gating of the NDMAR is achieved by regulating co-agonist availability[194]. D-serine release from astrocytes also regulates spine dynamics in newborn hippocampal neurons[116]. Altered D-serine levels have been found in schizophrenic patients[126, 127]. D-serine administration itself can improve both the positive and negative symptoms in patients[136, 137], but over time oral administration of D-serine becomes toxic[138] and pharmacologically targeting the enzymes involved in D-serine metabolism has proved difficult[195]. Discovering that astrocytes release D-serine downstream of the α7nAChR will help better inform drug discovery efforts in the future and may even uncover a class of novel, astrocyte-specific drug targets. While we have shown that activity regulates astrocytic release of D-serine, it remains unclear which behaviors rely on this astrocytic gating of neuronal circuits.

Here, we look at the role of both neurons and astrocytes in sensing cholinergic tone during behavioral tasks. Using all in vivo techniques, we have shown that astrocytes sense cholinergic signaling through the α7nAChR in order to modulate D-serine levels in the hippocampus. This effect was seen only in male mice. The ability of astrocytes to sense cholinergic tone through the α7nAChR was necessary for NDMAR-dependent behaviors including learning, short-term social memory, and contextual fear memory, but was not necessary for mediating other behaviors such as anxiety, anhedonia, body weight, or sleep. By pairing optogenetics with microdialysis, we showed that activation of the cholinergic projections could increase D-serine levels, suggesting that current

cholinergic modulators rely on the activation of astrocytes for their cognitive enhancement effects.

3.2 Materials and Methods

3.2.1 Mice

Experiments involving live animals were approved by the Animal Care and Use Committee at Tufts University. All animals received food and water ad libitum. Genotyping was performed on DNA from tail samples taken from pups at one week of age. Once animals had reached six-eight weeks of age, they were moved to a 12hour/12hour light-dark cycle. The following genetically altered mouse lines were used in experiments:

α7nAChR floxed mice (*B6-Chrna7^{LBDEx4007eHS}I*): These mice were generated in Dr. Kelly Dineley's lab at the University of Texas and described in Hernandez et al., 2014. They were back crossed to C57BL/6 mice and bred at Tufts University. Exon 4 of the CHRNA7 gene is flanked by loxP sites. This allows for temporal and spatial control of α7nAChR deletion.

Glast-creERT mice (Tg(Slc1a3-cre/ERT)1Nat/J): Heterozygous Glast-creERT2 BAC transgenic male mice were purchased from Jackson Laboratory (Stock #012586) and bred at Tufts University. Breeding crosses were established so that only heterozygous transgenic animals could be produced. These mice allow for the tamoxifen inducible expression of the cre protein downstream of the Glast promoter. The Glast-creERT2 mice were chosen to drive expression in CA1 astrocytes. This line was chosen for its specificity and efficiency in driving expression in CA1 astrocytes. It is also known that

the Glast promoter is active in some neurons in the dentate gyrus during development and in adulthood. By only activating the inducible cre-ERT2 molecule in adulthood, we limited the number of affected neurons in the dentate gyrus and there was no expression of the cre-ERT2 molecule in the CA1 region (Figure 3.1).

CamK-creERT mice (B6;129S6-Tg(Camk2a-cre/ERT2)1Aibs/J): Heterozygous male mice were purchased from Jackson Laboratories (Stock #014546) and bred at Tufts University. Breeding crosses were established so that only heterozygous transgenic animals could be produced. These mice allow for the tamoxifen inducible expression of the cre protein downstream of the CamK2 promoter.

Ai9 floxed mice (B6.Cg-*Gt(ROSA)26Sor*$^{tm9(CAG\text{-}tdTomato)Hze}$/J): Heterozygous male mice were purchased from Jackson Laboratory (Stock #007909) and bred at Tufts University. Both heterozygous and homozygous mice were produced for experiments. These mice allow for the expression of the tdTomato protein when cre has excised the stop codon inserted upstream of its coding region.

ChAT-ChR2 mice (*B6.Cg-Tg(Chat-COP4*H134R/EYFP)6Gfng/J*): Heterozygous male mice were purchased from Jackson Laboratory (Stock #014546) and bred at Tufts University. These mice express channel rhodopsin and GFP downstream of the ChAT promoter allowing for optogenetic activation of cholinergic neurons and their projections.

Offspring from the following genetic crosses were obtained for experiments:

Glast-creERT x α7nAChR floxed mice: Mice generated by breeding Glast-creERT and α7nAChR flox mouse lines result in the selective and conditional deletion of the α7nAChR primarily on astrocytes in the offspring. These mice require injections of 4-Hydroxytamoxifen (4-OHT) i.p. to activate the CreERT2 protein, which induces genetic recombination between loxP sites. The injections are performed at six weeks of age. Male and female mice were used for microdialysis experiments. Since there was no significant change in female hippocampal D-serine levels as measured by microdialysis, only male mice were used in the subsequent behavioral tests.

Glast-creERT x α7nAChR floxed x Ai9 floxed mice: Mice generated by breeding Glast-creERT2, α7nAChR floxed, and Ai9 floxed lines. As a result, these mice have no α7nAChRs and express creERT2 and the fluorescent reporter tdTomato in astrocytes after tamoxifen injections. These mice were only used for histological experiments. Both male and female brains were analyzed (female data not shown).

CamK-creERT x α7nAChR floxed mice: Mice generated by breeding CamK-creERT2 and α7nAChR floxed lines results in the ability to delete the α7nAChR in excitatory neurons in the offspring after tamoxifen injections. Male and female mice were used for microdialysis experiments. Since there was no significant change in female hippocampal D-serine levels as measured by microdialysis, only male mice were used in the subsequent behavioral tests.

CamK-creERT x α7nAChR floxed x Ai9 floxed mice: Mice generated by breeding CamK-creERT2, α7nAChR floxed, and Ai9 floxed lines. As a result, these mice have no α7nAChRs and express creERT2 and the fluorescent reporter tdTomato in neurons after tamoxifen injections. Both male and female brains were analyzed (female data not shown).

Glast-creERT x α7nAChR floxed x ChAT-ChR2 and CamK-creERT x α7nAChR floxed x ChAT-ChR2 mice: These mouse lines were generated for use in microdialysis experiments paired with optogenetics. The channel rhodopsin in cholinergic, ChAT positive neurons is activated optogenetically while microdialysis is being performed to measure D-serine levels in the hippocampus. Comparison of the D-serine levels during this experiment to the levels in mice that lack the α7nAChR on neurons rather than astrocytes were used to determine the contribution of each cell type in cholinergic D-serine regulation. Only male mice were used for these experiments, since our microdialysis data showed that the α7nAChR was not necessary for maintaining hippocampal D-serine levels in the hippocampus as measured by microdialysis.

3.2.2 Zeitgeber time

Zeitgeber time (ZT) is a universal notation system referring to the light cycle. This system allows for the comparison of time of day studies relative to the time at which experiments were performed relative to the light cycle rather than the clock time. ZT0 denotes the start of a 24 hour period and the onset of the light phase. Mice for these experiments experienced ZT0 at 9:00am and lights off, ZT12, at 9:00pm after six weeks of age.

3.2.3 Drugs

Drug	Supplier	Dose	Storage
Tamoxifen	Sigma	75mg/kg for 5 days	Prepared fresh daily in corn oil at a concentration of 20mg/mL and heated to 50C to aid in dissolution
D-serine	Sigma	50-100mg/kg	Dissolved in saline at 80mg/mL and stored at -80C
EVP-6124	MedChem Express	0.4mg/kg	Stored at -80C in DMSO aliquots and diluted freshly in saline before injection

Table 3.1: Pharmacological agents used in experiments.

3.2.4 Microdialysis

All procedures were approved by Tufts IACUC. During surgery at 6-8 weeks of age, mice were anesthetized using isoflurane. Buprenorphine (0.05mg/kg, sub cutaneous) was given pre-operative and post-operative as needed. Mice were implanted with a unilateral guide cannula (CMA P000138) over the hippocampus. To target the hippocampus, the following coordinates were used: -2mm from Bregma and 1.5mm left from the midline. The guide cannula was secured with dental cement and two contralateral anchor screws. Mice were allowed to recover 4-7 days singly housed before sampling. On the day of microdialysis, probes (CMA P000082) were inserted through the guide cannula at ZT0. ACSF (Harvard Apparatus, 597316) was perfused through the probe at a rate of 0.5µl/minute until ZT6. Dialysis samples were collected hourly and immediately frozen at -80C. Video monitoring was performed throughout the microdialysis experiment using Pinnacle Technologies cameras and Sirenia video capture

software. Targeting of the microdialysis cannula was confirmed at the end of the experiment. Briefly, brains were immersed in 4% PFA, cryoprotected, frozen, and sectioned. Target assessment was performed blind to the genotype of the mouse. If the cannula was not targeted to the hippocampus, the samples were excluded from HPLC analysis.

3.2.5 Microdialysis paired with optogenetics

Chat-ChR2 mice were used to optogenetically activate the cholinergic projections to the hippocampus while simultaneously measuring D-serine levels in awake male mice under partial constraint conditions. Briefly, adult male mice underwent the cannula implantation surgery during which a microdialysis guide cannula (Harvard Apparatus, CMAP000138) was implanted over the hippocampus (-2mm and left 1.5mm from Bregma) and an optogenetic guide cannula (Pinnacle Technologies, 7032) was implanted targeting the septum (1mm and 0.7mm left from Bregma at a 10° angle towards the midline). At the same time, a titanium head mount was attached to the skull with dental acrylic and contralateral anchor screws. Mice were single housed in Pinnacle cages and allowed to recover for four days before habituation to the recording chamber. During recording, mice were fixed via their head mount to a horizontal pole such that they were able to move the circular Styrofoam platform beneath them, but their head was fixed in place. Mice were exposed to this set up for three days prior to testing. They were first allowed to explore the set up freely, then head fixed for the remainder of the trial. Food rewards were presented to the mice during each trial. On the testing day, mice were head fixed at ZT0 on the mobile Styrofoam platform. The optogenetic and microdialysis guides were removed from the cannulas and the microdialysis (Harvard Apparatus,

CMAP000082) and optogenetic (Pinnacle Technologies, 7080-470-3) probes were inserted. Microdialysis samples were collected as described above. Optogenetic stimulation was added from ZT2 through ZT4 in 10s trains of 8Hz pulses with a pulse width of 10ms every 60s using the Sirenia software (Pinnacle Technologies). This stimulation was chosen based on its demonstrated ability to increase ACh levels in vivo.

3.2.6 Video scoring

Using videos recorded during microdialysis, animals were manually scored as active (mobile or immobile, but awake) or inactive (absence of movement and/or nested) in each minute of the 6 hour recording. An average activity score was obtained for each recording.

3.2.7 High performance liquid chromatography

D-serine measurements were performed with fluorescent detection after derivatization and separation on an Accucore C18 column (Thermo Fisher, 17126-152130). Samples were diluted in half with aqueous mobile phase and derivatized using o-Phthalaldehyde (Pickering, O120) and N-Acetyl-L-Cysteine (Sigma, A8199). Post derivatization, 1M acetic acid was added to normalize the pH. 1µl of derivatized sample was injected into the flow of the mobile phase. The mobile phases consisted of an organic phase (methanol) and an aqueous phase (50mM phosphate buffer, pH 4.34), which were perfused at a rate of 200µl/minute in a step-wise protocol: 0-6min 3% organic, 6.5-10min 20% organic, 11-14min 80% organic, and equilibrated at 3% organic for 7min. A standard curve was generated from D- and L-serine (Sigma) standard concentration solutions prepared at a ratio of 1:10. The area under the D-serine peak was used to calculate the concentration.

3.2.8 Immunohistochemistry and imaging

Brains were collected for immunohistochemistry after mice were anesthetized with isoflurane and transcardially perfused with phosphate buffered saline (PBS) and 4% paraformaldehyde (PFA). Once collected, brains were post-fixed and cryoprotected with 30% (w/v) sucrose in PBS at 4°C. Sections were collected using a sliding microtome (Leica SM2000R) at 40µm. For immunohistochemistry, sections were washed in PBS with 0.3% Triton X-100 (PBS-Tx), blocked with 5% bovine serum albumin (BSA) in PBS-Tx. Slices were incubated in primary antibodies diluted in blocking solution overnight at 4°C with gentle shaking. Sections were then washed in PBS-Tx and incubated with the appropriate AlexaFlour secondary antibody for 90 minutes at room temperature with gentle shaking. After incubation, sections were rinsed with PBS-Tx and mounted on Superfrost Plus slides (VWR) and coverslipped with Vectashield hardSet Mounting Medium containing DAPI (Vector Laboratories). Imaging was performed on a Nikon A1R confocal microscope with a 63x oil-immersion lens. Image resolution was set to 1024 x 1024 pixels. Images were adjusted for brightness and contrast, if necessary in Fiji (Schindelin et al., 2012). Fiji was also used for tracking manual cell counts of tdTomato+, NeuN+, and GFAP+ labeled cells.

Antibody	Concentration	Company	Product Number
NeuN	1:1000	Millipore	ABN78
GFAP	1:1000	AbCam	AB4674
Mouse and rabbit AlexaFlour 633	1:1000	Life Technologies	A-21052 A-21050

Table 3.2: Primary and secondary antibodies.

3.2.9 Behavior

Only adult male mice (6 to 10 weeks of age) were used for behavioral experiments. Mice were housed in groups of 2 to 4 and habituated to a 12hour/12hour light/dark cycle.

Fear conditioning: Baseline and rescue fear conditioning experiments were performed by the same male investigator (TJP). For rescue experiments, injections were performed by a separate investigator (MT). For baseline fear conditioning experiments, mice had previously been exposed to the three chamber social choice test, elevated plus maze, and pre-pulse inhibition (PPI). For rescue experiments, mice were not exposed to prior behavioral tests. Briefly, the fear conditioning set up consisted of four conditioning chambers (Coulbourn Instruments, H10-11R-TC) in a sound-attenuating isolation cabinet (Coulbourn Instruments, H10-24T). Mice were habituated to the metal grid that would later administer the foot shock. The shocks were administered at 0.5mA for 2 seconds by a precision shocker (Coulbourn Instruments, H13-15). During each session, the mouse's behavior was monitored by a camera mounted on the ceiling of the chamber (Panasonic, WV-BP334) and connected to a PCI-1410 (ACT-610) interface. FreezeFrame and FreezeView software (Coulbourn Instruments) was then used to automatically detect

freezing behavior. The threshold for freezing behavior was set at 1 second and consisted of complete absence of movement other than respiration. The training session lasted for 5 minutes and included three foot shocks administered with no auditory stimulus. For rescue experiments, littermates were randomly assigned to conditions and injected with either saline or 100mg/kg D-serine one hour prior to training. It has been shown that i.p. injections of 100mg/kg D-serine significantly increase hippocampal levels of D-serine (Figure 3.7A). After training, mice were returned to their home cage. Testing memory retrieval was performed 24 hours later during a single three minute session during which no shocks were administered. To assess freezing in a novel Context B, mice were placed in a second chamber which differed from the training and testing chamber in its visual, olfactory, tactile, lighting, and size.

Three chamber social choice: The three chamber social choice test is based on the animal's spontaneous preference for novelty. Mice were placed in a novel three chamber environment (Hamilton-Kinder LLC) where they were free to explore all three empty chambers for 10 minutes in the first trial. In the second trial, a novel, younger, conspecific mouse was introduced into a wire cage in the left chamber. Preference for the novel mouse is expressed as the amount of time spent in the left chamber relative to the total time spent exploring the other two chambers. In the third trial, the animal's ability to remember which mouse it has previously explored is shown by its preference for a second novel mouse placed in the right chamber. Total time spent in each chamber was measured using EthoVision (Noldus) and a video recording of each trial. These experiments were performed by a female experimenter (MT) between ZT0 and ZT3. One

hour prior to testing, mice in their home cage were moved into the testing room under red light.

Pre-pulse inhibition: To investigate sensory gating deficits, a short pre-pulse of 4ms is played 40ms before a startle response of 120dB. The degree to which the startle response is inhibited by the presence of the pre-pulse was recorded as the PPI. These experiments were performed by a female investigator (MT) at ZT4 on mice which had previously been exposed to the three chamber social choice test. Mice in their home cage were placed in the testing room one hour prior to the experiment. For testing, the mice were placed in individual acoustic startle chambers (Hamilton-Kinder LLC) and their startle response measured by the force (N) placed on a pressure sensitive platform (Hamilton-Kinder LLC). The trial consisted of 6 initial startle tones of 120dB followed by randomly distributed PPI trials and ending with a final 6 120dB startle tones. The whole experiment consisted of 72 trials and lasted 25 minutes. Mice were immediately removed from the acoustic startle chamber and placed back in their home cage at the conclusion of the experiment. The volume of the pre-pulse was randomly distributed throughout the trials at a level of 65, 73, 77, or 81dB. To confirm that cKO mice were exhibiting the same degree of startle response to the range of tones presented during testing, both control and cKO mice were exposed to a second startle experiment to generate an input output curve. The input output experiment was performed by the same female experimenter (MT) at least two days after the PPI experiment. Again, the mice were moved to the testing room one hour prior to the experiment at ZT4. 20ms startle tones ranging from 70 to 120dB were distributed randomly throughout the experiment, which lasted 30 minutes.

Sucrose preference test: The sucrose preference test was used as a corollary for anhedonia. Mice were singly housed to assess their preference for consuming a sucrose or water solution. These experiments were carried out by a male investigator (TJP).Using a standard two-bottle choice procedure[196], this preference was assessed over four days. Mice were habituated to using two bottles of drinking water in their home cage for three days. The amount of liquid consumed was measured as their baseline drinking behavior. To test for sucrose preference, the drinking water in one of the bottles was replaced with a 1% sucrose solution. The preference for consuming the sucrose solution was measured as the percent of sucrose consumed relative to total liquid consumed per day.

Elevated plus maze: The elevated plus maze was used to assess the level of anxiety in our mouse lines. Briefly, mice are placed at the central junction in a four-armed maze (Hamilton-Kinder). Two of the arms are open platforms and two of the arms have dark walls on all sides. The number of entries and amount of time spent in each arm is assessed by the number of beam crosses and video monitoring during the 10 minute trial. These experiments were conducted by a male investigator (TJP) between ZT0 and ZT1.

Home cage locomotion: In order to assess home cage locomotion, mice were singly housed for four days. The home cage was surrounded by infrared beam motion detectors (Hamilton-Kinder LLC). Each beam cross was recorded using Motor Monitor software (Hamilton-Kinder LLC). The hourly distance traveled was calculated for each mouse on the last day of recording. The average distance traveled was compared between genotypes and between the light and dark phases.

Home cage activity: Since microdialysis experiments were performed between ZT0 and ZT6 when the mice would normally be sleeping, we wanted to determine whether there was sleep deprivation occurring during this experiment compared to undisturbed mouse behavior between ZT0 and ZT6. Wild type mice, which had not undergone surgery, were allowed to habituate to single housing in Pinnacle cages (Pinnacle Technologies) for the same amount of time as mice that were about to undergo microdialysis. On the fourth day, mice were video monitored from ZT0 to ZT6 and the % of time each mouse was active over the six hours was then manually scored by assigning each minute of the recording as active or inactive. The average % of time undisturbed mice spent in the active state was compared to the average % of time mice were active while undergoing microdialysis

3.2.10 EEG/EMG

Electroencephalogram (EEG) paired with electromyography (EMG) was performed to assess sleep/wake behavior as well as cortical oscillation patterns. Briefly, surgeries were performed under isoflurane anesthesia to secure the EEG/EMG head mount (Pinnacle Technologies, 8201). The surface of the skull was exposed and four electrode screws were placed in the cortex and secured to the head mount with silver epoxy (Pinnacle Technology, 8226). The two EMG electrodes were inserted bilaterally into the nuchal muscles. The base of the head mount and surrounding skin was secured with dental acrylic. Buprenorphine (0.05mg/kg) and saline were administered i.p.. Mice were allowed to recover, singly housed, for four days in Pinnacle cages (Pinnacle Technologies). 0.5Hz low pass filter preamplifiers (Pinnacle Technologies, 8202-SL) were connected to the EEG/EMG head mount and the mice were allowed to habituate for

24 hours. EEG/EMG recordings were collected in the following 24 hours using Sirenia acquisition software equipped with infrared video monitoring (Pinnacle Technologies). EEG/EMG waveforms were analyzed as described in Papouin et al., 2017. Briefly, traces were analyzed by 10s epochs. Three frequency bands were analyzed for each epoch: δ (0.75-4Hz), θ (4-8Hz), and α (8-12Hz). These frequency bands in the EEG and the EMG amplitude were used to assign a vigilance state to each epoch: rapid eye movement (REM), non-REM, wakefulness, and quiet wakefulness.

3.3 Results

To assess the role of both neurons and astrocytes in mediating cholinergic signaling via the α7nAChR, we generated astrocyte (A-α7nAChR KO) and neuron (N-α7nAChR KO) specific conditional knockout lines using promoter specific, inducible creERT lines and the loxP system. In order to confirm that recombination was induced in the correct cell type, these KO lines were additionally crossed with the Ai9 line, which provided a fluorescent reporter allowing visualization of recombination activity via the expression of tdTomato. Cells which had undergone tamoxifen-induced recombination in the A-α7nAChR KO line had a high percentage of co-localization with glial fibrillary acidic protein (GFAP) and none with the neuronal nuclei marker (NeuN) in the CA1 region of the hippocampus (92.43%, N=6 mice, 124 cells and 0%, N=6 mice, 166 cells, respectively, Figure 3.1). tdTomato+ cells in the CA1 of N-α7nAChR KO mice showed no overlap with GFAP, but a high overlap with NeuN labeling (0%, N=5 mice, 294 cells, and 99.78%, N=5 mice, 364 cells, respectively, Figure 3.2). Both control (Glast or CamK-creERT$^{+/-}$, α7nAChR$^{+/+}$, and Ai9$^{f/+ \text{ or } f/f}$) and KO (Glast or CamK-creERT$^{+/-}$, α7nAChR$^{f/f}$, and Ai9$^{f/+ \text{ or } f/f}$) mice were used for quantification of recombination and

specificity. There was no significant difference in CA1 morphology, recombination rates, or specificity between the KO and control mice (data not shown).

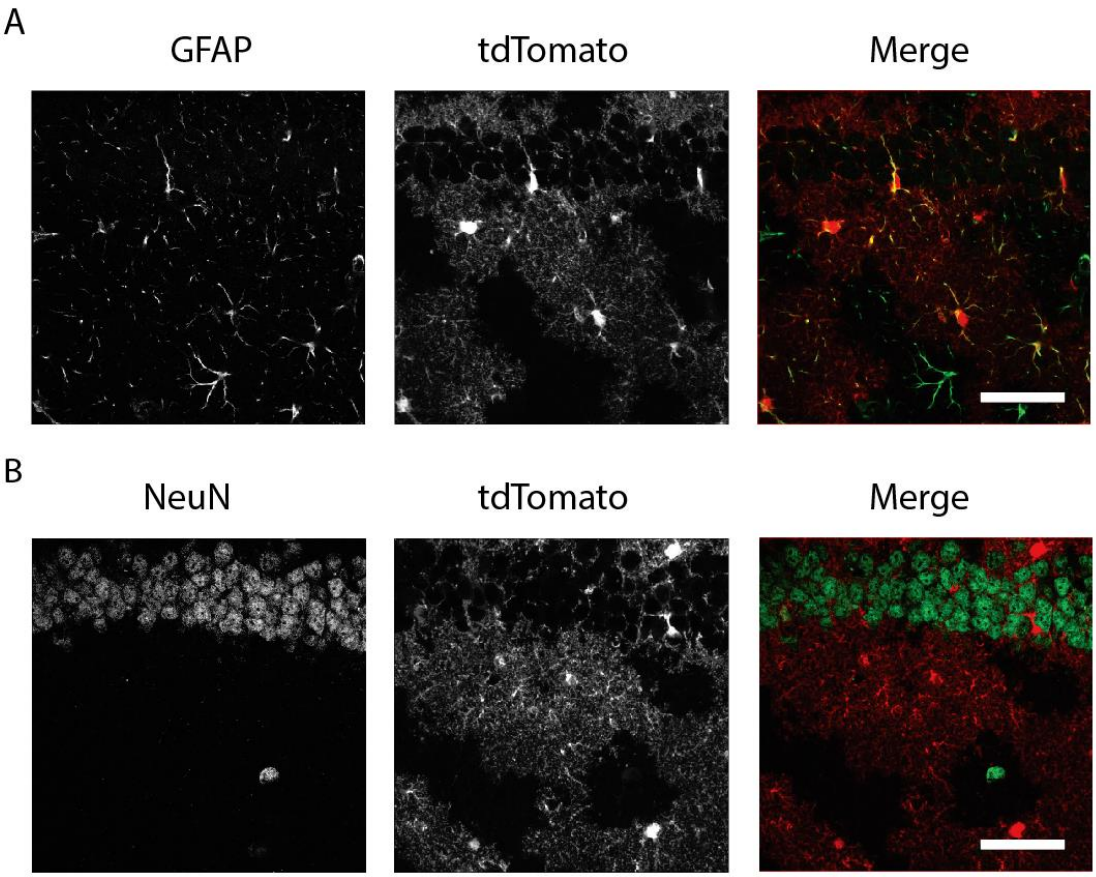

Figure 3.1: Specificity of GlastcreERT driven recombination in CA1 astrocytes. Representative images of GlastcreERT x α7nAChRflox x Ai9 floxed tdTomato reporter mice after five days of Tamoxifen treatment (Sigma, 75mg/kg). Images were taken using 60x magnification objective (N.A.=1.4) on a Nikon confocal microscope with gamma adjusted to view the fine processes. A) GFAP labeling astrocyte processes overlaps with tdTomato^{+} cells. B) NeuN labeling neuronal cell bodies does not overlap with tdTomato^{+} cells. Both control (Glast-creERT$^{+/-}$, α7nAChR$^{+/+}$, Ai9$^{f/+ \text{ or } f/f}$) and KO (Glast-creERT$^{+/-}$, α7nAChR$^{f/f}$, Ai9$^{f/+ \text{ or } f/f}$) mice were used. Scale bar = 50µm.

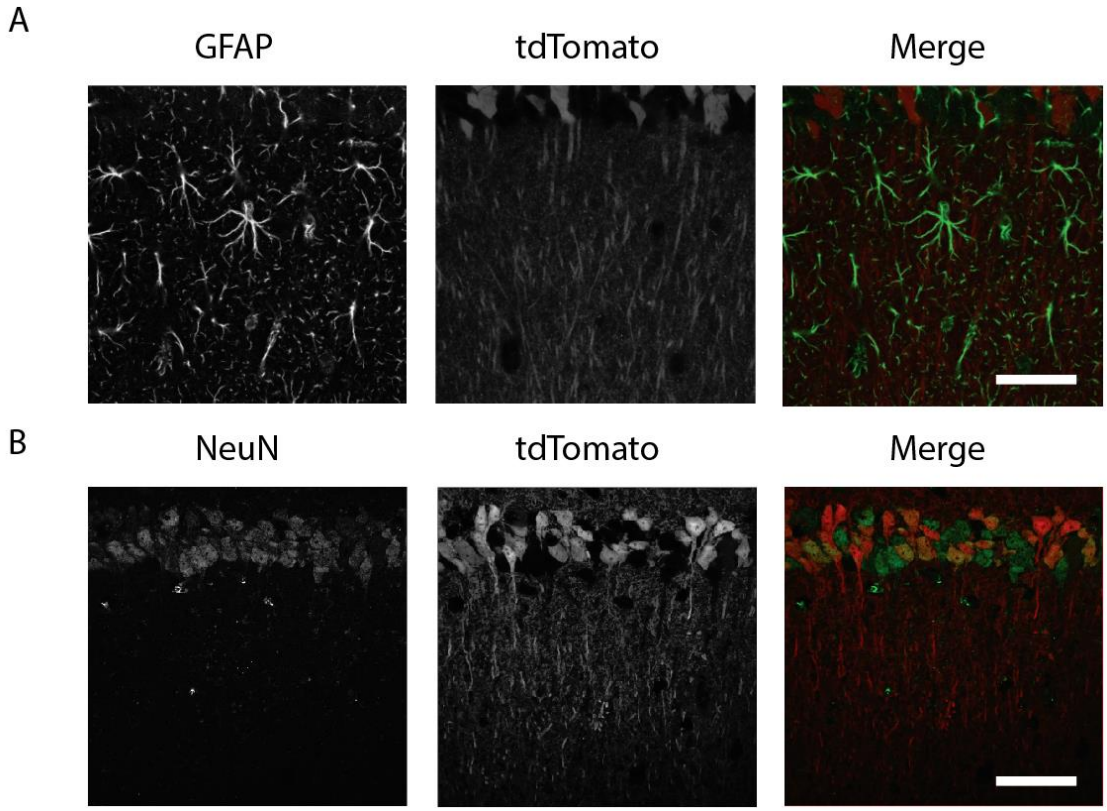

Figure 3.2: Specificity of CamK-creERT driven recombination in CA1 neurons. Representative images of CamK-creERT x α7nAChRflox x Ai9 floxed tdTomato reporter mice after five days of Tamoxifen treatment (Sigma, 75mg/kg). Images were taken using 60x magnification objective (N.A.=1.4) on a Nikon confocal microscope. A) GFAP labeling astrocyte processes do not overlap with tdTomato^{+} cells. B) NeuN labeling neuronal cell bodies does overlap with tdTomato^{+} cells. Both control (CamK-creERT$^{+/-}$, α7nAChR$^{+/+}$, Ai9$^{f/+ \text{ or } f/f}$) and KO (CamK-creERT$^{+/-}$, α7nAChR$^{f/f}$, Ai9$^{f/+ \text{ or } f/f}$) mice were used. Scale bar = 50µm.

In vivo microdialysis with video monitoring experiments were performed on adult A- and N-α7nAChR KO mice of both sexes. There was a significant decrease in hippocampal D-serine levels between ZT0 and ZT6 in male A-α7nAChR KO mice (p=0.003, Figure 3.4C), but loss of the α7nAChR had no effect on D-serine levels in A-α7nAChR KO female mice (p=0.561, Figure 3.4F) or N-α7nAChR KO mice (males: p=0.341, Figure 3.4B, females: p=0.66, Figure 3.4F). Since D-serine can be synthesized from L-serine via serine racemase[197], we also measured levels of L-serine in the A- and N-α7nAChR KO lines to investigate potential changes in the D-serine production

pathway. There were no differences in hippocampal L-serine levels in either sex of the A- or N-α7nAChR KO lines (A-α7nAChR KO males: p=0.418, Figure 3.4D, A-α7nAChR KO females: p=0.451, Figure 3.4H, N-α7nAChR KO males: p=0.113, Figure 3.4D, N-α7nAChR KO females: p=0.853, Figure 3.4H). Papouin et al., 2017 showed that D-serine levels in the hippocampus correlate with activity levels during microdialysis[1]. We saw no difference in activity levels during microdialysis, suggesting that changes in activity were not responsible for the changes seen in D-serine levels (A-α7nAChR KO males: p=0.409, Figure 3.4C, A-α7nAChR KO females: p=0.718, Figure 3.4G, N-α7nAChR KO males: p=0.355, Figure 3.4C, N-α7nAChR KO females: p=0.358, Figure 3.4G). Since microdialysis experiments were performed during the light phase when mice are normally sleeping, it was important to determine whether we were causing sleep deprivation during the microdialysis protocol. We video monitored mice under the same conditions as the microdialysis experiment, without the cannula implantation surgery or the presence of an experimenter between ZT0 and ZT6. There was no difference in the average percent of time undisturbed mice were active compared to mice undergoing microdialysis (p=0.682, Figure 3.5). These results show that the α7nAChR on astrocytes is crucial for sensing cholinergic tone and tuning extracellular D-serine availability.

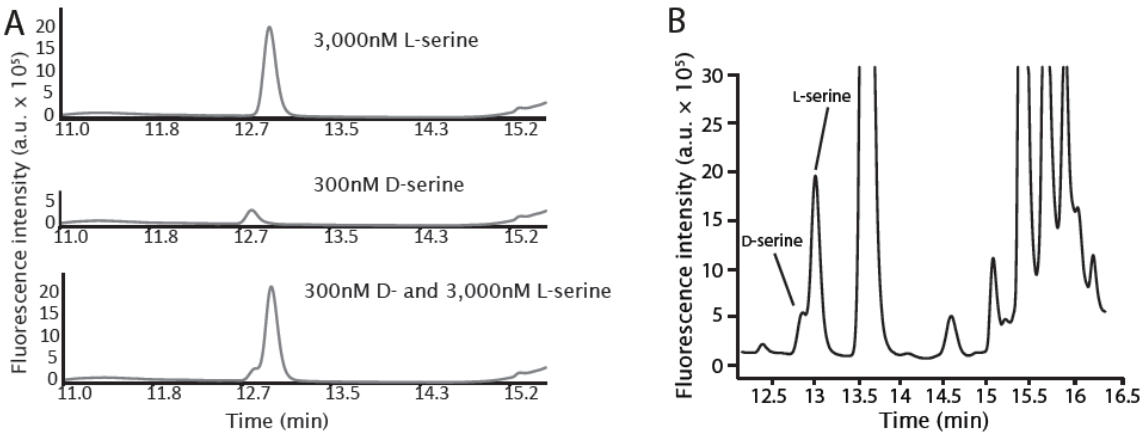

Figure 3.3: Measuring D- and L-serine using HPLC.

A) Representative chromatograms of 3,000nM of L-serine alone, 300nM D-serine alone, and D- and L-serine combined in solution. B) Representative trace showing D- and L-serine separated in a microdialysis sample.

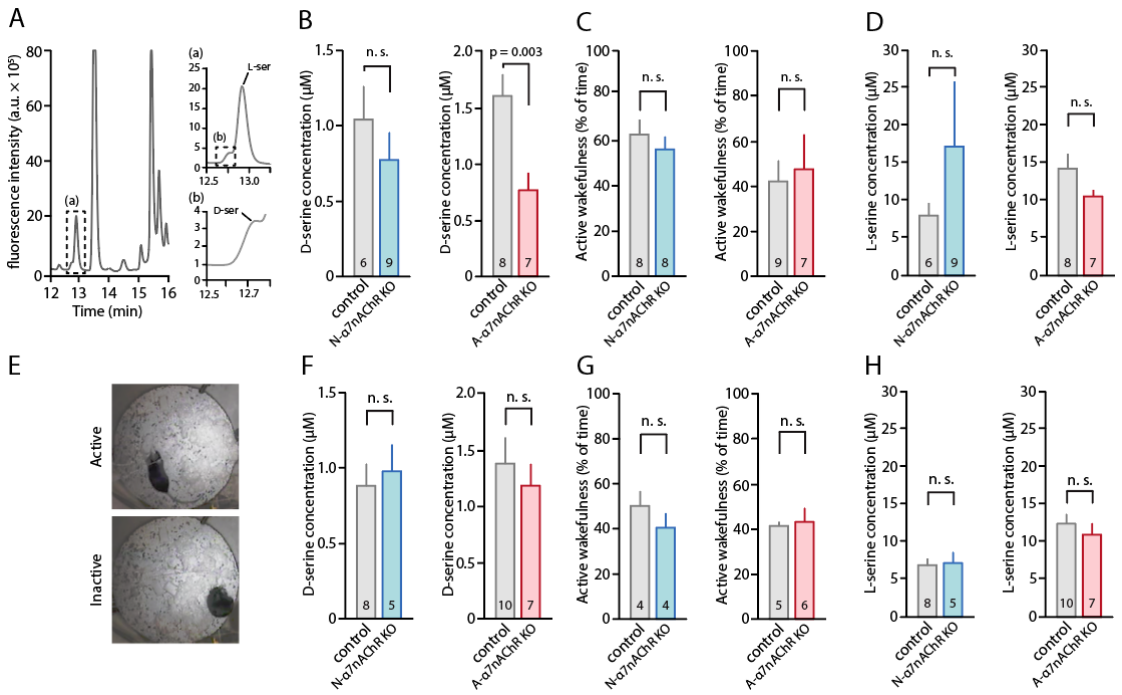

Figure 3.4: Astrocytic α7nAChRs are necessary for maintaining D-serine levels in the hippocampus of male mice.

A) Representative HPLC traces highlighting the D- and L-serine peaks in a hippocampal microdialysis sample. B) Average D-serine levels measured from microdialysis of the hippocampus between ZT0 and 6 in male A-α7nAChR KO (p=0.003) and male N-α7nAChR KO (p=0.341) mice. C) Average percent of time the mice were active during

the corresponding microdialysis experiments in B (p=0.355 and p=0.409, respectively). D) Average L-serine levels corresponding to B (p=0.113 and p=0.418, respectively). E) Screen shots from video monitoring during microdialysis illustrating the active and inactive state. F) Average D-serine levels measured from microdialysis of the hippocampus between ZT0 and 6 in female N-α7nAChR KO (p=0.66) and A-α7nAChR KO (p=0.561) and mice. G) Average percent of time the mice were active during the corresponding microdialysis experiments in F (p=0.358 and p=0.718, respectively). H) Average L-serine levels corresponding to F (p=0.853 and p=0.451, respectively). Statistics: t-test. Error bars = SEM.

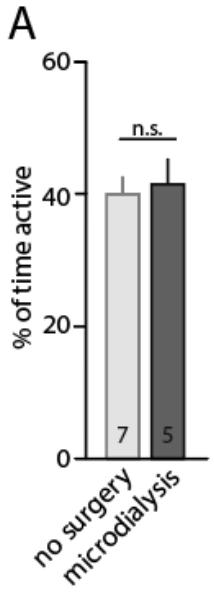

Figure 3.5: Microdialysis recording from ZT0-6 does not alter activity.

A) The microdialysis recording does not alter in the amount of time mice are active between ZT0 and 6 (p=0.682). Statistics: t-test. Error bars = SEM.

Cholinergic signaling pathways are well conserved throughout evolution and are essential for tuning the gain of neuronal circuitry so that it can perform the appropriate functions in a wide range of contexts. In order to determine what behaviors the α7nAChR modulates through astrocytes and neurons, we looked at sensory gating, learning, and memory behaviors in our A- and N-α7nAChR KO male mice. Both A- and N-α7nAChR KO lines responded to acoustic startle stimuli at the same level as their controls (p=0.336, Figure 3.6A and p=0.0975, Figure 3.6D, respectively). The N-α7nAChR KO mice tended

to show a deficit in PPI (p=0.0509, Figure 3.6E), whereas the A- α7nAChR KO mice showed a significant deficit in their ability to adjust their response to a startle stimulus in the PPI experiment (p=0.0058, Figure 3.6B). To assess short-term social memory in both α7nAChR cKO lines, we performed the three chamber social choice test. Both A- and N-α7nAChR KO mice and their littermate controls displayed normal social preference behavior (N-α7nAChR control: p<0.0001, N-α7nAChR KO: p=0.0002, A-α7nAChR control: p<0.0001, A-α7nAChR KO: p<0.0001, Figure 3.6$C_{2 \text{ and } 3}$). A-α7nAChR KO mice showed a deficit in short-term social memory in the third trial where they spent an equal amount of time in both the chamber with the novel mouse and the chamber with the familiar mouse (N-α7nAChR control: p<0.0001, N-α7nAChR KO: p=0.0011, A-α7nAChR control: p<0.0001, A-α7nAChR KO: p=0.419, Figure 3.6$F_{2 \text{ and } 3}$). The three chamber social choice test does not assess learning or long-term memory, so to directly look at these behaviors we performed contextual fear conditioning experiments. Both A- and N-α7nAChR KO mice exhibited learning by acquiring a freezing response to a context in which they received foot shocks (Figure 3.6G and J). The A-α7nAChR KO mice were slower to acquire this response, however, suggesting a deficit in learning (p=0.0015, Figure 3.6J). Since both lines acquired the same level of freezing as their controls during the training day, we were able to test their retrieval of this contextual fear memory 24 hours later. N-α7nAChR KO mice exhibited normal memory retrieval compared to their littermate controls (p>0.05, Figure 3.6H), whereas A-α7nAChR KO mice showed a deficit in memory retrieval at 24 hours by freezing significantly less than their littermate controls when reintroduced to the training context (p=0.0228, Figure 3.6K). There was no change in baseline freezing in a novel context, as shown for both N-

and A-α7nAChR KO mice 48 hours later in Context B ($p>0.05$, Figure 3.6I and $p>0.05$, Figure 3.6L, respectively). This deficit in contextual fear memory retrieval could be attributed to differences in sleep or activity in the A-α7nAChR KO mice. To investigate this, we looked at EEG/EMG recordings of A-α7nAChR KO mice and their controls as well as home cage locomotion over a 24 hour period. There were no differences in the power spectrum, time spent in each vigilance state, number of bouts, bout duration, or locomotion between the A-α7nAChR KO mice and their controls (Figure 3.7 and 3.8).

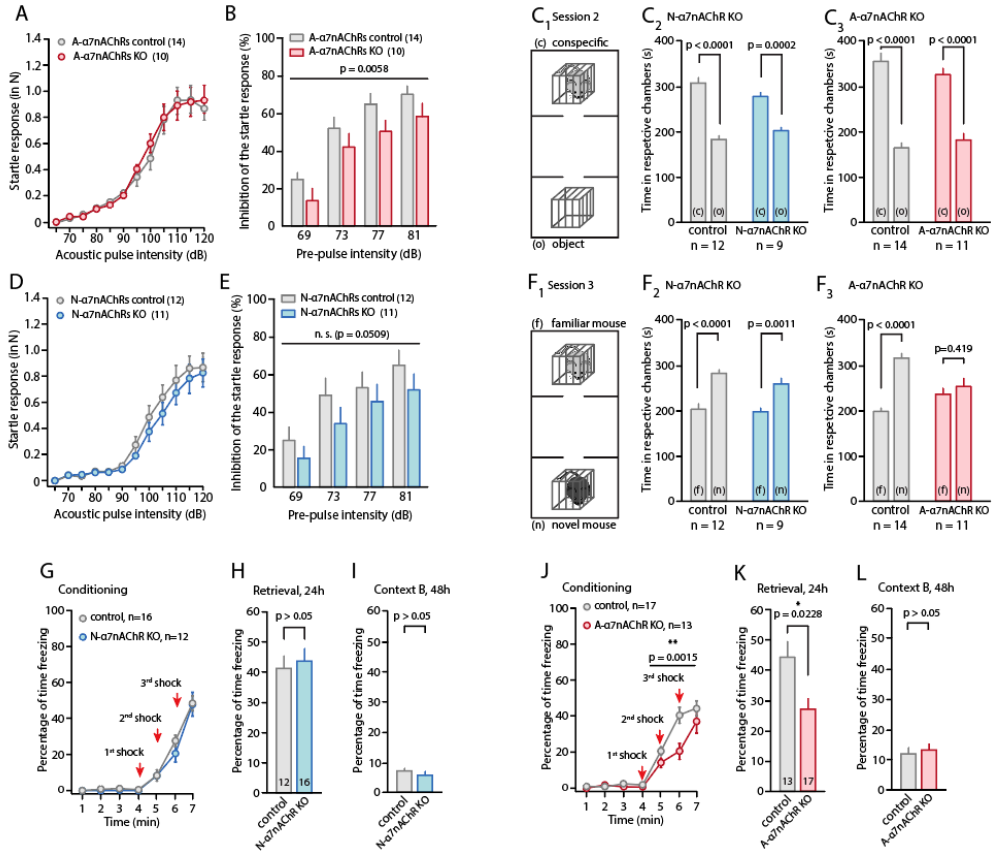

Figure 3.6: α7nAChRs modulate sensory gating, learning, and memory behaviors.

A) A-α7nAChR KO mice show no difference in the startle response input output curve compared to controls (p=0.336), but a deficit pre pulse inhibition (PPI) at ZT4 (p=0.0058, B). D) N-α7nAChR KO mice show no difference in the startle response input output curve compared to controls (p=0.0975) and a trend towards decreased PPI, but it does not reach significance (p=0.0509, E). Statistics: two way ANOVA, post hoc Bonferroni's test for multiple comparisons. C_1) Diagram of the three chamber set up for the second session. Both N- (C_2) and A- (C_3) α7nAChR KO mice and their controls exhibit preference for social novelty by spending more time in the chamber with the conspecific mouse. F_1) Diagram of the three chamber set up for the third session. A-α7nAChR KO mice do not exhibit the preference for social novelty when a novel mouse is introduced (F_3). N-α7nAChR KO mice exhibit a significant preference for the second novel mouse (F_2). Statistics: two way ANOVA, post hoc Bonferroni's test for multiple comparisons. G and J) both N- and A-α7nAChR KO mice are able to form a fear memory for a context in which they receive a foot shock. J) A-α7nAChR KO mice learn significantly slower than controls. Statistics: two way ANOVA. H) N-α7nAChR KO mice show the same level of freezing behavior when reintroduced to this context (p=0.517). K) A-α7nAChR KO mice freeze less than controls when reintroduced to this context (p=0.0228). I and L) Both N- and A-α7nAChR KO mice and their controls exhibit baseline levels of freezing when introduced to a second novel environment 48 hours later. Statistics: Student's t-test. Error bars = SEM.

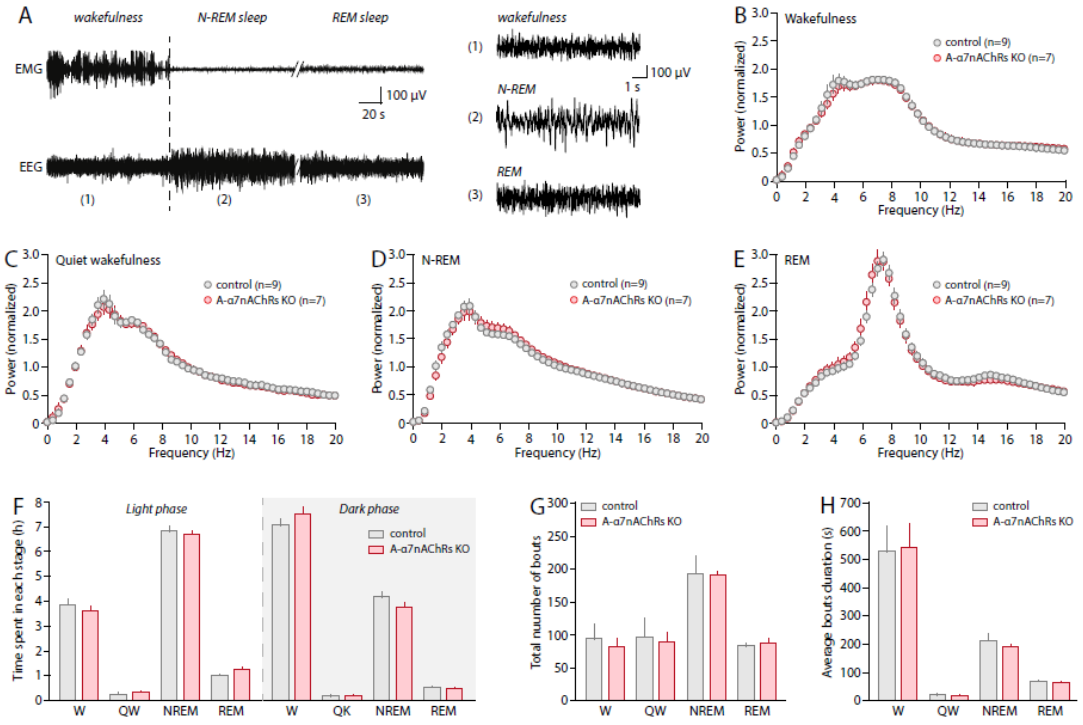

Figure 3.7: Cholinergic signaling through astrocytes does not mediate sleep behavior. A) Representative EEG and EMG traces during wakefulness, non-REM, and REM sleep. B-E) Normalized power spectra showing no difference between A- α7nAChR KO mice and controls. F) Average time spent in each phase per mouse. G) Total number of bouts in each phase. H) Average bout duration across the 24 hour period. There was no difference between controls and A- α7nAChR KO mice in any of these parameters.

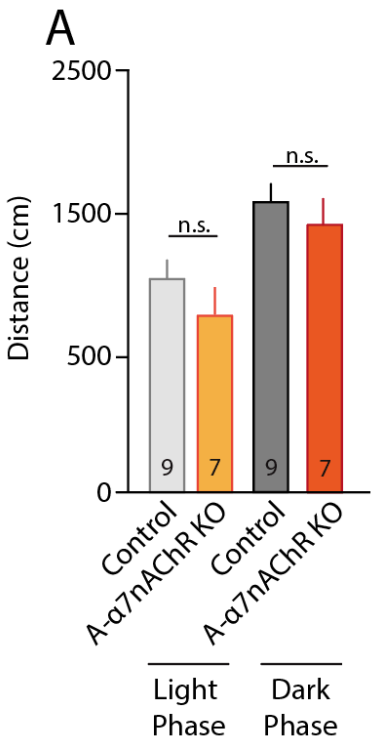

Figure 3.8: A-α7nAChR KO mice do not travel longer distances than control mice.

A) Home cage measurements of distance traveled measured by beam crosses. There is no difference between the male A-α7nAChR KO mice and their controls in either the light or the dark phase (p=0.236 and p=0.671, respectively). Statistics: t-test. Error bars = SEM.

To further investigate the specific role of astrocytes in tuning neuronal circuits to cholinergic signals, we looked at additional behaviors in the A-α7nAChR KO mice. There was no difference in body weight (p=0.092, Figure 3.10), suggesting that metabolism and feeding behavior was not grossly altered. To assess anhedonia, we performed the sucrose preference test. There were no differences in daily liquid consumption or sucrose preference between the A-α7nAChR KO mice and their controls (Figure 3.9A). Prior to the sucrose preference test, mice were moved into new singly housed cages. Nesting behavior was assessed at 4 and 48 hours after the move. A-α7nAChR KO mice showed a significant deficit in nesting behavior at the 4 hour time point, but were able to produce the same level of nesting as their controls by 48 hours (4

hours: p=0.034, 48 hours: p>0.05, Figure 3.9H). To determine if this initial deficit in nesting behavior was due to altered anxiety levels in the A-α7nAChR KO mice, we performed the elevated plus maze. While the A-α7nAChR KO mice exhibited a trend towards spending less time in the open arms, there was no significant difference from controls (p=0.0801, Figure 3.9D). The additional investigation of the A-α7nAChR KO line shows that the main behavioral deficits are in NMDAR dependent behaviors.

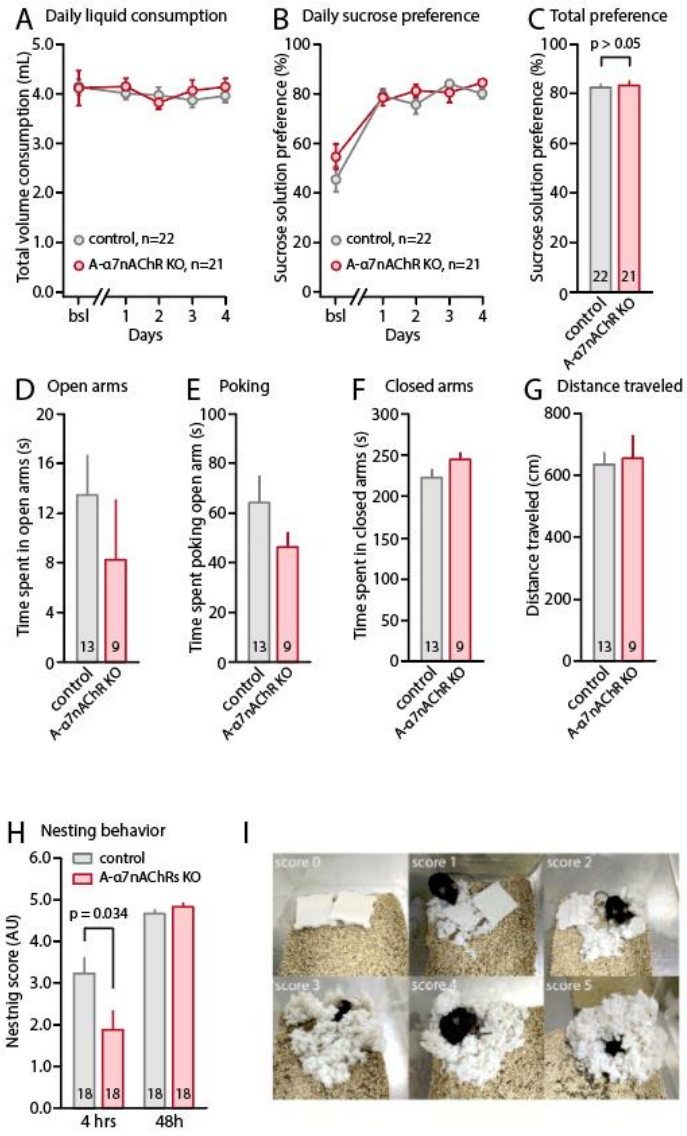

Figure 3.9: Behavioral profiling of A- α7nAChR KO mice
A) A- α7nAChR KO mice consumed the same amount of liquid over the five day experiment compared to controls and the same amount of sucrose solution, B). C) Shows no difference in sucrose preference over the four days of testing. D and E) A- α7nAChR KO mice did not spend significantly more time in (Mann Whitney, p=0.0801) or poking into the open arms of the elevated plus maze. They also did not show significant differences from control sin time spent in the closed arms or total distance traveled, F and G, respectively. H) A- α7nAChR KO mice are slower to nest build when first placed in a single-housed clean cage. This difference is gone by 48 hours. I) Representative images of each nesting score from 0-5. Statistics: Student's t-test, unless otherwise specified. Error bars = S.E.M.

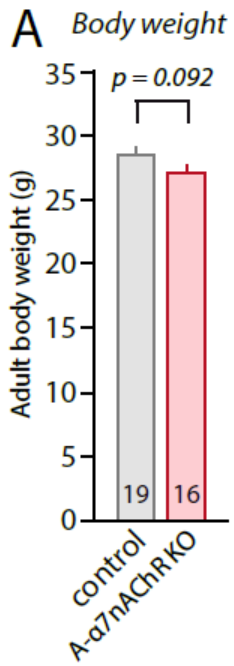

Figure 3.10: α7nAChRs on astrocytes do not modulate adult bodyweight.

A) A- α7nAChR KO mice do not have significantly different bodyweights than their littermate controls in adulthood. Statistics: Student's t-test. Error bars = S.E.M.

Our baseline behavioral studies show that astrocytes are responsible for sensing cholinergic signaling through the α7nAChR and that this results in modulation of learning and memory behaviors. To determine whether D-serine is the downstream molecule responsible for the behavioral deficits seen in the A-α7nAChR KO mice, we performed a D-serine rescue experiment. To confirm that i.p. injections of D-serine increase hippocampal D-serine levels within the time we are testing, we performed microdialysis after injecting saline, 50, or 100mg/kg D-serine i.p. and found that both doses significantly increased D-serine, but not L-serine, levels in the hippocampus (50mg/kg: $p=0.009$, 100mg/kg: $p<0.01$, Figure 3.11A). For the rescue experiments, A-α7nAChR KO and control mice were injected with either 100mg/kg D-serine one hour before contextual fear conditioning. 24 hours later, retrieval of the fear memory was

tested by reintroducing the mice to the context in which they were shocked and measuring the amount of freezing. A-α7nAChR KO mice now exhibited the same level of freezing as control mice (Figure 3.11C).

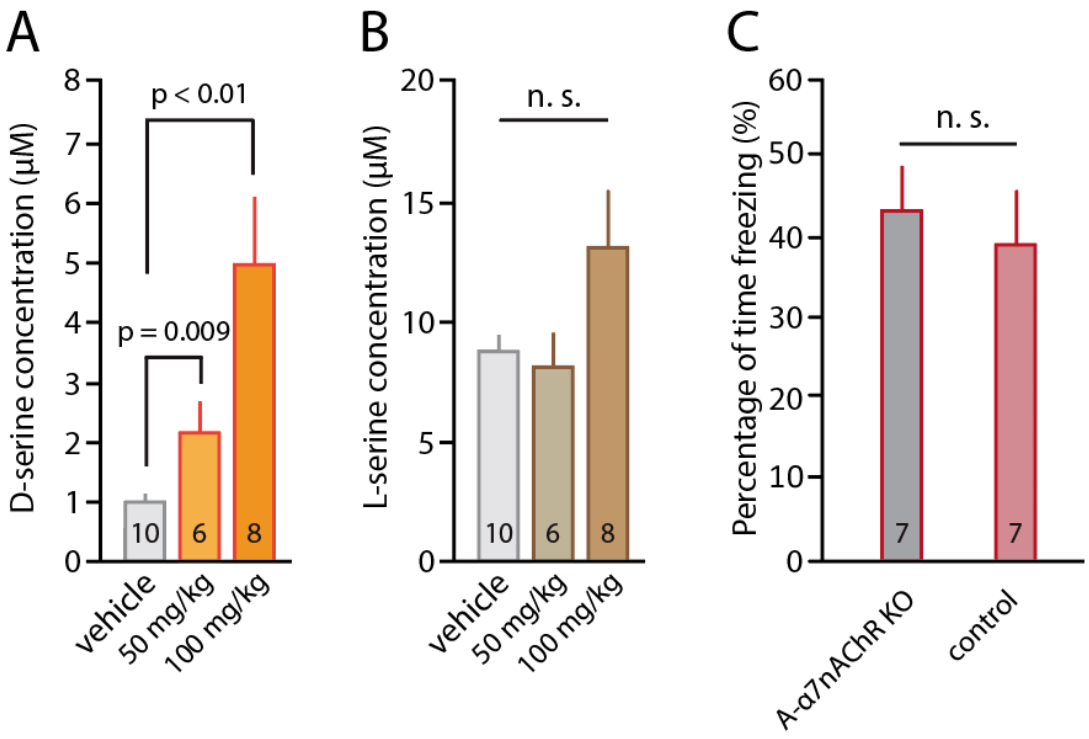

Figure 3.11: Intraperitoneal injections of D-serine significantly increase hippocampal D-serine levels.
A) Both 50mg/kg and 100mg/kg D-serine i.p. at ZT0 significantly increase the amount of D-serine measured in the hippocampus from ZT2-6. B) There is no significant change in L-serine levels after ZT0 D-serine injections (p=0.081). C) Treating A-α7nAChR KO mice with 100mg/kg D-serine 1 hour prior to fear contextual fear conditioning rescues the deficit in fear memory retrieval 24 hours later compared to controls (p=0.635). Statistics: t-test. Error bars = SEM.

Since D-serine levels are decreased in cognitive disorders such as schizophrenia[127], it is crucial to better understand pathways that can increase D-serine in vivo. Using optogenetics paired with in vivo microdialysis, we activated the cholinergic neurons projecting to the hippocampus while simultaneously collecting dialysis samples from the hippocampus. Chat-ChR2+ mice showed an increase in D-serine levels during

the two hours of stimulation compared to ChR2- controls (p=0.007, Figure 3.12B). Recovery samples were collected two hours post stimulation and we observed that D-serine returned to baseline levels in the ChR2+ mice (p=0.372, Figure 3.12B).

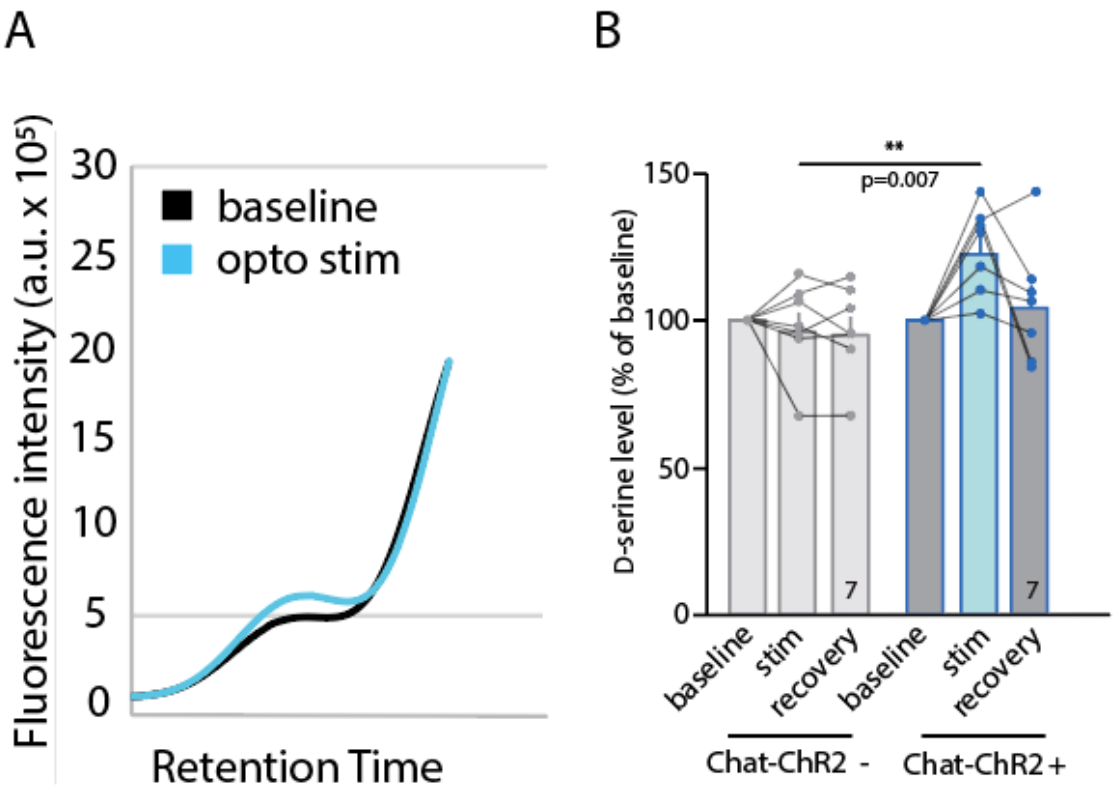

Figure 3.12: Optogenetic stimulation of cholinergic projections increases hippocampal D-serine levels.
A) Representative HPLC trace showing D-serine levels from hippocampal microdialysis samples before and after optogenetic stimulation of the cholinergic projections. B) Average hippocampal. D-serine levels before, during, and after optogenetic stimulation of the cholinergic projections. D-serine is increased in Chat-ChR2 + compared to controls during optogenetic stimulation. This increase is reversible, since there is no difference between D-serine levels in the recovery phase (p=0.372). Statistics: Student's t-test. Error bars = S.E.M.

3.4 Discussion

With these results, we demonstrate that astrocytes sense cholinergic tone and modulate learning and memory, but not for sleep, hedonic, or anxiety behaviors. This expands on our understanding of the astrocytes role at the tripartite synapse. Previously,

we showed that astrocytes were the key mediators sensing cholinergic tone and adjusting D-serine availability in a wakefulness dependent manner[1]. Here, we have tested the importance of this pathway at the behavioral level. We have shown that the astrocyte's ability to sense cholinergic tone through the α7nAChR is necessary for not only maintaining D-serine levels, but for exhibiting normal hippocampal, NMDAR dependent behaviors. Equally important for the understanding of cholinergic mechanisms and future drug discovery efforts, we have shown that this α7nAChR dependent pathway is not necessary for sleep, anxiety, or hedonic behaviors. Activating the cholinergic neurons in the medial septum can effectively increase D-serine levels in the hippocampus. These findings highlight the therapeutic potential of this pathway in diseases where there are deficits in D-serine, learning, and/or memory. It also suggests that current cholinergic modulators rely on the activation of astrocytes to produce their nootropic effects.

While broad cholinergic activators have been approved and prescribed for their cognitive enhancement effects[75, 76], more specific agonists and partial agonists for the α7nAChR have also been recently investigated[23, 80]. While there have been challenges in the development of these drugs due to their activation of cholinergic receptors in the periphery[63], our work can help better inform future drug discovery efforts in this field in two ways. First, we show that the α7nAChR is necessary for normal performance on learning and memory behaviors, specifically. This should be carefully considered when designing behavioral paradigms to test the efficacy of α7nAChR activators. Second, we show that the α7nAChR is not necessary for maintaining D-serine levels in female mice. This has huge implications for understanding sex ratios in diseases such as schizophrenia, clinical trial design, and patient treatment. Others have shown that there are sex

differences in D-serine related enzymes[198]. It is also known that the NMDAR antagonist Ketamine has differential effects in males versus females due to estrogen and progesterone signaling[199]. Lastly, our work highlights the importance of experimental and clinical trial design when investigating the activation of the cholinergic pathway. Since cholinergic signaling is high after periods of wakefulness or rapid eye movement sleep (REM) and low after periods of non-REM sleep[200], it is important to consider the time of day and the behavioral state of the mouse or human prior to activating the cholinergic system and test learning and memory behaviors.

It has been known that astrocytes play key roles at the synapse[83]. Emerging evidence highlights their role in sensing more global signals, like neuromodulators, responding with increased intracellular calcium activity, and translating the contextual tone into altered availability of gliotransmitters at the synapse[10, 88]. Though neurons also play a role in sensing acetylcholine levels directly[8, 9], our results show that activation of the α7nAChR on neurons is not necessary for tuning performance in learning and memory behaviors. Further experiments are required to investigate the downstream effects of activating the α7nAChR on neurons and ultimately which behaviors that pathway is responsible for modulating. While many previous studies have focused on the production, release, and uptake of D-serine in astrocytes versus neurons[111, 112], the effect of activating each cell type specifically and how it impacts behavior will be the most important results for informing future drug discovery efforts.

Our results show that a new class of glial specific drug targets could hold significant potential for the treatment of disorders, such as schizophrenia, while also overcoming the challenges faced with current small molecules in the pipeline. As

previously mentioned, α7nAChR agonists and partial allosteric modulators have been clinically developed for the treatment of Alzheimer's disease and schizophrenia[23, 80]. Off target effects and desensitization of the receptor have caused problems for these molecules, however[63]. D-serine administration itself can affect both positive and negative symptoms of schizophrenia[123], but has to be given at such high doses that it becomes toxic. Since we have demonstrated that the α7nAChR on astrocytes plays a key role in regulating D-serine availability, future drug discovery efforts could focus on developing activators of key players that act downstream of the α7nAChR on astrocytes to modulate D-serine release. It is also likely that other parallel receptor pathways are able to activate D-serine release from astrocytes. Previous work in hippocampal slices has shown that the α7nAChR rather than other cholinergic or neuradrenergic receptors is the key mediator, but it is possible that other endogenous systems, such as the dopaminergic and hormonal pathways, or designer systems can play a role in D-serine regulation when activated in the hippocampus or even other brain regions.

Chapter 4: General Discussion

This work has explored a novel role for astrocytes in the brain. By establishing and validating multiple in vivo techniques and genetic mouse lines, we have shown that astrocytes modulate neuronal networks by sensing cholinergic signaling through the α7nAChR and modulating D-serine levels. Our results have uncovered a novel cholinergic pathway, opened the door for a new class of drug targets, and allows for better understanding of the cholinergic modulators currently used in the clinic.

By first establishing the technique of in vivo microdialysis, I was able to sample D-serine levels in the hippocampus in awake and behaving mice. Measuring D-serine under unanaesthetized conditions was crucial for future experiments, since it is known that anesthesia significantly alters astrocyte calcium signaling[201]. In order to investigate the activation of the cholinergic system in vivo, I also paired in vivo microdialysis with optogenetic stimulation to look at the validity of activating the cholinergic system as a treatment option for disorders with low D-serine levels. Others have used either indirect measurements (NDMAR current recordings) or chemical biosensors to measure D-serine levels[1, 202]. The most accurate and sensitive measurement of D-serine concentrations is through fluorescent detection and HPLC[203]. In establishing this technique in the lab, I was able to separate D- and L-serine from microdialysis samples and measure their concentrations independently. In the first application of these tools, I was able to validate the in situ finding that D-serine levels in the hippocampus correlate with activity and wakefulness. I also validated the use of video monitoring activity levels during microdialysis as a measurement for wakefulness through its strong correlation to measurements of wakefulness using EEG/EMG recordings.

Once the in vivo correlation between D-serine and activity was confirmed, I narrowed in on the mechanism of this pathway by developing cell type specific knockout mouse lines for the α7nAChR gene, CHRNA7. Using astrocyte (A- α7nAChR) and neuron (N- α7nAChR) specific conditional knockout (KO) lines, I was able to assess the role of each cell type in sensing cholinergic tone and modulating D-serine levels. The α7nAChR pathway was not involved in regulating activity levels between ZT0 and ZT6 or L-serine levels. The activation of α7nAChRs on astrocytes was necessary for maintaining D-serine levels in the hippocampus of male mice, but not necessary in female mice. The loss of astrocytic α7nAChRs in the male A- α7nAChR mice had significant consequences for performance in learning and memory behavioral tasks. These deficits can be explained by hypofunctioning of the NMDAR. Behaviors that do not primarily rely on NDMAR signaling were not affected (i.e. sleep, hedonia, and anxiety).

Though acetylcholine was one of the very first neurotransmitters described[2], we still do not fully understand the mechanisms underlying its role as a neuromodulator. Our findings not only showed a novel role for specifically the α7nAChR in acetylcholine's neuromodulatory activity, but we also identified that the activation of astrocytes is necessary for the downstream tuning of NMDARs and neuronal networks. This finding could lead to a new class of drug targets focused on astrocyte activation. Astrocytes have been known to participate in signaling at the synapse[83] and exhibit altered calcium signaling in response to neuromodulators[10, 88]. Our work adds to the growing body of evidence suggesting that astrocytes sense wide range signals, integrate that information, and serve as gate keepers for neuronal networks, allowing them to perform the

appropriate functions in each brain state. As the key signaling molecule in this pathway, our work established an integral role for D-serine. Though alterations in D-serine levels have been shown in disease states[123, 126], the upstream mechanisms regulating its extracellular availability have remained a mystery. By identifying one such pathway, we can better modulate D-serine levels in both health and disease states. Another important implication from our findings involves differences between cellular mechanisms in male versus female brains. Sex differences have not been emphasized in many basic research studies where only male animals were used. Our data suggests that the mechanisms involving cholinergic signaling and D-serine regulation differ significantly between males and females. This could have serious implications for future drug development and the current use of cholinergic modulators in the clinic.

Previous work looking at the regulation of D-serine release, transport, and production has tried to assign clear roles for astrocytes and neurons in these processes[104-106]. Limited by the tools available and differences in the experimental designs have led to inconclusive results. Here, we have sought to investigate the cell type specific role of the α7nAChR specifically in extracellular D-serine availability in the hippocampus. Using the most specific and advanced tools available, we have shown that the α7nAChR on neurons is not necessary for maintaining hippocampal D-serine levels in male or female mice. The α7nAChR on astrocytes, however, is very necessary for maintaining hippocampal D-serine levels in male mice. It is possible that the α7nAChR on both cell types is partially responsible for modulating D-serine, but if neuronal α7nAChRs were a primary source of regulation, we would have expected to see compensation in the A-α7nAChR KO mice, which we did not. The degree to which D-serine was altered in the

A- α7nAChR KO mice also suggests that this is an important pathway for D-serine modulation. To date, there is only one other manipulation that has caused a more dramatic drop in in vivo D-serine levels: whole brain knockout of the enzyme that synthesizes D-serine, serine racemase[103]. Further experiments are needed to identify the machinery responsible for modulating D-serine downstream of α7nAChR activation on astrocytes. From our results, it is possible that activation of the α7nAChR is inducing shuttling of D- or L-serine to neurons which in turn affect extracellular levels. It is unlikely that this is the case, however, since blocking vesicular release from astrocytes also causes a decrease in D-serine levels, which cannot be rescued by exogenous application of L-serine[1]. D-serine uptake and degradation pathways could also be involved in this mechanism. To account for the decrease in D-serine levels that we measure with microdialysis, D-serine uptake and/or degradation would have to be potentiated. It is unlikely that knocking out a receptor that induced intracellular calcium transients would release inhibition on a transporter or the D-amino acid oxidase enzyme, but further studies using pharmacology or looking at enzyme levels could address this possibility.

Though we have shown that the cholinergic, α7nAChR pathway is important for modulating D-serine levels, it is possible that other neuromodulator or signaling pathways are able to play a similar role. Astrocytes express adrenergic receptors and have been shown to respond to changes in norepinephrine levels with altered calcium transients in vivo[88]. Through pharmacology, we have shown that the adrenergic receptors do not modulate D-serine as measured by NMDAR currents, however[1]. Astrocytes also express receptors for circulating hormones and dopamine[204-210]. Recent work in vitro has

shown that astrocytes respond to changes in dopamine concentrations via calcium transients and morphological changes[204]. Investigating astrocytic signaling pathways in vitro and with pharmacology limits the strength of the conclusions, however. Future work using cell type specific genetic knock out lines is needed to better understand astrocyte signaling in vivo and to determine whether other pathways are necessary or sufficient to modulate D-serine levels.

Our findings not only showed a novel mechanism for cholinergic signaling through astrocytes, but have also showed that the activation or suppression of this pathway could be a new therapeutic option for cognitive disorders where D-serine is dysregulated. Using both pharmacological and optogenetic activation, we were able to increase D-serine levels and subsequently potentiate NMDAR currents. This contributes to our mechanistic understanding of currently prescribed noortropic drugs targeting both cholinergic enzymes and the NMDAR in Alzheimer's disease as well as supports the notion that boosting this pathway could have therapeutic potential for other cognitive disorders such as schizophrenia. α7nAChR agonists and positive allosteric modulators have started to enter clinical trials[23]. At this point, there are still substantial hurdles that these molecules need to overcome before being approved for safe and effective use in patients. One of the largest challenges is peripheral activation of the α7nAChR. The α7nAChR is expressed in the gut[63] and the harmful effects of activating of this peripheral population has so far outweighed the benefits of the molecule's ability to act in the CNS. To circumvent this, Karuna Pharmaceuticals is investigating the co-administration of α7nAChR agonists with α7nAChR antagonists that cannot pass through the blood-brain barrier. The strength of the activation also has to be carefully considered. Over activation

of the α7nAChR can cause internalization. Therefore, future work with α7nAChR agonists or positive allosteric modulators should carefully consider cholinergic tone at the time of dosing, interactions with other medications, and the presence of other activators such as nicotine. In clinical trial for schizophrenia, smoking is a particularly difficult variable to control since more than 60% of schizophrenic patients smoke cigarettes[211].

Adding to the evidence showing that this pathway is important in the etiology of schizophrenia, it has been shown that direct oral dosing of D-serine can modulate both positive and negative symptoms in schizophrenic patients[123, 136-138]. As a treatment option, this could bypass the complexities of targeting the cholinergic system or the α7nAChR directly. Unfortunately, the amount that is needed to dose orally becomes toxic when given over time. Fueled by the growing appreciation for the 'Glutamate Hypothesis' and the role of the NDMAR in schizophrenia pathology, others have tried to target the enzyme that degrades D-serine, D-amino acid oxidase, to potentiate NMDAR functioning[212]. As the α7nAChR and D-serine pathway is repeatedly implicated in cognitive disease etiologies, the need to effectively target this pathway increases. The mechanistic understanding that our work contributes to this field opens valuable new avenues for drug development efforts.

Future research efforts in this area should focus on four key aspects. First, identifying the molecular pathway linking α7nAChR activation and D-serine release. Since α7nAChR is an ion channel primarily permeable to calcium, calcium sensitive molecules in astrocytes could be prime targets for activating D-serine release and avoiding the complications with targeting the α7nAChR itself. Second, a more complete, in vivo exploration of pathways that influence D-serine levels. Though most of the key

neuromodulatory signaling pathways have been investigated in situ or in vitro with pharmacology, finding receptor targets other than the α7nAChR that can be activated to increase D-serine levels in vivo would have great therapeutic potential. Third, more work is needed in many research areas, but particularly in regards to the α7nAChR and D-serine pathway, to determine the mechanistic differences between male and female brains. This line of research could explain why the prevalence for cognitive disorders differs drastically between males and females[213] or uncover new therapeutic targets by utilizing pathways that are active in one sex, but not the other. Fourth, the role of astrocytes in cognitive disease pathology and mediating the effects of noortropic drugs is just beginning to be explored. Further investigation into cell type specific involvement in both of these areas can lead to the development of more specific and effective drug targets.

Appendix

List of M.T. contributions by figure:

Figure 1.1: None
Figure 1.2: None
Figure 1.3: None
Figure 2.1: None
Figure 2.2: None
Figure 2.3: Performed EEG/EMG surgery and collected data.
Figure 2.4: All - performed MD surgery, collection, and analysis via HPLC. Performed EEG/EMG surgery and video monitoring comparison.
Figure 2.5: All - performed video monitoring and EEG/EMG comparison. Performed microdialysis surgery, sample collection, and analysis via HPLC.
Figure 2.6: None
Figure 2.7: None
Figure 2.8: None
Figure 2.9: None
Figure 2.10: None
Figure 2.11: None
Figure 2.12: None
Figure 2.13: None
Figure 2.14: None
Figure 2.15: None
Figure 3.1: Generated mice, collected brains, performed immunohistochemistry, imaged, and quantified.
Figure 3.2: Generated mice, collected brains, performed immunohistochemistry, imaged, and quantified.
Figure 3.3: Developed HPLC method for separating D- and L-serine in standard and microdialysis solutions.
Figure 3.4: Performed microdialysis surgery, collected samples, and analyzed D- and L-serine concentrations. Analyzed videos for activity measurement.
Figure 3.5: Collected videos and performed activity analysis.
Figure 3.6: Generated mice, performed input output curve, PPI experiment, and three chamber social choice test.
Figure 3.7: Performed EEG/EMG surgery and collected data.
Figure 3.8: Performed locomotion experiment and analyzed data.
Figure 3.9: Generated mice.
Figure 3.10: Generated mice.
Figure 3.11: Performed microdialysis surgery, collected samples, and analyzed D- and L-serine levels via HPLC. Injected mice with 100mg/kg D-serine prior to learning during the contextual fear conditioning protocol.
Figure 3.12: Performed optogenetic/microdialysis cannula implantation surgery, collected samples, and analyzed D-serine levels via HPLC.

Bibliography

1. Papouin T, Dunphy JM, Tolman M, Dineley KT, Haydon PG. Septal Cholinergic Neuromodulation Tunes the Astrocyte-Dependent Gating of Hippocampal NMDA Receptors to Wakefulness. *Neuron* May 17 2017;94(4):840-854 e847.

2. Dale D. Hydrogen ion concentrations limiting automaticity in different regions of the frog's heart. *J Physiol* Feb 27 1914;47(6):493-508.

3. Tansey EM. Henry Dale and the discovery of acetylcholine. *C R Biol* May-Jun 2006;329(5-6):419-425.

4. Zoli M, Jansson A, Sykova E, Agnati LF, Fuxe K. Volume transmission in the CNS and its relevance for neuropsychopharmacology. *Trends Pharmacol Sci* Apr 1999;20(4):142-150.

5. Okuda T, Haga T, Kanai Y, Endou H, Ishihara T, Katsura I. Identification and characterization of the high-affinity choline transporter. *Nat Neurosci* Feb 2000;3(2):120-125.

6. Ren J, Qin C, Hu F, Tan J, Qiu L, Zhao S, Feng G, Luo M. Habenula "cholinergic" neurons co-release glutamate and acetylcholine and activate postsynaptic neurons via distinct transmission modes. *Neuron* Feb 10 2011;69(3):445-452.

7. Mesulam MM. Cholinergic pathways and the ascending reticular activating system of the human brain. *Ann N Y Acad Sci* May 10 1995;757:169-179.

8. Changeux JP. Nicotine addiction and nicotinic receptors: lessons from genetically modified mice. *Nat Rev Neurosci* Jun 2010;11(6):389-401.

9. Drever BD, Riedel G, Platt B. The cholinergic system and hippocampal plasticity. *Behav Brain Res* Aug 10 2011;221(2):505-514.

10. Takata N, Mishima T, Hisatsune C, Nagai T, Ebisui E, Mikoshiba K, Hirase H. Astrocyte calcium signaling transforms cholinergic modulation to cortical plasticity in vivo. *J Neurosci* Dec 7 2011;31(49):18155-18165.

11. Navarrete M, Araque A. Basal synaptic transmission: astrocytes rule! *Cell* Sep 2 2011;146(5):675-677.

12. Changeux JP, Bertrand D, Corringer PJ, et al. Brain nicotinic receptors: structure and regulation, role in learning and reinforcement. *Brain Res Brain Res Rev* May 1998;26(2-3):198-216.

13. Picciotto MR, Caldarone BJ, Brunzell DH, Zachariou V, Stevens TR, King SL. Neuronal nicotinic acetylcholine receptor subunit knockout mice: physiological and behavioral phenotypes and possible clinical implications. *Pharmacol Ther* Nov-Dec 2001;92(2-3):89-108.

14. Fabian-Fine R, Skehel P, Errington ML, Davies HA, Sher E, Stewart MG, Fine A. Ultrastructural distribution of the alpha7 nicotinic acetylcholine receptor subunit in rat hippocampus. *J Neurosci* Oct 15 2001;21(20):7993-8003.

15. Mansvelder HD, Keath JR, McGehee DS. Synaptic mechanisms underlie nicotine-induced excitability of brain reward areas. *Neuron* Mar 14 2002;33(6):905-919.

16. Grady SR, Meinerz NM, Cao J, et al. Nicotinic agonists stimulate acetylcholine release from mouse interpeduncular nucleus: a function mediated by a different nAChR than dopamine release from striatum. *J Neurochem* Jan 2001;76(1):258-268.

17. Parikh V, Ji J, Decker MW, Sarter M. Prefrontal beta2 subunit-containing and alpha7 nicotinic acetylcholine receptors differentially control glutamatergic and cholinergic signaling. *J Neurosci* Mar 3 2010;30(9):3518-3530.
18. Wess J, Duttaroy A, Zhang W, et al. M1-M5 muscarinic receptor knockout mice as novel tools to study the physiological roles of the muscarinic cholinergic system. *Receptors Channels* 2003;9(4):279-290.
19. Douglas CL, Baghdoyan HA, Lydic R. Prefrontal cortex acetylcholine release, EEG slow waves, and spindles are modulated by M2 autoreceptors in C57BL/6J mouse. *J Neurophysiol* Jun 2002;87(6):2817-2822.
20. Raiteri M, Leardi R, Marchi M. Heterogeneity of presynaptic muscarinic receptors regulating neurotransmitter release in the rat brain. *J Pharmacol Exp Ther* Jan 1984;228(1):209-214.
21. Zhang W, Yamada M, Gomeza J, Basile AS, Wess J. Multiple muscarinic acetylcholine receptor subtypes modulate striatal dopamine release, as studied with M1-M5 muscarinic receptor knock-out mice. *J Neurosci* Aug 1 2002;22(15):6347-6352.
22. McCormick DA, Prince DA. Two types of muscarinic response to acetylcholine in mammalian cortical neurons. *Proc Natl Acad Sci U S A* Sep 1985;82(18):6344-6348.
23. Jones CK, Byun N, Bubser M. Muscarinic and nicotinic acetylcholine receptor agonists and allosteric modulators for the treatment of schizophrenia. *Neuropsychopharmacology* Jan 2012;37(1):16-42.
24. Galey D, Destrade C, Jaffard R. Relationships between septo-hippocampal cholinergic activation and the improvement of long-term retention produced by medial septal electrical stimulation in two inbred strains of mice. *Behav Brain Res* Feb 28 1994;60(2):183-189.
25. Buzsaki G, Csicsvari J, Dragoi G, Harris K, Henze D, Hirase H. Homeostatic maintenance of neuronal excitability by burst discharges in vivo. *Cereb Cortex* Sep 2002;12(9):893-899.
26. Huerta PT, Lisman JE. Bidirectional synaptic plasticity induced by a single burst during cholinergic theta oscillation in CA1 in vitro. *Neuron* Nov 1995;15(5):1053-1063.
27. Jiang L, Lopez-Hernandez GY, Lederman J, Talmage DA, Role LW. Optogenetic studies of nicotinic contributions to cholinergic signaling in the central nervous system. *Rev Neurosci* 2014;25(6):755-771.
28. Morishita H, Miwa JM, Heintz N, Hensch TK. Lynx1, a cholinergic brake, limits plasticity in adult visual cortex. *Science* Nov 26 2010;330(6008):1238-1240.
29. Overstreet DH. The Flinders sensitive line rats: a genetic animal model of depression. *Neurosci Biobehav Rev* Spring 1993;17(1):51-68.
30. Mineur YS, Obayemi A, Wigestrand MB, Fote GM, Calarco CA, Li AM, Picciotto MR. Cholinergic signaling in the hippocampus regulates social stress resilience and anxiety- and depression-like behavior. *Proc Natl Acad Sci U S A* Feb 26 2013;110(9):3573-3578.
31. Mark GP, Rada PV, Shors TJ. Inescapable stress enhances extracellular acetylcholine in the rat hippocampus and prefrontal cortex but not the nucleus accumbens or amygdala. *Neuroscience* Oct 1996;74(3):767-774.

32. Nijholt I, Farchi N, Kye M, et al. Stress-induced alternative splicing of acetylcholinesterase results in enhanced fear memory and long-term potentiation. *Mol Psychiatry* Feb 2004;9(2):174-183.
33. Slimak MA, Ables JL, Frahm S, Antolin-Fontes B, Santos-Torres J, Moretti M, Gotti C, Ibanez-Tallon I. Habenular expression of rare missense variants of the beta4 nicotinic receptor subunit alters nicotine consumption. *Front Hum Neurosci* 2014;8:12.
34. Wang JC, Grucza R, Cruchaga C, et al. Genetic variation in the CHRNA5 gene affects mRNA levels and is associated with risk for alcohol dependence. *Mol Psychiatry* May 2009;14(5):501-510.
35. English BA, Hahn MK, Gizer IR, et al. Choline transporter gene variation is associated with attention-deficit hyperactivity disorder. *J Neurodev Disord* Dec 2009;1(4):252-263.
36. Huerta PT, Lisman JE. Heightened synaptic plasticity of hippocampal CA1 neurons during a cholinergically induced rhythmic state. *Nature* Aug 19 1993;364(6439):723-725.
37. Bell LA, Bell KA, McQuiston AR. Synaptic muscarinic response types in hippocampal CA1 interneurons depend on different levels of presynaptic activity and different muscarinic receptor subtypes. *Neuropharmacology* Oct 2013;73:160-173.
38. Grigoryan GA, Mitchell SN, Hodges H, Sinden JD, Gray JA. Are the cognitive-enhancing effects of nicotine in the rat with lesions to the forebrain cholinergic projection system mediated by an interaction with the noradrenergic system? *Pharmacol Biochem Behav* Nov 1994;49(3):511-521.
39. Bell KA, Shim H, Chen CK, McQuiston AR. Nicotinic excitatory postsynaptic potentials in hippocampal CA1 interneurons are predominantly mediated by nicotinic receptors that contain alpha4 and beta2 subunits. *Neuropharmacology* Dec 2011;61(8):1379-1388.
40. Berg L, Andersson CD, Artursson E, Hornberg A, Tunemalm AK, Linusson A, Ekstrom F. Targeting acetylcholinesterase: identification of chemical leads by high throughput screening, structure determination and molecular modeling. *PLoS One* 2011;6(11):e26039.
41. Gu Z, Yakel JL. Timing-dependent septal cholinergic induction of dynamic hippocampal synaptic plasticity. *Neuron* Jul 14 2011;71(1):155-165.
42. Gu Z, Lamb PW, Yakel JL. Cholinergic coordination of presynaptic and postsynaptic activity induces timing-dependent hippocampal synaptic plasticity. *J Neurosci* Sep 5 2012;32(36):12337-12348.
43. Nagode DA, Tang AH, Karson MA, Klugmann M, Alger BE. Optogenetic release of ACh induces rhythmic bursts of perisomatic IPSCs in hippocampus. *PLoS One* 2011;6(11):e27691.
44. English BA, Dortch M, Ereshefsky L, Jhee S. Clinically significant psychotropic drug-drug interactions in the primary care setting. *Curr Psychiatry Rep* Aug 2012;14(4):376-390.
45. Navarrete M, Perea G, Fernandez de Sevilla D, Gomez-Gonzalo M, Nunez A, Martin ED, Araque A. Astrocytes mediate in vivo cholinergic-induced synaptic plasticity. *PLoS Biol* Feb 2012;10(2):e1001259.

46. Tsanov M. Septo-hippocampal signal processing: breaking the code. *Prog Brain Res* 2015;219:103-120.
47. Michalk A, Stricker S, Becker J, et al. Acetylcholine receptor pathway mutations explain various fetal akinesia deformation sequence disorders. *Am J Hum Genet* Feb 2008;82(2):464-476.
48. Sabatelli M, Eusebi F, Al-Chalabi A, et al. Rare missense variants of neuronal nicotinic acetylcholine receptor altering receptor function are associated with sporadic amyotrophic lateral sclerosis. *Hum Mol Genet* Oct 15 2009;18(20):3997-4006.
49. Sciamanna G, Hollis R, Ball C, et al. Cholinergic dysregulation produced by selective inactivation of the dystonia-associated protein torsinA. *Neurobiol Dis* Sep 2012;47(3):416-427.
50. Muller JS, Baumeister SK, Schara U, et al. CHRND mutation causes a congenital myasthenic syndrome by impairing co-clustering of the acetylcholine receptor with rapsyn. *Brain* Oct 2006;129(Pt 10):2784-2793.
51. Schliebs R, Arendt T. The significance of the cholinergic system in the brain during aging and in Alzheimer's disease. *J Neural Transm (Vienna)* Nov 2006;113(11):1625-1644.
52. Burke SN, Barnes CA. Neural plasticity in the ageing brain. *Nat Rev Neurosci* Jan 2006;7(1):30-40.
53. Szutowicz A, Bielarczyk H, Gul S, Ronowska A, Pawelczyk T, Jankowska-Kulawy A. Phenotype-dependent susceptibility of cholinergic neuroblastoma cells to neurotoxic inputs. *Metab Brain Dis* Sep 2006;21(2-3):149-161.
54. Bierer LM, Haroutunian V, Gabriel S, et al. Neurochemical correlates of dementia severity in Alzheimer's disease: relative importance of the cholinergic deficits. *J Neurochem* Feb 1995;64(2):749-760.
55. Wang HY, Lee DH, D'Andrea MR, Peterson PA, Shank RP, Reitz AB. beta-Amyloid(1-42) binds to alpha7 nicotinic acetylcholine receptor with high affinity. Implications for Alzheimer's disease pathology. *J Biol Chem* Feb 25 2000;275(8):5626-5632.
56. Dineley KT, Bell KA, Bui D, Sweatt JD. beta -Amyloid peptide activates alpha 7 nicotinic acetylcholine receptors expressed in Xenopus oocytes. *J Biol Chem* Jul 12 2002;277(28):25056-25061.
57. Bartus RT, Dean RL, 3rd, Beer B, Lippa AS. The cholinergic hypothesis of geriatric memory dysfunction. *Science* Jul 30 1982;217(4558):408-414.
58. Giacobini E, Gold G. Alzheimer disease therapy--moving from amyloid-beta to tau. *Nat Rev Neurol* Dec 2013;9(12):677-686.
59. Lane RM, Potkin SG, Enz A. Targeting acetylcholinesterase and butyrylcholinesterase in dementia. *Int J Neuropsychopharmacol* Feb 2006;9(1):101-124.
60. Drachman DA, Leavitt J. Human memory and the cholinergic system. A relationship to aging? *Arch Neurol* Feb 1974;30(2):113-121.
61. Bodick NC, Offen WW, Levey AI, et al. Effects of xanomeline, a selective muscarinic receptor agonist, on cognitive function and behavioral symptoms in Alzheimer disease. *Arch Neurol* Apr 1997;54(4):465-473.

62. Bodick NC, Offen WW, Shannon HE, Satterwhite J, Lucas R, van Lier R, Paul SM. The selective muscarinic agonist xanomeline improves both the cognitive deficits and behavioral symptoms of Alzheimer disease. *Alzheimer Dis Assoc Disord* 1997;11 Suppl 4:S16-22.
63. Deardorff WJ, Shobassy A, Grossberg GT. Safety and clinical effects of EVP-6124 in subjects with Alzheimer's disease currently or previously receiving an acetylcholinesterase inhibitor medication. *Expert Rev Neurother* Jan 2015;15(1):7-17.
64. Lewis G. Schizophrenia: concepts and clinical management. *BMJ* Feb 26 2000;320(7234):586A.
65. Lisman JE, Coyle JT, Green RW, Javitt DC, Benes FM, Heckers S, Grace AA. Circuit-based framework for understanding neurotransmitter and risk gene interactions in schizophrenia. *Trends Neurosci* May 2008;31(5):234-242.
66. Marin O. Interneuron dysfunction in psychiatric disorders. *Nat Rev Neurosci* Jan 18 2012;13(2):107-120.
67. Noetzel MJ, Rook JM, Vinson PN, et al. Functional impact of allosteric agonist activity of selective positive allosteric modulators of metabotropic glutamate receptor subtype 5 in regulating central nervous system function. *Mol Pharmacol* Feb 2012;81(2):120-133.
68. Sarter M, Lustig C, Taylor SF. Cholinergic contributions to the cognitive symptoms of schizophrenia and the viability of cholinergic treatments. *Neuropharmacology* Mar 2012;62(3):1544-1553.
69. Sullivan PF, Daly MJ, O'Donovan M. Genetic architectures of psychiatric disorders: the emerging picture and its implications. *Nat Rev Genet* Jul 10 2012;13(8):537-551.
70. Crook JM, Tomaskovic-Crook E, Copolov DL, Dean B. Decreased muscarinic receptor binding in subjects with schizophrenia: a study of the human hippocampal formation. *Biol Psychiatry* Sep 1 2000;48(5):381-388.
71. Dean B, Crook JM, Opeskin K, Hill C, Keks N, Copolov DL. The density of muscarinic M1 receptors is decreased in the caudate-putamen of subjects with schizophrenia. *Mol Psychiatry* Mar 1996;1(1):54-58.
72. Zavitsanou K, Katsifis A, Mattner F, Huang XF. Investigation of m1/m4 muscarinic receptors in the anterior cingulate cortex in schizophrenia, bipolar disorder, and major depression disorder. *Neuropsychopharmacology* Mar 2004;29(3):619-625.
73. Miwa JM, Freedman R, Lester HA. Neural systems governed by nicotinic acetylcholine receptors: emerging hypotheses. *Neuron* Apr 14 2011;70(1):20-33.
74. Adler LE, Hoffer LD, Wiser A, Freedman R. Normalization of auditory physiology by cigarette smoking in schizophrenic patients. *Am J Psychiatry* Dec 1993;150(12):1856-1861.
75. Forette F, Anand R, Gharabawi G. A phase II study in patients with Alzheimer's disease to assess the preliminary efficacy and maximum tolerated dose of rivastigmine (Exelon). *Eur J Neurol* Jul 1999;6(4):423-429.
76. Feldman HH, Lane R, Study G. Rivastigmine: a placebo controlled trial of twice daily and three times daily regimens in patients with Alzheimer's disease. *J Neurol Neurosurg Psychiatry* Oct 2007;78(10):1056-1063.

77. Leonard S, Gault J, Hopkins J, et al. Association of promoter variants in the alpha7 nicotinic acetylcholine receptor subunit gene with an inhibitory deficit found in schizophrenia. *Arch Gen Psychiatry* Dec 2002;59(12):1085-1096.
78. Court J, Spurden D, Lloyd S, et al. Neuronal nicotinic receptors in dementia with Lewy bodies and schizophrenia: alpha-bungarotoxin and nicotine binding in the thalamus. *J Neurochem* Oct 1999;73(4):1590-1597.
79. Shekhar A, Potter WZ, Lightfoot J, et al. Selective muscarinic receptor agonist xanomeline as a novel treatment approach for schizophrenia. *Am J Psychiatry* Aug 2008;165(8):1033-1039.
80. Olincy A, Harris JG, Johnson LL, et al. Proof-of-concept trial of an alpha7 nicotinic agonist in schizophrenia. *Arch Gen Psychiatry* Jun 2006;63(6):630-638.
81. Freedman R, Olincy A, Buchanan RW, et al. Initial phase 2 trial of a nicotinic agonist in schizophrenia. *Am J Psychiatry* Aug 2008;165(8):1040-1047.
82. Hanin G, Shenhar-Tsarfaty S, Yayon N, et al. Competing targets of microRNA-608 affect anxiety and hypertension. *Hum Mol Genet* Sep 1 2014;23(17):4569-4580.
83. Araque A, Parpura V, Sanzgiri RP, Haydon PG. Tripartite synapses: glia, the unacknowledged partner. *Trends Neurosci* May 1999;22(5):208-215.
84. Heller JP, Rusakov DA. Morphological plasticity of astroglia: Understanding synaptic microenvironment. *Glia* Dec 2015;63(12):2133-2151.
85. Morel L, Higashimori H, Tolman M, Yang Y. VGluT1+ neuronal glutamatergic signaling regulates postnatal developmental maturation of cortical protoplasmic astroglia. *J Neurosci* Aug 13 2014;34(33):10950-10962.
86. Ding F, O'Donnell J, Thrane AS, Zeppenfeld D, Kang H, Xie L, Wang F, Nedergaard M. alpha1-Adrenergic receptors mediate coordinated Ca2+ signaling of cortical astrocytes in awake, behaving mice. *Cell Calcium* Dec 2013;54(6):387-394.
87. Chen N, Sugihara H, Sharma J, Perea G, Petravicz J, Le C, Sur M. Nucleus basalis-enabled stimulus-specific plasticity in the visual cortex is mediated by astrocytes. *Proc Natl Acad Sci U S A* Oct 9 2012;109(41):E2832-2841.
88. Paukert M, Agarwal A, Cha J, Doze VA, Kang JU, Bergles DE. Norepinephrine controls astroglial responsiveness to local circuit activity. *Neuron* Jun 18 2014;82(6):1263-1270.
89. Monai H, Ohkura M, Tanaka M, et al. Calcium imaging reveals glial involvement in transcranial direct current stimulation-induced plasticity in mouse brain. *Nat Commun* Mar 22 2016;7:11100.
90. Schmitt LI, Sims RE, Dale N, Haydon PG. Wakefulness affects synaptic and network activity by increasing extracellular astrocyte-derived adenosine. *J Neurosci* Mar 28 2012;32(13):4417-4425.
91. Gordon GR, Baimoukhametova DV, Hewitt SA, Rajapaksha WR, Fisher TE, Bains JS. Norepinephrine triggers release of glial ATP to increase postsynaptic efficacy. *Nat Neurosci* Aug 2005;8(8):1078-1086.
92. Rollenhagen JE, Olson CR. Low-frequency oscillations arising from competitive interactions between visual stimuli in macaque inferotemporal cortex. *J Neurophysiol* Nov 2005;94(5):3368-3387.

93. Papouin T, Ladepeche L, Ruel J, et al. Synaptic and extrasynaptic NMDA receptors are gated by different endogenous coagonists. *Cell* Aug 3 2012;150(3):633-646.
94. Pascual O, Casper KB, Kubera C, et al. Astrocytic purinergic signaling coordinates synaptic networks. *Science* Oct 7 2005;310(5745):113-116.
95. Pan HC, Chou YC, Sun SH. P2X7 R-mediated Ca(2+) -independent d-serine release via pannexin-1 of the P2X7 R-pannexin-1 complex in astrocytes. *Glia* May 2015;63(5):877-893.
96. Han KS, Woo J, Park H, Yoon BJ, Choi S, Lee CJ. Channel-mediated astrocytic glutamate release via Bestrophin-1 targets synaptic NMDARs. *Mol Brain* Jan 16 2013;6:4.
97. Halassa MM, Fellin T, Haydon PG. The tripartite synapse: roles for gliotransmission in health and disease. *Trends Mol Med* Feb 2007;13(2):54-63.
98. Martineau M, Parpura V, Mothet JP. Cell-type specific mechanisms of D-serine uptake and release in the brain. *Front Synaptic Neurosci* 2014;6:12.
99. Labrie V, Clapcote SJ, Roder JC. Mutant mice with reduced NMDA-NR1 glycine affinity or lack of D-amino acid oxidase function exhibit altered anxiety-like behaviors. *Pharmacol Biochem Behav* Feb 2009;91(4):610-620.
100. Labrie V, Lipina T, Roder JC. Mice with reduced NMDA receptor glycine affinity model some of the negative and cognitive symptoms of schizophrenia. *Psychopharmacology (Berl)* Oct 2008;200(2):217-230.
101. DeVito LM, Balu DT, Kanter BR, Lykken C, Basu AC, Coyle JT, Eichenbaum H. Serine racemase deletion disrupts memory for order and alters cortical dendritic morphology. *Genes Brain Behav* Mar 2011;10(2):210-222.
102. Sattar Yea. A review of the mechanism of antagonism of N-methyl-D-aspartate receptor by ketamine in treatment-resistant depression. *Cureus* 5/18/2018 2018;10(5).
103. Basu AC, Tsai GE, Ma CL, et al. Targeted disruption of serine racemase affects glutamatergic neurotransmission and behavior. *Mol Psychiatry* Jul 2009;14(7):719-727.
104. Wolosker H, Blackshaw S, Snyder SH. Serine racemase: a glial enzyme synthesizing D-serine to regulate glutamate-N-methyl-D-aspartate neurotransmission. *Proc Natl Acad Sci U S A* Nov 9 1999;96(23):13409-13414.
105. Schell MJ, Molliver ME, Snyder SH. D-serine, an endogenous synaptic modulator: localization to astrocytes and glutamate-stimulated release. *Proc Natl Acad Sci U S A* Apr 25 1995;92(9):3948-3952.
106. Schell MJ, Brady RO, Jr., Molliver ME, Snyder SH. D-serine as a neuromodulator: regional and developmental localizations in rat brain glia resemble NMDA receptors. *J Neurosci* Mar 1 1997;17(5):1604-1615.
107. Kartvelishvily E, Shleper M, Balan L, Dumin E, Wolosker H. Neuron-derived D-serine release provides a novel means to activate N-methyl-D-aspartate receptors. *J Biol Chem* May 19 2006;281(20):14151-14162.
108. Miya K, Inoue R, Takata Y, et al. Serine racemase is predominantly localized in neurons in mouse brain. *J Comp Neurol* Oct 20 2008;510(6):641-654.

109. Panatier A, Theodosis DT, Mothet JP, Touquet B, Pollegioni L, Poulain DA, Oliet SH. Glia-derived D-serine controls NMDA receptor activity and synaptic memory. *Cell* May 19 2006;125(4):775-784.
110. Martineau M, Shi T, Puyal J, et al. Storage and uptake of D-serine into astrocytic synaptic-like vesicles specify gliotransmission. *J Neurosci* Feb 20 2013;33(8):3413-3423.
111. Yasuda E, Ma N, Semba R. Immunohistochemical evidences for localization and production of D-serine in some neurons in the rat brain. *Neurosci Lett* Feb 16 2001;299(1-2):162-164.
112. Benneyworth MA, Li Y, Basu AC, Bolshakov VY, Coyle JT. Cell selective conditional null mutations of serine racemase demonstrate a predominate localization in cortical glutamatergic neurons. *Cell Mol Neurobiol* May 2012;32(4):613-624.
113. Rosenberg D, Artoul S, Segal AC, et al. Neuronal D-serine and glycine release via the Asc-1 transporter regulates NMDA receptor-dependent synaptic activity. *J Neurosci* Feb 20 2013;33(8):3533-3544.
114. Sason H, Billard JM, Smith GP, et al. Asc-1 Transporter Regulation of Synaptic Activity via the Tonic Release of d-Serine in the Forebrain. *Cereb Cortex* Feb 1 2017;27(2):1573-1587.
115. Shigetomi E, Jackson-Weaver O, Huckstepp RT, O'Dell TJ, Khakh BS. TRPA1 channels are regulators of astrocyte basal calcium levels and long-term potentiation via constitutive D-serine release. *J Neurosci* Jun 12 2013;33(24):10143-10153.
116. Sultan S, Li L, Moss J, et al. Synaptic Integration of Adult-Born Hippocampal Neurons Is Locally Controlled by Astrocytes. *Neuron* Dec 2 2015;88(5):957-972.
117. Yamasaki M, Yamada K, Furuya S, Mitoma J, Hirabayashi Y, Watanabe M. 3-Phosphoglycerate dehydrogenase, a key enzyme for l-serine biosynthesis, is preferentially expressed in the radial glia/astrocyte lineage and olfactory ensheathing glia in the mouse brain. *J Neurosci* Oct 1 2001;21(19):7691-7704.
118. Yang JH, Wada A, Yoshida K, et al. Brain-specific Phgdh deletion reveals a pivotal role for L-serine biosynthesis in controlling the level of D-serine, an N-methyl-D-aspartate receptor co-agonist, in adult brain. *J Biol Chem* Dec 31 2010;285(53):41380-41390.
119. Ehmsen JT, Ma TM, Sason H, Rosenberg D, Ogo T, Furuya S, Snyder SH, Wolosker H. D-serine in glia and neurons derives from 3-phosphoglycerate dehydrogenase. *J Neurosci* Jul 24 2013;33(30):12464-12469.
120. Klomp LW, Bull LN, Knisely AS, et al. A missense mutation in FIC1 is associated with greenland familial cholestasis. *Hepatology* Dec 2000;32(6):1337-1341.
121. Ribeiro CS, Reis M, Panizzutti R, de Miranda J, Wolosker H. Glial transport of the neuromodulator D-serine. *Brain Res* Mar 8 2002;929(2):202-209.
122. Rutter AR, Fradley RL, Garrett EM, Chapman KL, Lawrence JM, Rosahl TW, Patel S. Evidence from gene knockout studies implicates Asc-1 as the primary transporter mediating d-serine reuptake in the mouse CNS. *Eur J Neurosci* Mar 2007;25(6):1757-1766.

123. Cho SE, Na KS, Cho SJ, Kang SG. Low d-serine levels in schizophrenia: A systematic review and meta-analysis. *Neurosci Lett* Nov 10 2016;634:42-51.
124. Sacchi S, Caldinelli L, Cappelletti P, Pollegioni L, Molla G. Structure-function relationships in human D-amino acid oxidase. *Amino Acids* Nov 2012;43(5):1833-1850.
125. Balu DT, Li Y, Puhl MD, Benneyworth MA, Basu AC, Takagi S, Bolshakov VY, Coyle JT. Multiple risk pathways for schizophrenia converge in serine racemase knockout mice, a mouse model of NMDA receptor hypofunction. *Proc Natl Acad Sci U S A* Jun 25 2013;110(26):E2400-2409.
126. Hashimoto K, Fukushima T, Shimizu E, et al. Decreased serum levels of D-serine in patients with schizophrenia: evidence in support of the N-methyl-D-aspartate receptor hypofunction hypothesis of schizophrenia. *Arch Gen Psychiatry* Jun 2003;60(6):572-576.
127. Bendikov I, Nadri C, Amar S, Panizzutti R, De Miranda J, Wolosker H, Agam G. A CSF and postmortem brain study of D-serine metabolic parameters in schizophrenia. *Schizophr Res* Feb 2007;90(1-3):41-51.
128. Calcia MA, Madeira C, Alheira FV, et al. Plasma levels of D-serine in Brazilian individuals with schizophrenia. *Schizophr Res* Dec 2012;142(1-3):83-87.
129. Morita Y, Ujike H, Tanaka Y, et al. A genetic variant of the serine racemase gene is associated with schizophrenia. *Biol Psychiatry* May 15 2007;61(10):1200-1203.
130. Boks MP, Rietkerk T, van de Beek MH, Sommer IE, de Koning TJ, Kahn RS. Reviewing the role of the genes G72 and DAAO in glutamate neurotransmission in schizophrenia. *Eur Neuropsychopharmacol* Sep 2007;17(9):567-572.
131. Caldinelli L, Sacchi S, Molla G, Nardini M, Pollegioni L. Characterization of human DAAO variants potentially related to an increased risk of schizophrenia. *Biochim Biophys Acta* Mar 2013;1832(3):400-410.
132. Ma TM, Abazyan S, Abazyan B, et al. Pathogenic disruption of DISC1-serine racemase binding elicits schizophrenia-like behavior via D-serine depletion. *Mol Psychiatry* May 2013;18(5):557-567.
133. Pritchett D, Hasan S, Tam SK, et al. d-amino acid oxidase knockout (Dao(-/-)) mice show enhanced short-term memory performance and heightened anxiety, but no sleep or circadian rhythm disruption. *Eur J Neurosci* May 2015;41(9):1167-1179.
134. Sakurai S, Ishii S, Umino A, Shimazu D, Yamamoto N, Nishikawa T. Effects of psychotomimetic and antipsychotic agents on neocortical and striatal concentrations of various amino acids in the rat. *J Neurochem* Sep 2004;90(6):1378-1388.
135. Verrall L, Walker M, Rawlings N, Benzel I, Kew JN, Harrison PJ, Burnet PW. d-Amino acid oxidase and serine racemase in human brain: normal distribution and altered expression in schizophrenia. *Eur J Neurosci* Sep 2007;26(6):1657-1669.
136. Tsai G, Yang P, Chung LC, Lange N, Coyle JT. D-serine added to antipsychotics for the treatment of schizophrenia. *Biol Psychiatry* Dec 1 1998;44(11):1081-1089.
137. Heresco-Levy U, Javitt DC, Ebstein R, Vass A, Lichtenberg P, Bar G, Catinari S, Ermilov M. D-serine efficacy as add-on pharmacotherapy to risperidone and olanzapine for treatment-refractory schizophrenia. *Biol Psychiatry* Mar 15 2005;57(6):577-585.

138. Kantrowitz JT, Malhotra AK, Cornblatt B, et al. High dose D-serine in the treatment of schizophrenia. *Schizophr Res* Aug 2010;121(1-3):125-130.
139. Ohnuma T, Sakai Y, Maeshima H, et al. Changes in plasma glycine, L-serine, and D-serine levels in patients with schizophrenia as their clinical symptoms improve: results from the Juntendo University Schizophrenia Projects (JUSP). *Prog Neuropsychopharmacol Biol Psychiatry* Dec 12 2008;32(8):1905-1912.
140. Billard JM. D-Amino acids in brain neurotransmission and synaptic plasticity. *Amino Acids* Nov 2012;43(5):1851-1860.
141. Barnes CA, Rao G, Shen J. Age-related decrease in the N-methyl-D-aspartateR-mediated excitatory postsynaptic potential in hippocampal region CA1. *Neurobiol Aging* Jul-Aug 1997;18(4):445-452.
142. Javitt DC. Current and emergent treatments for symptoms and neurocognitive impairment in schizophrenia. *Curr Treat Options Psychiatry* Jun 2015;1(2):107-120.
143. Moghaddam B, Javitt D. From revolution to evolution: the glutamate hypothesis of schizophrenia and its implication for treatment. *Neuropsychopharmacology* Jan 2012;37(1):4-15.
144. Johnson JW, Ascher P. Glycine potentiates the NMDA response in cultured mouse brain neurons. *Nature* Feb 5-11 1987;325(6104):529-531.
145. Kleckner NW, Dingledine R. Requirement for glycine in activation of NMDA-receptors expressed in Xenopus oocytes. *Science* Aug 12 1988;241(4867):835-837.
146. Henneberger C, Papouin T, Oliet SH, Rusakov DA. Long-term potentiation depends on release of D-serine from astrocytes. *Nature* Jan 14 2010;463(7278):232-236.
147. Bergersen LH, Morland C, Ormel L, et al. Immunogold detection of L-glutamate and D-serine in small synaptic-like microvesicles in adult hippocampal astrocytes. *Cereb Cortex* Jul 2012;22(7):1690-1697.
148. Labrie V, Wong AH, Roder JC. Contributions of the D-serine pathway to schizophrenia. *Neuropharmacology* Mar 2012;62(3):1484-1503.
149. Freedman R. alpha7-nicotinic acetylcholine receptor agonists for cognitive enhancement in schizophrenia. *Annu Rev Med* 2014;65:245-261.
150. Teles-Grilo Ruivo LM, Mellor JR. Cholinergic modulation of hippocampal network function. *Front Synaptic Neurosci* 2013;5:2.
151. Marrosu F, Portas C, Mascia MS, Casu MA, Fa M, Giagheddu M, Imperato A, Gessa GL. Microdialysis measurement of cortical and hippocampal acetylcholine release during sleep-wake cycle in freely moving cats. *Brain Res* Feb 13 1995;671(2):329-332.
152. Lee MG, Hassani OK, Alonso A, Jones BE. Cholinergic basal forebrain neurons burst with theta during waking and paradoxical sleep. *J Neurosci* Apr 27 2005;25(17):4365-4369.
153. Zant JC, Kim T, Prokai L, et al. Cholinergic Neurons in the Basal Forebrain Promote Wakefulness by Actions on Neighboring Non-Cholinergic Neurons: An Opto-Dialysis Study. *J Neurosci* Feb 10 2016;36(6):2057-2067.

154. Kirkwood A, Rozas C, Kirkwood J, Perez F, Bear MF. Modulation of long-term synaptic depression in visual cortex by acetylcholine and norepinephrine. *J Neurosci* Mar 1 1999;19(5):1599-1609.
155. Lin H, Hsu FC, Baumann BH, Coulter DA, Lynch DR. Cortical synaptic NMDA receptor deficits in alpha7 nicotinic acetylcholine receptor gene deletion models: implications for neuropsychiatric diseases. *Neurobiol Dis* Mar 2014;63:129-140.
156. Markram H, Segal M. Acetylcholine potentiates responses to N-methyl-D-aspartate in the rat hippocampus. *Neurosci Lett* May 18 1990;113(1):62-65.
157. Yang Y, Paspalas CD, Jin LE, Picciotto MR, Arnsten AF, Wang M. Nicotinic alpha7 receptors enhance NMDA cognitive circuits in dorsolateral prefrontal cortex. *Proc Natl Acad Sci U S A* Jul 16 2013;110(29):12078-12083.
158. Zappettini S, Grilli M, Olivero G, et al. Nicotinic alpha7 receptor activation selectively potentiates the function of NMDA receptors in glutamatergic terminals of the nucleus accumbens. *Front Cell Neurosci* 2014;8:332.
159. Hirase H, Iwai Y, Takata N, Shinohara Y, Mishima T. Volume transmission signalling via astrocytes. *Philos Trans R Soc Lond B Biol Sci* Oct 19 2014;369(1654):20130604.
160. Sharma G, Vijayaraghavan S. Nicotinic cholinergic signaling in hippocampal astrocytes involves calcium-induced calcium release from intracellular stores. *Proc Natl Acad Sci U S A* Mar 27 2001;98(7):4148-4153.
161. Shen JX, Yakel JL. Functional alpha7 nicotinic ACh receptors on astrocytes in rat hippocampal CA1 slices. *J Mol Neurosci* Sep 2012;48(1):14-21.
162. Singh NS, Paul RK, Ramamoorthy A, Torjman MC, Moaddel R, Bernier M, Wainer IW. Nicotinic acetylcholine receptor antagonists alter the function and expression of serine racemase in PC-12 and 1321N1 cells. *Cell Signal* Dec 2013;25(12):2634-2645.
163. Vardjan N, Parpura V, Zorec R. Loose excitation-secretion coupling in astrocytes. *Glia* May 2016;64(5):655-667.
164. Pinto L, Goard MJ, Estandian D, et al. Fast modulation of visual perception by basal forebrain cholinergic neurons. *Nat Neurosci* Dec 2013;16(12):1857-1863.
165. Su M, Hu H, Lee Y, d'Azzo A, Messing A, Brenner M. Expression specificity of GFAP transgenes. *Neurochem Res* Nov 2004;29(11):2075-2093.
166. Paoletti P, Neyton J. NMDA receptor subunits: function and pharmacology. *Curr Opin Pharmacol* Feb 2007;7(1):39-47.
167. Paoletti P, Bellone C, Zhou Q. NMDA receptor subunit diversity: impact on receptor properties, synaptic plasticity and disease. *Nat Rev Neurosci* Jun 2013;14(6):383-400.
168. Vecsey CG, Wimmer ME, Havekes R, Park AJ, Perron IJ, Meerlo P, Abel T. Daily acclimation handling does not affect hippocampal long-term potentiation or cause chronic sleep deprivation in mice. *Sleep* Apr 1 2013;36(4):601-607.
169. Fukushima T, Kawai J, Imai K, Toyo'oka T. Simultaneous determination of D- and L-serine in rat brain microdialysis sample using a column-switching HPLC with fluorimetric detection. *Biomed Chromatogr* Dec 2004;18(10):813-819.
170. Dale N, Hatz S, Tian F, Llaudet E. Listening to the brain: microelectrode biosensors for neurochemicals. *Trends Biotechnol* Aug 2005;23(8):420-428.

171. Matus-Amat P, Higgins EA, Sprunger D, Wright-Hardesty K, Rudy JW. The role of dorsal hippocampus and basolateral amygdala NMDA receptors in the acquisition and retrieval of context and contextual fear memories. *Behav Neurosci* Aug 2007;121(4):721-731.
172. Schenberg EE, Oliveira MG. Effects of pre or posttraining dorsal hippocampus D-AP5 injection on fear conditioning to tone, background, and foreground context. *Hippocampus* 2008;18(11):1089-1093.
173. Maingret N, Girardeau G, Todorova R, Goutierre M, Zugaro M. Hippocampo-cortical coupling mediates memory consolidation during sleep. *Nat Neurosci* Jul 2016;19(7):959-964.
174. Balu DT, Takagi S, Puhl MD, Benneyworth MA, Coyle JT. D-serine and serine racemase are localized to neurons in the adult mouse and human forebrain. *Cell Mol Neurobiol* Apr 2014;34(3):419-435.
175. Wolosker H, Radzishevsky I. The serine shuttle between glia and neurons: implications for neurotransmission and neurodegeneration. *Biochem Soc Trans* Dec 2013;41(6):1546-1550.
176. Gahring LC, Persiyanov K, Dunn D, Weiss R, Meyer EL, Rogers SW. Mouse strain-specific nicotinic acetylcholine receptor expression by inhibitory interneurons and astrocytes in the dorsal hippocampus. *J Comp Neurol* Jan 12 2004;468(3):334-346.
177. Duffy AM, Fitzgerald ML, Chan J, Robinson DC, Milner TA, Mackie K, Pickel VM. Acetylcholine alpha7 nicotinic and dopamine D2 receptors are targeted to many of the same postsynaptic dendrites and astrocytes in the rodent prefrontal cortex. *Synapse* Dec 2011;65(12):1350-1367.
178. Zhang Y, Chen K, Sloan SA, et al. An RNA-sequencing transcriptome and splicing database of glia, neurons, and vascular cells of the cerebral cortex. *J Neurosci* Sep 3 2014;34(36):11929-11947.
179. Aston-Jones G, Bloom FE. Norepinephrine-containing locus coeruleus neurons in behaving rats exhibit pronounced responses to non-noxious environmental stimuli. *J Neurosci* Aug 1981;1(8):887-900.
180. Beinat C, Banister SD, Herrera M, Law V, Kassiou M. The therapeutic potential of alpha7 nicotinic acetylcholine receptor (alpha7 nAChR) agonists for the treatment of the cognitive deficits associated with schizophrenia. *CNS Drugs* Jul 2015;29(7):529-542.
181. Prickaerts J, van Goethem NP, Chesworth R, et al. EVP-6124, a novel and selective alpha7 nicotinic acetylcholine receptor partial agonist, improves memory performance by potentiating the acetylcholine response of alpha7 nicotinic acetylcholine receptors. *Neuropharmacology* Feb 2012;62(2):1099-1110.
182. Zhao S, Ting JT, Atallah HE, et al. Cell type-specific channelrhodopsin-2 transgenic mice for optogenetic dissection of neural circuitry function. *Nat Methods* Sep 2011;8(9):745-752.
183. Clements JD. Transmitter timecourse in the synaptic cleft: its role in central synaptic function. *Trends Neurosci* May 1996;19(5):163-171.

184. Orozco-Ibarra M, Medina-Campos ON, Sanchez-Gonzalez DJ, et al. Evaluation of oxidative stress in D-serine induced nephrotoxicity. *Toxicology* Jan 5 2007;229(1-2):123-135.
185. Vandecasteele M, Varga V, Berenyi A, Papp E, Bartho P, Venance L, Freund TF, Buzsaki G. Optogenetic activation of septal cholinergic neurons suppresses sharp wave ripples and enhances theta oscillations in the hippocampus. *Proc Natl Acad Sci U S A* Sep 16 2014;111(37):13535-13540.
186. Paul S, Jeon WK, Bizon JL, Han JS. Interaction of basal forebrain cholinergic neurons with the glucocorticoid system in stress regulation and cognitive impairment. *Front Aging Neurosci* 2015;7:43.
187. Ashford JW. Treatment of Alzheimer's Disease: The Legacy of the Cholinergic Hypothesis, Neuroplasticity, and Future Directions. *J Alzheimers Dis* 2015;47(1):149-156.
188. Foster DJ, Jones CK, Conn PJ. Emerging approaches for treatment of schizophrenia: modulation of cholinergic signaling. *Discov Med* Dec 2012;14(79):413-420.
189. Colucci L, Bosco M, Rosario Ziello A, Rea R, Amenta F, Fasanaro AM. Effectiveness of nootropic drugs with cholinergic activity in treatment of cognitive deficit: a review. *J Exp Pharmacol* 2012;4:163-172.
190. Yamamoto T, Ochalski A, Hertzberg EL, Nagy JI. On the organization of astrocytic gap junctions in rat brain as suggested by LM and EM immunohistochemistry of connexin43 expression. *J Comp Neurol* Dec 22 1990;302(4):853-883.
191. Halassa MM, Fellin T, Takano H, Dong JH, Haydon PG. Synaptic islands defined by the territory of a single astrocyte. *J Neurosci* Jun 13 2007;27(24):6473-6477.
192. Kugler P, Schleyer V. Developmental expression of glutamate transporters and glutamate dehydrogenase in astrocytes of the postnatal rat hippocampus. *Hippocampus* 2004;14(8):975-985.
193. Zhang Q, Haydon PG. Roles for gliotransmission in the nervous system. *J Neural Transm (Vienna)* Jan 2005;112(1):121-125.
194. Fossat P, Turpin FR, Sacchi S, et al. Glial D-serine gates NMDA receptors at excitatory synapses in prefrontal cortex. *Cereb Cortex* Mar 2012;22(3):595-606.
195. Smith SM, Uslaner JM, Hutson PH. The Therapeutic Potential of D-Amino Acid Oxidase (DAAO) Inhibitors. *Open Med Chem J* May 27 2010;4:3-9.
196. Takeda M, Imaizumi M, Fushiki T. Preference for vegetable oils in the two-bottle choice test in mice. *Life Sci* 2000;67(2):197-204.
197. De Miranda J, Santoro A, Engelender S, Wolosker H. Human serine racemase: moleular cloning, genomic organization and functional analysis. *Gene* Oct 3 2000;256(1-2):183-188.
198. Konno R, Yasumura Y. Mouse mutant deficient in D-amino acid oxidase activity. *Genetics* Feb 1983;103(2):277-285.
199. Carrier N, Kabbaj M. Sex differences in the antidepressant-like effects of ketamine. *Neuropharmacology* Jul 2013;70:27-34.
200. Vazquez J, Baghdoyan HA. Basal forebrain acetylcholine release during REM sleep is significantly greater than during waking. *Am J Physiol Regul Integr Comp Physiol* Feb 2001;280(2):R598-601.

201. Thrane AS, Rangroo Thrane V, Zeppenfeld D, Lou N, Xu Q, Nagelhus EA, Nedergaard M. General anesthesia selectively disrupts astrocyte calcium signaling in the awake mouse cortex. *Proc Natl Acad Sci U S A* Nov 13 2012;109(46):18974-18979.

202. Polcari D, Kwan A, Van Horn MR, Danis L, Pollegioni L, Ruthazer ES, Mauzeroll J. Disk-shaped amperometric enzymatic biosensor for in vivo detection of D-serine. *Anal Chem* Apr 1 2014;86(7):3501-3507.

203. El-Tallawy HN, Saleem TH, El-Ebidi AM, Hassan MH, Gabra RH, Farghaly WM, Abo El-Maali N, Sherkawy HS. Clinical and biochemical study of d-serine metabolism among schizophrenia patients. *Neuropsychiatr Dis Treat* 2017;13:1057-1063.

204. Galloway A, Adeluyi A, O'Donovan B, et al. Dopamine triggers CTCF-dependent morphological and genomic remodeling of astrocytes. *J Neurosci* Apr 30 2018.

205. Langle SL, Poulain DA, Theodosis DT. Induction of rapid, activity-dependent neuronal-glial remodelling in the adult rat hypothalamus in vitro. *Eur J Neurosci* Jul 2003;18(1):206-214.

206. Frago LM, Chowen JA. Involvement of Astrocytes in Mediating the Central Effects of Ghrelin. *Int J Mol Sci* Mar 2 2017;18(3).

207. Morte B, Gil-Ibanez P, Bernal J. Regulation of Gene Expression by Thyroid Hormone in Primary Astrocytes: Factors Influencing the Genomic Response. *Endocrinology* May 1 2018;159(5):2083-2092.

208. Pearson-Leary J, Osborne DM, McNay EC. Role of Glia in Stress-Induced Enhancement and Impairment of Memory. *Front Integr Neurosci* 2015;9:63.

209. Acaz-Fonseca E, Sanchez-Gonzalez R, Azcoitia I, Arevalo MA, Garcia-Segura LM. Role of astrocytes in the neuroprotective actions of 17beta-estradiol and selective estrogen receptor modulators. *Mol Cell Endocrinol* May 25 2014;389(1-2):48-57.

210. Wang C, Jie C, Dai X. Possible roles of astrocytes in estrogen neuroprotection during cerebral ischemia. *Rev Neurosci* 2014;25(2):255-268.

211. Sagud M, Mihaljevic-Peles A, Muck-Seler D, Pivac N, Vuksan-Cusa B, Brataljenovic T, Jakovljevic M. Smoking and schizophrenia. *Psychiatr Danub* Sep 2009;21(3):371-375.

212. Lane HY, Lin CH, Green MF, et al. Add-on treatment of benzoate for schizophrenia: a randomized, double-blind, placebo-controlled trial of D-amino acid oxidase inhibitor. *JAMA Psychiatry* Dec 2013;70(12):1267-1275.

213. Li R, Ma X, Wang G, Yang J, Wang C. Why sex differences in schizophrenia? *J Transl Neurosci (Beijing)* Sep 2016;1(1):37-42.